

**Electrocatalytic-Frustrated Lewis Pair Hydrogen
Oxidation Using Novel Benzothiazolium Salts**



Sarah Jane Woodhouse

A thesis submitted in accordance with the requirements for the degree of Doctor of
Philosophy (PhD) from the University of East Anglia

School of Chemistry, University of East Anglia

September 2020

© This copy of the thesis has been supplied on condition that anyone who consults it is understood to recognise that its copyright rests with the author and that use of any information derived there from must be in accordance with current UK Copyright Law. In addition, any quotation or extract must include full attribution.

Abstract

The aim this project was to synthesise benzothiazolines/benzothiazolium salts with a variety of functional groups on the C2 aryl ring, in order to fine tune the acidity of the C2-H for electrocatalytic hydrogen oxidation. The synthesis was successful and a variety of different compounds were made and the functionality did affect the acidity of the C2-H (Chapter 4). However, problems arose with the frustrated Lewis pair activation of the cycle with adduct formation. This is discussed further in Chapter 5.

In chapter 1, several different ways of hydrogen production are discussed, from steam reformation to hydrogenases. Also included is the utilisation of hydrogen, from hydrogen fuel cells to hydrogen cleavage/activation, for use in chemical transformations, using frustrated Lewis pairs.

Chapter 2 shows the successful synthesis of a variety of different molecules, from di-thiol linked, substituted imines to benzothiazolium salts to *N*-methyl-2-(aryl)benzothiazolines.

Chapter 3 includes the results and discussion of the syntheses, discussing the unexpected synthesis of di-thiol linked substituted imines, and the successful synthesis of a variety of novel *N*-methyl-2-(aryl)benzothiazolines.

In chapter 4, the electrochemical analysis of a variety of synthesised *N*-methyl-2-(aryl)benzothiazolines is discussed. Analysis of the variable scan rate (VSR) cyclic voltammetry produced Randles-Sevcik plots in order to determine the relationship between peak current and v_{scan} rate. For electrochemically reversible electron transfer processes that involve freely diffusing redox species, this relationship is linear.

Chapter 5 introduces the hydride transfer experiments for the *N*-methyl-2-(4-nitrophenyl)benzothiazolium salt, which indicated successful transfer, although a slow transformation. Investigations into alternative boranes were undertaken and the results are discussed.

Access Condition and Agreement

Each deposit in UEA Digital Repository is protected by copyright and other intellectual property rights, and duplication or sale of all or part of any of the Data Collections is not permitted, except that material may be duplicated by you for your research use or for educational purposes in electronic or print form. You must obtain permission from the copyright holder, usually the author, for any other use. Exceptions only apply where a deposit may be explicitly provided under a stated licence, such as a Creative Commons licence or Open Government licence.

Electronic or print copies may not be offered, whether for sale or otherwise to anyone, unless explicitly stated under a Creative Commons or Open Government license. Unauthorised reproduction, editing or reformatting for resale purposes is explicitly prohibited (except where approved by the copyright holder themselves) and UEA reserves the right to take immediate 'take down' action on behalf of the copyright and/or rights holder if this Access condition of the UEA Digital Repository is breached. Any material in this database has been supplied on the understanding that it is copyright material and that no quotation from the material may be published without proper acknowledgement.

Acknowledgements

I would firstly like to thank Dr Greg Wildgoose for giving me the opportunity to undertake the project. I extend my gratitude to the rest of the Wildgoose group who were there when I started; especially Dr Robin Blagg and Dr James Courtney for their continued support even after their departures.

I would like to thank The Leverhulme Trust for their financial aid, funding the project. I would not have been able to do a PhD without the funding.

I wholeheartedly thank my current supervisor Dr Joseph Wright for all his help and guidance; taking me under his wing when Greg left academia. Thanks also goes to Dr Anna Fuller for jumping on board to become my secondary supervisor and proofreading chapters when writing. I extend my thanks to Dr David Hughes for his help with the crystallography.

A special thank you goes to Dr Elisé Wright and Dr Ryan Tinson, whose support throughout has been top notch; through my darkest days they were always there and I do not know how I could repay them for their kindness.

I am also grateful for the support from Dr Derek Warren, Dr Anna Mullen, Mike O'Sullivan and Alex Morrith. They have all been there through my multiple breakdowns and crying episodes when I didn't think I could do it! Thanks is also extended to Samwell Piper for listening to all my moaning at home and being there to participate in our 'girlie nights' when I needed cheering up after an awful day/week at uni.

I am most grateful for the support from my friends and family back home. My granny and mum have given me financial support throughout and when my funding ended. My nearest and dearest friends have listened to my moaning and are my biggest cheerleaders. I hope I make every single one of them proud.

Lastly, I would like to thank the wider UEA community. It has been an emotional rollercoaster, with trips to Student services, but I made it to submission and I will forever be grateful for the opportunity to study at UEA. #UEAiswonderful

Contents

1.	Introduction	6
1.1	Summary	6
1.2	Hydrogen production	8
1.3	Hydrogen catalysts	10
1.3.1	Hydrogenases	10
1.3.2	Molecular catalysts	11
1.3.3	Transition metal catalysts	11
1.3.4	Metal-free catalysts	12
1.4	Hydrogen fuel cells	14
1.5	Hydrogen storage	17
1.6	Frustrated Lewis pairs (FLPs)	18
1.6.1	Lewis adducts and the history of FLPs	18
1.6.2	Phosphorus-Boron FLPs	19
1.6.3	Beyond phosphines as Lewis bases	21
1.6.4	Expanding Lewis acid research	22
1.6.5	Metal FLP-like systems	24
1.6.6	Carbon-based Lewis acids	24
2.	Experimental	27
2.1	Synthesis of dithiol-linked, aryl-substituted imines	27
2.2	Synthesis of [<i>N</i> -methyl-2-(aryl)benzothiazolium] zinc salts	32
2.3	Synthesis of <i>N</i> -Methyl-2-(aryl)benzothiazoline	35
2.4	Other syntheses	41
2.5	X-ray crystallographic data	45
3.	Synthesis: results and discussion	49
3.1	Background	49
3.2	Synthesis of dithiol-linked, aryl-substituted compounds	54
3.3	Synthesis of <i>N</i> -methyl-2-(aryl)benzothiazolines	62
3.4	Synthesis of [<i>N</i> -methyl-2-(aryl)benzothiazolium] zinc salts	71
3.5	Synthesis of [<i>N</i> -methyl-2-(aryl)benzothiazolium][BARF ₂₀] salts	77
4.	Electrochemistry	78
4.1	Electrochemical equilibria	80
4.2	Electrode kinetics	82
4.3	Mass transport – diffusion, migration and convection	83
4.4	Supporting electrolyte	84
4.5	Chronoamperometry	86
4.6	Electrochemical analysis of various <i>N</i> -methyl-2-arylbenzothiazolines	87
5.	Hydride transfer from activated frustrated Lewis pairs to <i>N</i> -methyl-2-arylbenzothiazolium cations	94
5.1	Background	94
5.2	Initial hydride transfer experiments	97
5.3	Adduct formation	108
5.4	Boranes	112
6.	Conclusions and future work	118
7.	Appendix	119
8.	References	123

Abbreviations

BArF ₁₅	Tris(pentafluorophenyl)borane
BArF ₁₈	Tris[3,5-bis(trifluoromethyl)phenyl]borane
BArF ₂₀	Tetrakis(pentafluorophenyl)borate
FLP	Frustrated Lewis pair
H ₄ MPT	Tetrahydromethanopterin
MP	Melting point
NAD(P)	Nicotinamide adenine dinucleotide
NR	No reaction
RTP	Room temperature and pressure (25 °C and 1 atm)
THF	Tetrahydrofuran

1. Introduction

This project was to synthesise a variety of *N*-methyl(aryl)benzothiazolines/*N*-methyl(aryl)benzothiazolium salts to be used as electrocatalysts for hydrogen oxidation, in conjunction with a Frustrated Lewis Pair (FLP). Discussed in this section is the background to hydrogen as a fuel, its storage, hydrogen oxidation using FLPs and prior work done in this area of research.

1.1 Summary

Hydrogen is the most abundant element on Earth but less than 1% is available as dihydrogen, H₂, as the majority is bound in water and some bound in hydrocarbons.¹ Hydrogen has been used as an energy source since the 1800s and makes up to 50% of 'syngas' from gasification of coal. 'Syngas' is a synthetic gas produced from the combustion of coal and generally consists of carbon monoxide, hydrogen, carbon dioxide and methane². It has been used in the US to heat urban homes since 1800s to 1940s when it was overtaken by the use of natural gas.³ The use (and combustion of) natural gas has contributed significantly to the increase in greenhouse gases (such as carbon dioxide) and climate change. Climate change is responsible for the rise in sea levels and since 1993 thermal expansion of oceans has contributed 57% to the rise in sea levels; while a 28% contribution has come from a decrease in glaciers and ice caps with the remainder attributed to losses from polar ice sheets.⁴ Fossil fuel oil (e.g. crude oil) accounts for 97% of global liquid fuels and the peak of production can be estimated to occur before 2031.⁵ Oil resources are said to be sufficient to meet the anticipated demand of growth until a similar time⁶ after which an alternative energy would need to be sourced. Hydrogen is an energy vector that we want to exploit as a renewable energy source. Oxidation of hydrogen produces water as shown in Equation 1.1.1.



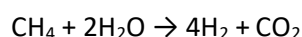
Equation 1.1.1 - The oxidation of hydrogen to form water as the only product

This reaction is highly exothermic ($\Delta H = -286 \text{ kJ mol}^{-1}$).⁷ Hydrogen is considered a clean energy source, as the only product of the reaction is water and therefore has the greatest potential, environmentally.³ It is the only energy carrier which can be produced and used with negligible environmental impact.⁸ This is very important as the current fuels used produce carbon

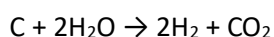
dioxide and are therefore said to be the cause of global warming which has led to climate change. Hydrogen can be used in fuel cells, which harness this energy and produce electrical current. The production of hydrogen is, therefore, crucial for use as an energy source.

1.2 Hydrogen production

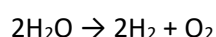
Hydrogen is of great interest in the fuel industry as a renewable energy vector and the sustainable production of hydrogen is essential for a future hydrogen economy.⁹ There are currently three main ways in which hydrogen is produced industrially which include steam reforming (Equation 1.2.1), coal gasification (Equation 1.2.2) and water electrolysis (Equation 1.2.3).¹⁰



Equation 1.2.1 – Steam reforming of methane which produces hydrogen and carbon dioxide

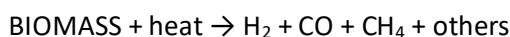


Equation 1.2.2 – Coal gasification which produces hydrogen and carbon dioxide

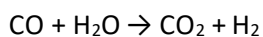


Equation 1.2.3 – Electrolysis of water which produces hydrogen and oxygen

Steam reforming and coal gasification rely on fossil fuels and therein lies the problem as there is a finite supply of fossil fuels. As previously mentioned, the burning of fossil fuels produces carbon dioxide which causes global warming, which has led to climate change. There are other processes for hydrogen production which include thermochemical (pyrolysis of biomass, Equation 1.2.4) production and biological (water-gas shift, Equation 1.2.5) production.



Equation 1.2.4 – Pyrolysis of biomass which produces hydrogen, carbon monoxide, methane and others¹¹



Equation 1.2.5 – Water-gas shift process produces carbon dioxide and hydrogen¹²

The by-products of the above mentioned processes include CO_x .¹³ Pyrolysis produces other gases such as methane; not just hydrogen.¹⁴ Methane is another greenhouse gas which causes global warming. Steam reforming is the most common process of hydrogen production but relies on high temperatures and pressures (675–1000 K and 30 bar),¹⁵ which is very costly and therefore not effective.

There are several sustainable pathways for hydrogen production that harness renewable energy sources⁹ which are shown in Figure 1.2.1.

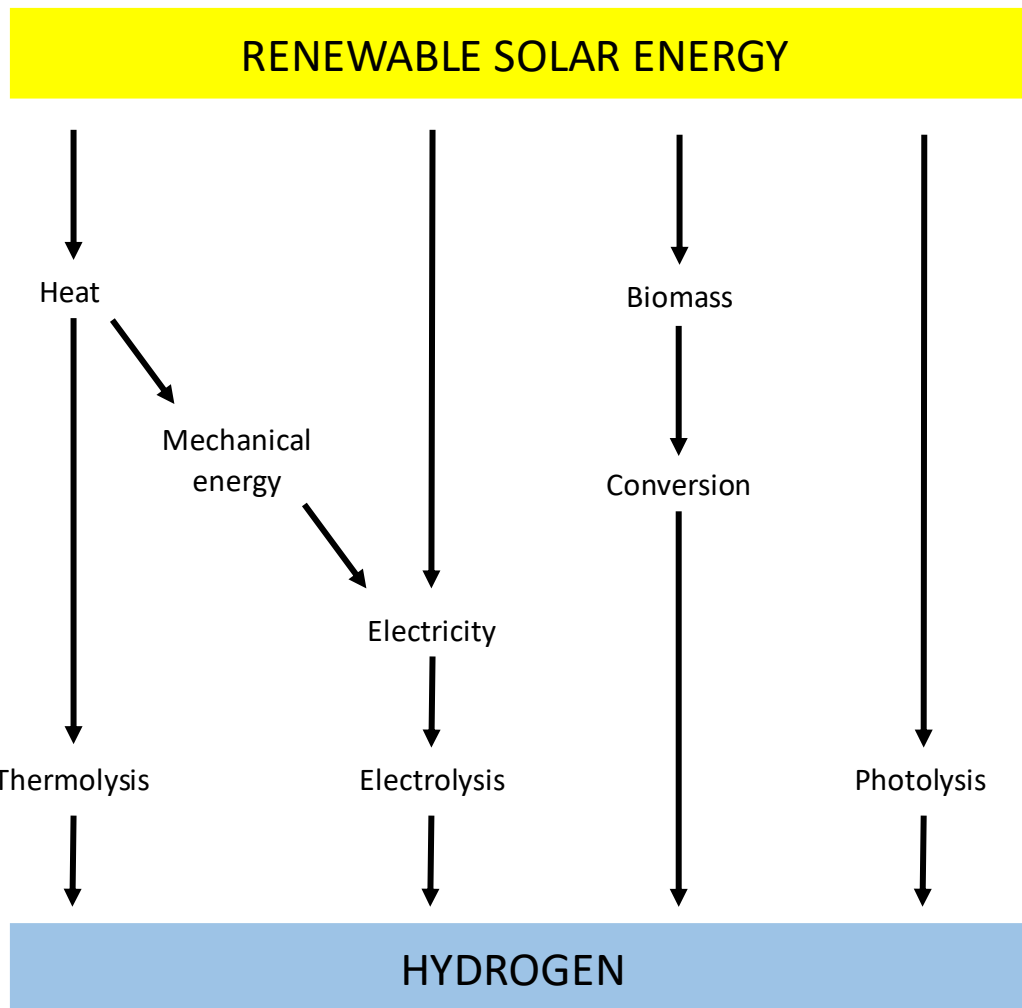


Figure 1.2.1 - Sustainable pathways for hydrogen production from renewable solar energy. Figure redrawn from reference 9

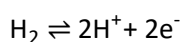
Most hydrogen is used for industrial purposes such as petroleum refining and ammonia production for fertilisers.⁹ Hydrogen plays a vital role in chemical processes in production of fragrances, detergents, emulsifiers and lubricants¹⁶, as well as pharmaceuticals.¹⁷ There has been a plethora of research into the chemical splitting of hydrogen for many chemical transformations and this will be discussed in Section 1.5.

1.3 Hydrogen catalysts

There are several systems that catalyse the production/oxidation of hydrogen already known. These will be discussed individually below.

1.3.1 Hydrogenases

Hydrogenases are biological enzymes that catalyse the reversible oxidation of hydrogen as shown in Equation 1.3.1.1.



Equation 1.3.1.1 - The half equation for the oxidation of hydrogen to form two protons and two electrons¹⁸

These enzymes are of great interest due to their catalytic capability in the production and oxidation of hydrogen. However, there is a problem with hydrogenases in that most are oxygen-sensitive; binding of which renders the enzyme inactive, and so these enzymes work in anaerobic conditions. In nature there are three main types of hydrogenases, stratified based on the components in the active site. These are [Fe]-, [FeFe]- and [NiFe]-hydrogenases, and it is in the latter group that oxygen-tolerant hydrogenases can be found.¹⁹

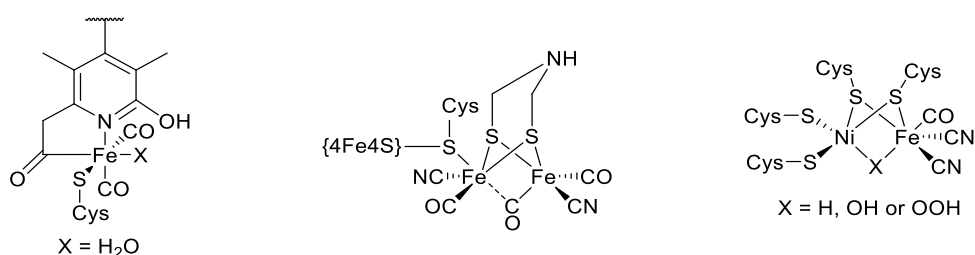


Figure 1.3.1.1 – The active sites of the [Fe]- (left), [FeFe]- (middle), and [NiFe]-hydrogenases (right). Active sites redrawn from references 19, 20 and 21.

The [Fe]- (or mono-iron) hydrogenase has a single transition metal centre and catalyses the reduction of methenyl-H₄MPT⁺ (*N*⁵,*N*¹⁰-methenyl-tetrahydromethanopterin) to methylene-H₄MPT (*N*⁵,*N*¹⁰-methylene-tetrahydromethanopterin) using hydrogen. This single metal-centred enzyme is redox inactive and therefore cannot catalyse the reverse reaction.²⁰

The [FeFe]- (or Fe-only) hydrogenase can be found in many prokaryotes and eukaryotes²² and differs from the mono-iron hydrogenase in the fact that it can catalyse both the oxidation of

hydrogen and the reduction of protons, coupled to energy-conserving electron transfer reactions, which allow energy to be obtained from either hydrogen or from the oxidation of substrates with lower potential.²³

The [NiFe]-hydrogenase is similar to the iron-only hydrogenase with respect to the bimetallic active site. However, this hydrogenase is thought of as an 'uptake' hydrogenase; it will use hydrogen rather than produce it and the electrons are used to reduce NAD(P).²⁴

A lot of research has focussed on 'biomimetic' catalysts for hydrogen production, trying to mimic the active site of the hydrogenase with varying rates of success.²⁵⁻²⁸ The hydrogenase activity site mimics haven't produced catalysts with true enzyme-like activity and it is for this reason that we have decided against this route for our research.

1.3.2 Molecular catalysts

Similarly to the 'biomimetic' hydrogen catalysts, 'bio-inspired' catalysts have also been at the forefront of research recently. There have been many catalysts synthesised, using Nickel as the metal centre. They incorporate the Ni similarly to that in the active site of the [NiFe]-hydrogenase but deviate with the use of phosphine or nitrogen-containing ligands.²⁹

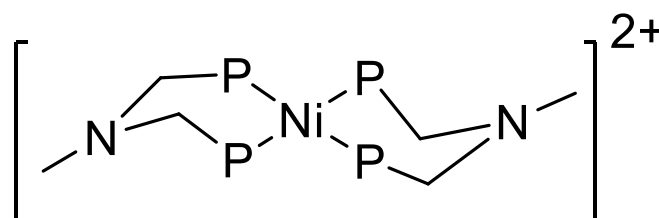


Figure 1.3.2.1 – A DuBois bioinspired hydrogen catalyst, $[\text{Ni}(\text{PNP})_2]^{2+}$ (PNP is bis(diethylphosphinomethyl)methylamine). Redrawn from reference 29.

1.3.3 Transition metal catalysts

Most of the hydrogen production/oxidation catalysts are transition metal-containing,³⁰⁻³⁴ as mentioned above. Transition metal catalysts have been very useful in the hydrogenation of alkenes.³⁵ One such catalyst for this is Wilkinson's catalyst which contains a rhodium metal centre.³⁶ This, like many other transition metal catalysts, splits hydrogen by oxidative addition (homolytic cleavage), as shown in Figure 1.3.3.1.

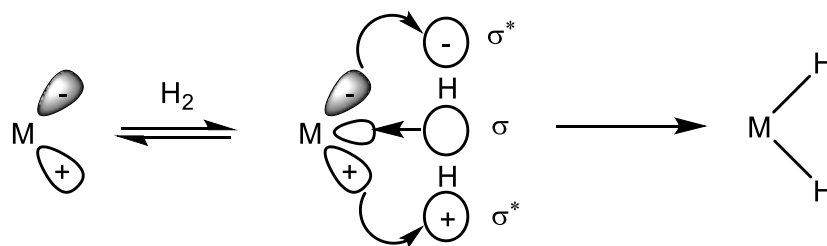


Figure 1.3.3.1 – Homolytic cleavage of H_2 by a transition metal centre

Homolytic cleavage of hydrogen occurs due to the back-donation from a filled d-orbital on the metal centre, to the anti-bonding σ^* orbital of hydrogen (Figure 1.3.3.1).³⁷

Platinum is another transition metal which has been extensively researched for its properties as a catalyst in water splitting to produce hydrogen and its use in hydrogen fuel cells. This will be further discussed in Section 1.4.

There is a huge problem with using transition metals, such as platinum. Platinum is a rare metal (37 ppb in the Earth's crust) and is expensive (over 50 US\$ g^{-1} , with an all-time high of 80US\$ g^{-1} in 2008).³⁸ It is therefore vital that an inexpensive, abundant, preferably non-metal catalyst be found.

1.3.4 Metal-free catalysts

A metal-free electrocatalyst for both hydrogen evolution and hydrogen oxidation has been reported by Haddad *et al.*³⁹ The zinc complex (Figure 1.3.4.1 – Top) has exhibited one of the highest turnover frequencies (TOF) of any hydrogen oxidation electrocatalysts. However, the free ligand (Figure 1.3.4.1 – Bottom) has electrocatalytic activity comparable to that of the zinc complex. It could, therefore, be argued that the zinc is unnecessary and could therefore be classed as a metal-free electrocatalyst for both hydrogen evolution and oxidation.

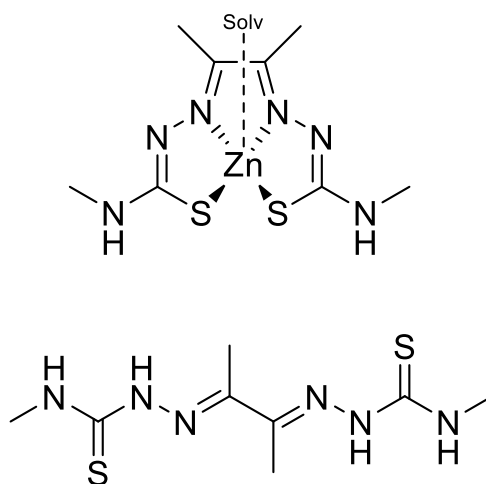


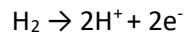
Figure 1.3.4.1 – The zinc diacetyl-bis(*N*-4-methyl-3-thiosemicarbazide) complex (top) and the free ligand diacetyl-bis(*N*-4-methyl-3-thiosemicarbazone) (bottom) reported by Haddad *et al.* for both the hydrogen evolution and hydrogen oxidation reactions

A hydrogen evolution electrocatalyst has been developed by Zheng *et al.*, coupling graphitic-carbon nitride and N-doped graphene. This hybrid catalyst reduces water to molecular hydrogen with comparable activity to some well-developed metallic catalysts.⁴⁰

In recent years many metal-free (or noble-metal-free) electrocatalysts have been reported for hydrogen evolution,^{40,41} oxygen reduction^{42–46} and oxygen evolution,⁴⁷ nitrogen fixation^{48–49} and even carbon dioxide reduction,^{50–51} but reports of efficient hydrogen oxidation electrocatalysts seem to be lacking. This could be due to the high efficiency of noble-metals to do such a job in fuel cells (Section 1.4).

1.4 Hydrogen fuel cells

Hydrogen fuel cells are electrochemical cells which convert chemical energy into electricity using hydrogen (Equation 1.4.1).



Equation 1.4.1 – Half equation for the oxidation of hydrogen, producing 2 protons and 2 electrons

In the fuel cell, hydrogen oxidation occurs at the anode and the electrons are passed through a circuit. At the cathode oxygen is reduced, which is then combined with the protons, forming water (Figure 1.4.1). Hydrogen in fuel cells has high efficiency due to its small ionic size and fast diffusion properties,⁵² which are required for the selective transport of protons across the electrolyte membrane⁵³ in order to form water with the reduced oxygen.

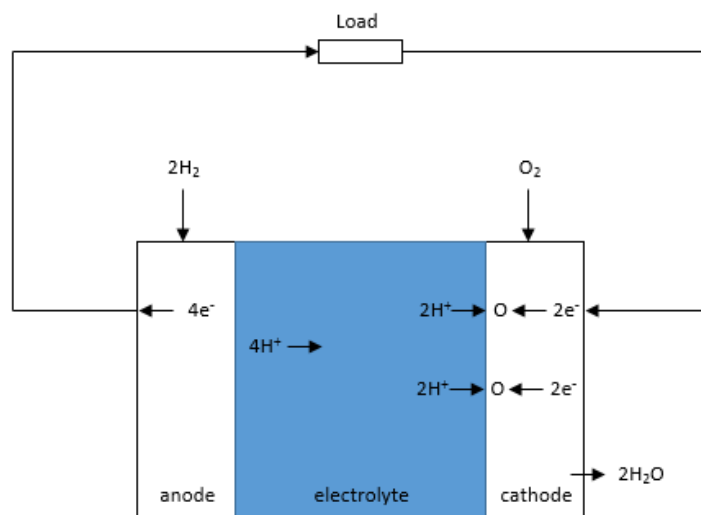


Figure 1.4.1 – Principle of hydrogen fuel cell operation (adapted from reference 7)

The first example of a fuel cell was engineered by Grove in 1839. Tubes of hydrogen and oxygen were inverted over platinum electrodes, alternating the tubes of gas (Figure 1.4.1) and was then submerged in aqueous sulphuric acid. After 26 of these were connect in series, the current generated was enough to drive the electrolysis of water.⁵⁴

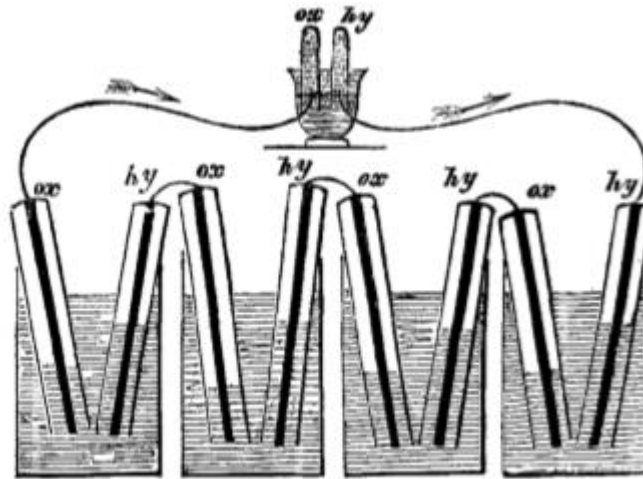


Figure 1.4.2 – The gaseous voltaic battery engineered by Grove – the first hydrogen fuel cell (reproduced from reference 54).

Figure 1.4.3 shows the equations for the electrolysis of water. Hydrogen fuel cells are opposite to the electrolysis of water, using hydrogen to produce water rather than splitting water to produce hydrogen. Therefore, two hydrogen molecules are required for every one molecule of oxygen, to form two water molecules. In a fuel cell, 4 electrons are passed through the circuit, producing electricity.

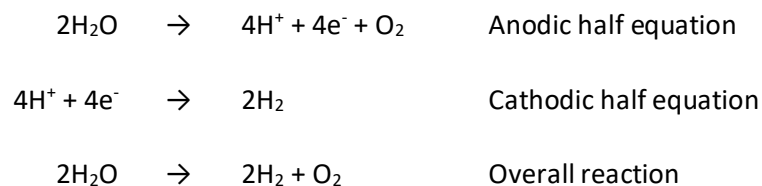


Figure 1.4.3 – The equations for the electrolysis of water⁷

Alkaline fuel cells (AFCs) use potassium hydroxide as the electrolyte. AFCs are poisoned by carbon dioxide, which is present in steam reforming of natural gas to about 20%⁵⁵ (Equation 1.2.1). As previously mentioned, steam reforming is the most common process for hydrogen production.¹⁵ Separation of hydrogen from natural gas creates about the same amount of greenhouse gases as using petrol⁵⁶ and is therefore environmentally unsustainable. Another issue with fuel cells is the use of platinum as the electrodes. Not only is platinum costly and in limited supply⁵⁷ but it is poisoned by carbon monoxide, which can be present in the atmosphere.⁵⁸⁻⁵⁹ These factors put limits on the applications of fuel cells⁵⁵ and make them commercially impractical.²⁹

Fuel cell use does have some advantages though. In contrast to internal combustion engines, which emit greenhouse gases⁶⁰ such as carbon dioxide and nitrogen oxides, the only product from fuel cells is water and some heat.⁷ This means fuel cells have zero emissions of air pollutants.⁶⁰ Fuel cells do not degrade or discharge over time,⁶¹ unlike batteries, and as long as there is a fuel source the fuel cell will work.⁶²

There are many practical issues with the use of hydrogen fuel cells in transportation. Although hydrogen has a high specific energy (based on mass), 9.5 kg would be required to give the same energy content as 25 kg of petrol;⁶³ this equates to 114,000 L (at standard RTP: 25 °C and 1 atm). Storing this volume of gas in cylinders (at 200 bar of pressure) would still require a volume 5 times greater than the corresponding volume of petrol.⁵⁵ Storage of this volume of hydrogen is not feasible for use of hydrogen fuel cell vehicles. However, there are hydrogen vehicles available commercially in several countries.⁶⁴ Better hydrogen storage devices are still being developed.

1.5 Hydrogen storage

Hydrogen is a gas so, for viable use, the problems with volumetric energy density need to be overcome. Molecular systems for hydrogen storage are advantageous over cylinders of hydrogen gas.⁶⁵ Reversible metal hydrides are a viable option for a molecular system⁵⁵ e.g. $\text{LaNi}_5\text{H}_{6.5}$. This example is already sold in metal-hydride batteries, but is not feasible for use in vehicles as it is less than 2% hydrogen (by mass) and 4–5 % (by mass) is required.¹ Also, the use of transition metals for hydrogen activation is less desirable than carbon-based storage systems due to the higher molecular weight; a lower weight is more practical for transportation.⁶⁵ Hydrogen stored as a cryogenic liquid is another possibility; requiring roughly the same volume of liquid hydrogen to give the same range as petrol.⁵⁵ However, this is impractical for transportation as it requires a heavy cryogenic tank. Hydrogen bound in another substance (hydrogen carrier) is another option. The substance would need to reversibly release hydrogen.⁶⁶ Mg-Li amides have been reported to demonstrate reversible hydrogen storage capacity of 5 wt%.⁶⁷ Research into compounds which reversibly release hydrogen is ongoing, with significant focus on frustrated Lewis pairs⁷² which could be considered a viable hydrogen storage device.

1.6 Frustrated Lewis pairs (FLPs)

1.6.1 Lewis adducts and the history of FLPs

Lewis acids and Lewis bases have long been known to form a classical Lewis adduct (Figure 1.6.1.1), with a Lewis acid being an electron pair acceptor and a Lewis base being an electron pair donor and hence forming a dative bond. However, sterically hindered Lewis acid/base pairs do not form an adduct and this is due to steric hindrance. As far back as 1942, Brown and co-workers reported the non-formation of an adduct, between 2,6-lutidine and trimethylborane.⁶⁸ This was attributed to sterics, with the nitrogen shielded by the *ortho*-methyl groups in addition to interactions with the methyl groups of the borane (Figure 1.6.1.2).



Figure 1.6.1.1 – Example of the formation of a classical Lewis adduct, from the reaction between tetrahydrofuran (Lewis base) and BH_3 (Lewis acid)

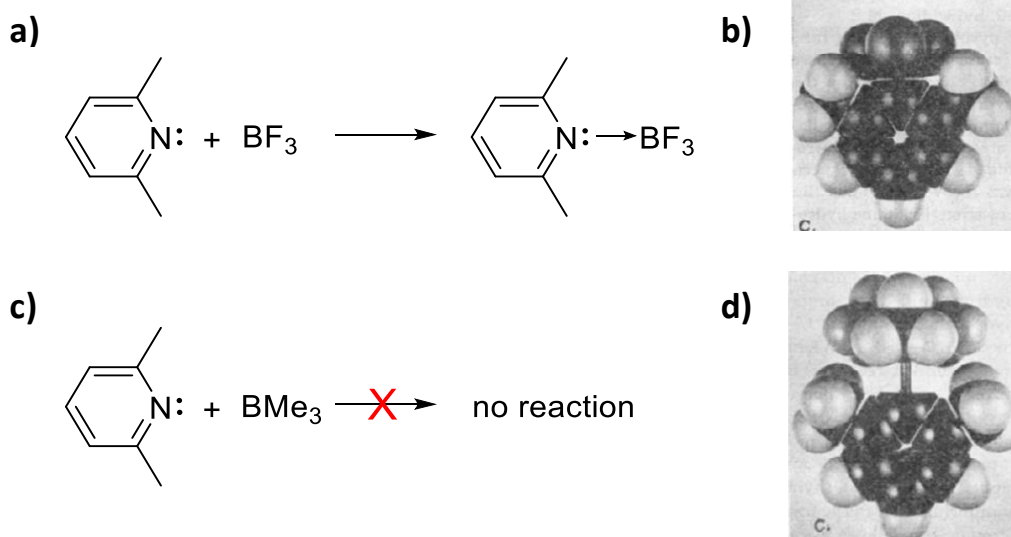


Figure 1.6.1.2 – The formation of a classical Lewis adduct (a), Brown's molecular model of the Lewis adduct (b), no Lewis adduct formation (c), and Brown's molecular model for no adduct formation (d). Photos taken from reference 68.

Figure 1.6.1.3 shows the history of FLP chemistry, from Brown's discovery in 1942, to 2007 when Stephan and Erker reported olefin hydrogenation catalysed by an FLP.^{69–70} In 1996,

Piers and co-workers reported the hydrosilylation of ketones using BARF_{15} , where it was reported that BARF_{15} activated the Si–H bond. This has since been recognised as the first example of FLP chemistry as we know it today.⁷¹

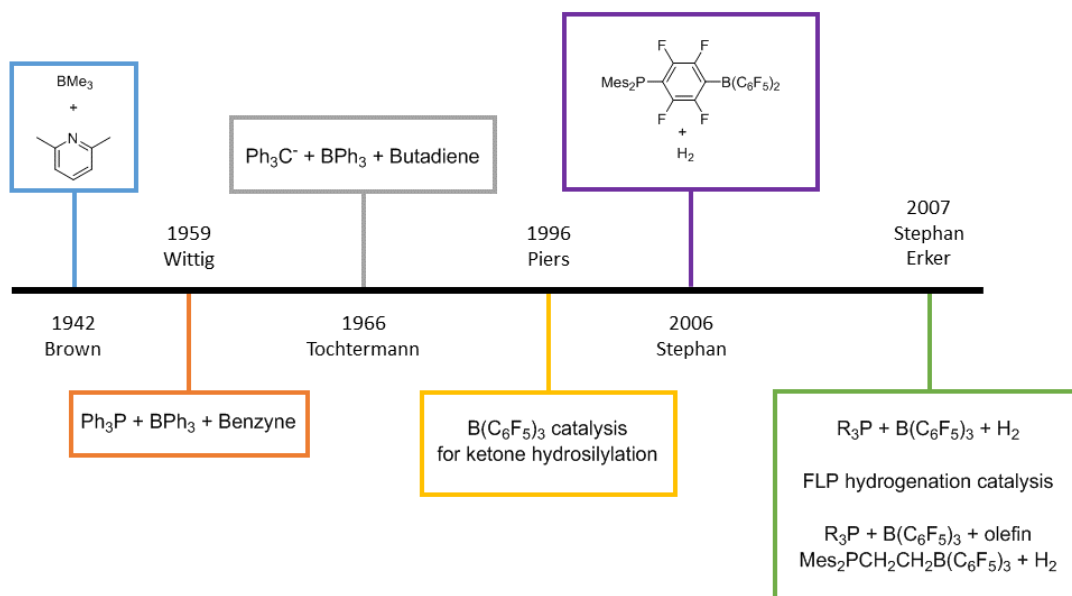


Figure 1.6.1.3 - The history of Frustrated Lewis pair chemistry, from 1942 to 2007⁷¹

It was a decade later that Stephan and co-workers reported the first FLP system to heterolytically cleave hydrogen.⁷²

1.6.2 Phosphorus-Boron FLPs

A decade after Piers and co-workers reported the use of BARF_{15} as a catalyst in the hydrosilylation of ketones, Stephan and co-workers reported the first FLP system to heterolytically cleave hydrogen⁷³ (Figure 1.6.2.1). The system was intramolecular, and exploited the Lewis acidic properties of the boron and Lewis basic properties of the phosphorus.

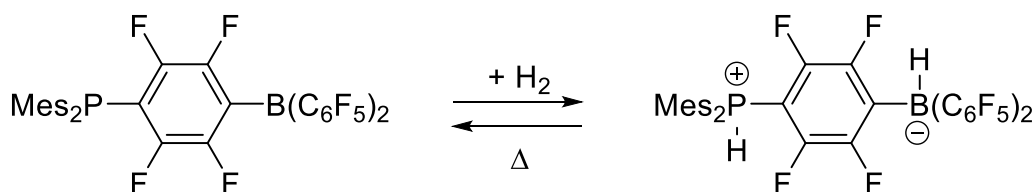


Figure 1.6.2.1 - The first example of heterolytic hydrogen cleavage using an intramolecular FLP⁷³

Since this first example of an intramolecular FLP system there have been strides made to expand FLP chemistry, with the use of other intramolecular systems⁷⁴ (Figure 1.6.2.2).

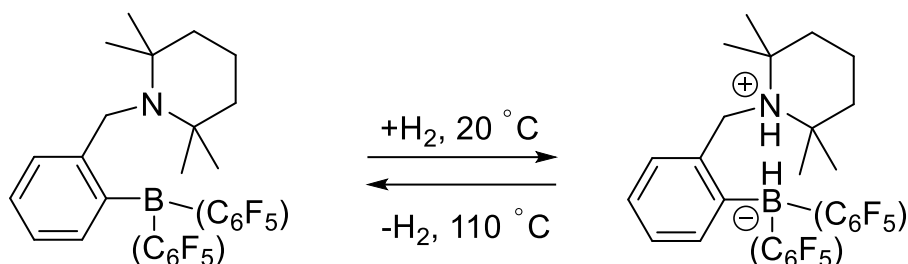


Figure 1.6.2.2 – An intramolecular FLP system containing boron (Lewis acid) and nitrogen (Lewis base) functionalities for the heterolytic, reversible cleavage of hydrogen⁷⁴

Hydrogen cleavage has long been dominated by the use of precious metals for this reaction, with oxidative addition of hydrogen across the metal centre. However, research has moved on, into an area which uses a more sustainable methodology moving away from precious metals. However, research into the use of metals in FLP-like systems is still ongoing and will be discussed further in Section 1.6.5. There has been substantial work, not only with intramolecular systems but, probing intermolecular FLP systems using boranes and phosphines,⁷⁵ since Stephan *et al.* reported the intramolecular use of these two functionalities. The archetypal intermolecular FLP system has combined the Lewis acid, BArF₁₅ and a sterically encumbered phosphine such as P(^tBu)₃ which, on the addition of hydrogen, forms the borohydride and phosphonium cation. However, many other phosphines have since been reported, in conjunction with BArF₁₅ in FLP systems.^{70,76}

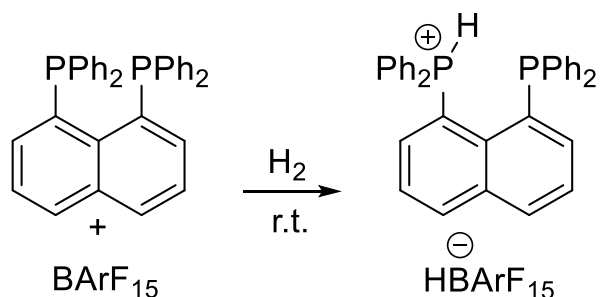


Figure 1.6.2.3 - Hydrogen activation using 1,8-bis(diphenylphosphino)naphthalene and BArF₁₅ as an FLP⁷⁰

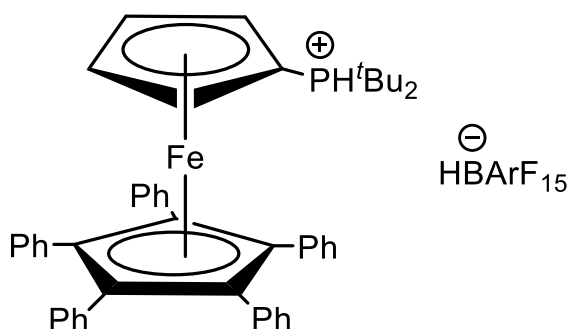


Figure 1.6.2.4 - The product of hydrogen activation using a mono-phosphinoferrrocene and BArF_{15} to form a ferrocenylphosphonium borate⁷⁶

Figure 1.6.2.3 and 1.6.2.4 show examples of the type of intermolecular FLP system for reversible hydrogen activation, which uses the Lewis acid, BArF_{15} . A lot of research has probed the use of other boranes such as BPh_3 , but it was found that there was no reaction with a variety of bulky amines.⁷⁴ This supports a view that hydrogen cleavage occurs under favourable steric and electronic conditions. Not only must the sterics preclude the formation of an amine-borane adduct, but the Lewis acidity and basicity must match in strength for heterolytic hydrogen cleavage to occur.⁷⁷ There has also been a plethora of research into different Lewis bases, moving away from the use of bulky phosphines.

1.6.3 Beyond phosphines as Lewis bases

Since the pioneering work by Stephan *et al.*, research has expanded from the archetypal phosphine Lewis base moiety, to include nitrogen-based Lewis bases such as N-heterocyclic carbenes⁷⁸⁻⁸⁰ (Figure 1.6.3.1) and bulky pyridines⁸¹⁻⁸² (Figure 1.6.3.2).

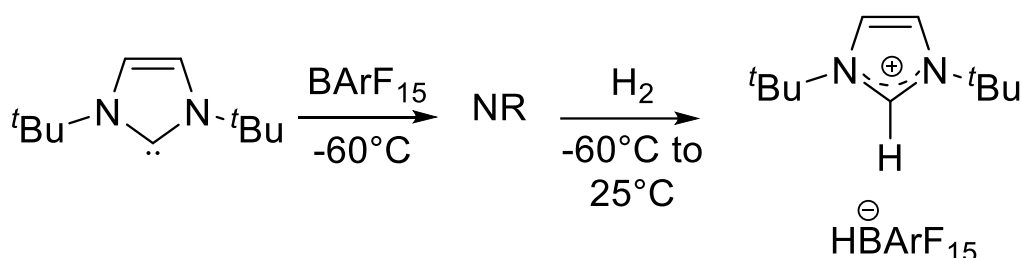


Figure 1.6.3.1 - The reaction of 1,3-di-*tert*-butyl-1,3-imidazol-2-ylidene with BArF_{15} for heterolytic hydrogen cleavage. NR = no reaction⁷⁸

The cleavage of hydrogen by the carbene is irreversible (Figure 1.6.3.1), even upon heating to 150 °C for 4 days. This suggests that the carbene displays greater basicity compared to

phosphines previously used in FLP systems.⁷⁸ Carbenes have been reported to exhibit transition-metal-like reactivity and cleave hydrogen in a formal oxidative addition fashion⁸³ with an sp^2 -type lone pair and empty p orbital, displaying the same donation/back donation process as seen for transition metals (Figure 1.3.3.1).⁸⁴

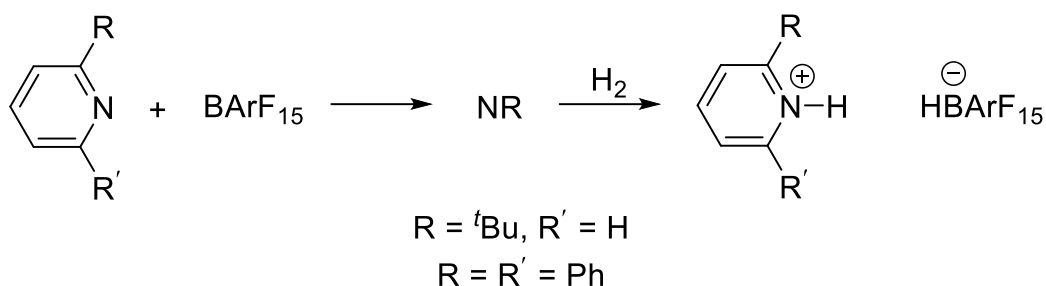


Figure 1.6.3.2 - Heterolytic cleavage of hydrogen using bulky pyridines and BArF_{15} as an FLP. NR = no reaction⁸¹

Both the N-heterocyclic carbenes (NHCs) and the bulky substituted-pyridines show no reaction when in solution with BArF_{15} but on addition of hydrogen, heterolytic cleavage is noted. In contrast, when 2,6-lutidine and BArF_{15} are in solution together, there is an equilibrium between free molecules and adduct formation. However, on the addition of hydrogen this system still acts as an FLP and hydrogen is cleaved heterolytically (Figure 1.6.3.3).⁸²

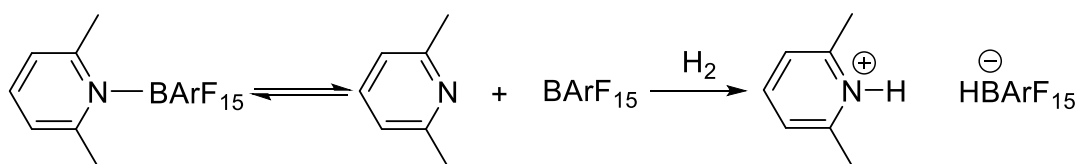


Figure 1.6.3.3 – Heterolytic cleavage of hydrogen using 2,6-lutidine and BArF_{15} as an FLP⁸²

1.6.4 Expanding Lewis acid research

A great majority of the literature has focussed on the Lewis acid, BArF_{15} , but there has since been other Lewis acids used which include other halogenated triarylboranes^{85–88} (Figure 1.6.4.1), borenium cations^{89–90} (Figure 1.6.4.2) and triaryl aluminium species^{91–92} (Figure 1.6.4.3).

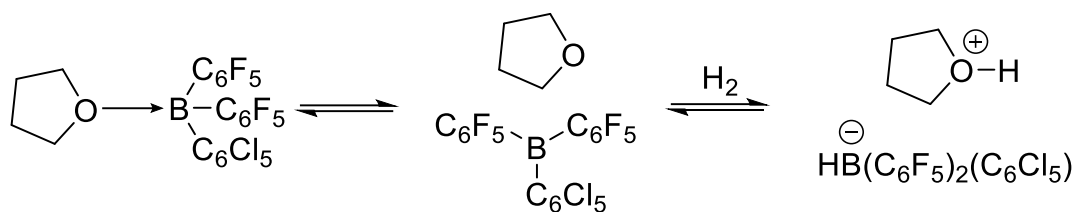


Figure 1.6.4.1 - Reversible hydrogen activation using $B(C_6F_5)_2(C_6Cl_5)$ in THF⁸⁷

Figure 1.6.4.1 shows that the substitution of a pentafluorophenyl ring for a pentachlorophenyl ring still activates hydrogen in an FLP-type mechanism, and the solvent (THF) is used as the Lewis base.

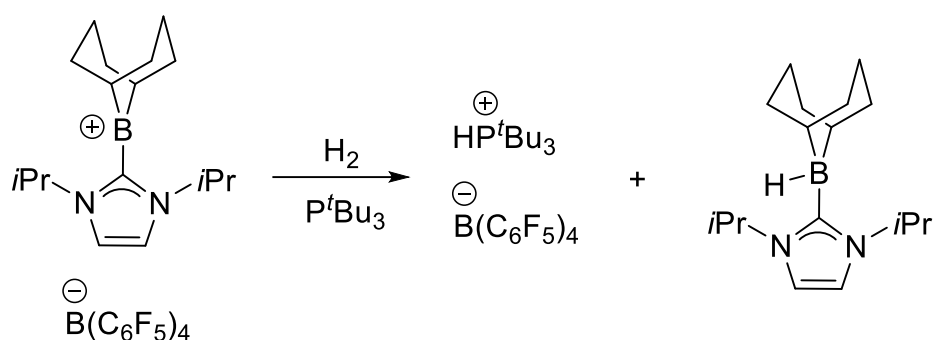


Figure 1.6.4.2 - Hydrogen activation using a borenium salt⁸⁹

Figure 1.6.4.2 shows the activation of hydrogen using a borenium cation with the addition of a Lewis base (tri-*tert*-butylphosphine) and is also effective with a bulkier phosphine such as trimesitylphosphine.⁸⁹

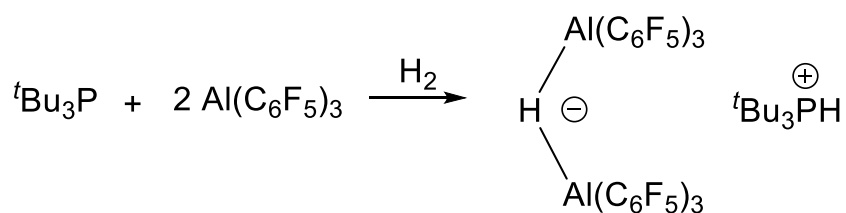


Figure 1.6.4.3 - Hydrogen activation using a triaryl aluminium species and a phosphine as an FLP⁹¹

Figure 1.6.4.3 shows the activation of hydrogen using an FLP system of a bulky phosphine and a triaryl aluminium species. The aluminium species in this example is similar to $BARF_{15}$, but it can be noted that a bridging hydride is formed when hydrogen is added to this system

whereas when hydrogen is added to an FLP system containing BARF₁₅ a terminal hydride species is formed.

1.6.5 Metal FLP-like systems

As previously mentioned, metals such as platinum are still the most commonly used for hydrogen splitting. A significant amount of research has been reported for hydrogen splitting using other platinum group metals such as rhodium,^{93–96} ruthenium^{97–99} and iridium¹⁰⁰ for this reaction, other expensive transition metals such as titanium,^{101–102} zirconium¹⁰³ and even gold.¹⁰⁴ Hydrogen splitting has also been seen using cheaper and more abundant transition metals such as nickel¹⁰⁵ and iron,¹⁰⁶ and even group 13 elements.¹⁰⁷

Although there are a significant number of metals seen to cleave hydrogen, the argument can be made that there still needs to be a more sustainable route for this process. This could be with the use of carbon-based systems.

1.6.6 Carbon-based Lewis acids

In 2010, Ines and co-workers reported a carbon-based Lewis acid moiety (Figure 1.6.6.1) with a lower Lewis acidity than polyfluorinated boranes, but in the order of that of triphenoxyborane (B(OPh)₃).¹⁰⁸

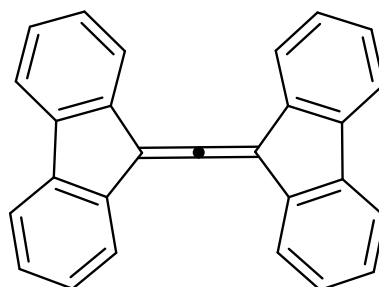


Figure 1.6.6.1 – Structure of the Lewis acidic allene reported by Ines *et al.*¹⁰⁸

The allene in Figure 1.5.6.1 is a completely carbon Lewis acid and has been used in an FLP system with a carbon-based Lewis base (1,3-bis-(2',6'-diisopropylphenyl)imidazole-2-

ylidene); a carbene. Although this system does not cleave hydrogen, it does activate the weaker, non-polar, covalent disulfide bond.¹⁰⁸

In 2016, the first metal-free hydrogen oxidation catalytic system was reported, using *N*-methylacridinium, a carbon-based Lewis acid, coupled to a frustrated Lewis pair (FLP) of BArF₁₈ (Tris[3,5-bis(trifluoromethyl)phenyl]borane) and 2,6-lutidine (Figure 1.6.6.2).¹⁰⁹

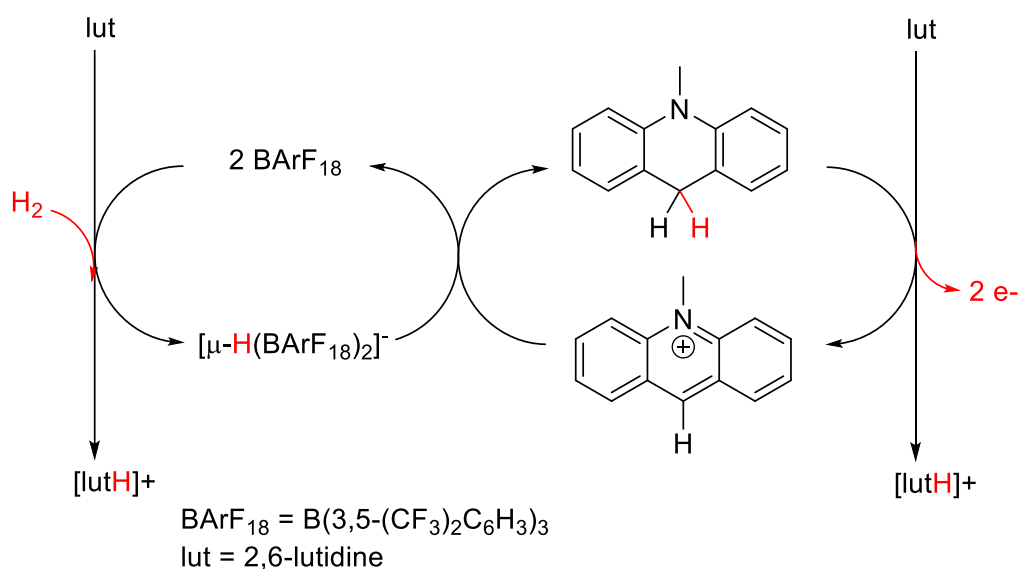


Figure 1.6.6.2 – Electrocatalytic cycle for the oxidation of hydrogen using BArF₁₈ and 2,6-lutidine as the FLP system and the *N*-methylacridinium cation as a hydride shuttle

In the above system hydrogen is split by the FLP (BArF₁₈ and 2,6-lutidine) and the bridging hydride is then transferred to the *N*-methylacridinium cation to form *N*-methylacridane. At the electrode the hydride is converted to a proton and 2 electrons.¹⁰⁹

Work by Ingleson and co-workers reported a set of compounds (*N*-methylbenzothiazolium salts) that demonstrated comparable Lewis acidity towards hydride for that of the well-established triarylboranes.¹¹⁰ The hydride ion affinity (HIA) of *N*-methyl-2-phenylbenzothiazolium cation was computationally determined to be comparable to that of BArF₁₅ (-45kcal/mol and -41kcal/mol respectively).¹¹⁰ At -41kcal/mol, the HIA of *N*-methyl-2-phenylbenzothiazolium cation was less than that of *N*-methylacridinium cation and therefore would be more reducing than *N*-methylacridane.¹¹⁰ With the acridinium/acridane couple reported as an electrocatalyst for hydrogen oxidation, it was highlighted that the *N*-methyl-2-arylbenzothiazoline/*N*-methyl-2-arylbenzothiazolium cation couple could also be of use in electrocatalytic hydrogen oxidation. It was thought that introducing different substituents on the aryl ring could fine tune the hydricity of the C2 position of these

compounds. This was the beginning of continued research into metal-free electrocatalysts for hydrogen oxidation and why this thesis focuses on this subset of carbon-based Lewis acids (*N*-methylbenzothiazoliums) for their application in this field.

The aims of the project were:

- To synthesise a variety of *N*-methyl-2-arylbenzothiazolines/*N*-methyl-2-arylbenzothiazolium salts with electron-donating substituents and electron-withdrawing substituents, to see the effects of these substituents of the oxidising/reducing capability and to fine-tune the hydricity of the C2 position
- To electrochemically analyse the different compounds to see the effects of the different electron-donating and electron-withdrawing substituents
- To oxidise hydrogen using a variety of synthesised *N*-methyl-2-arylbenzothiazolium salts, in conjunction with a viable FLP system

2. Experimental

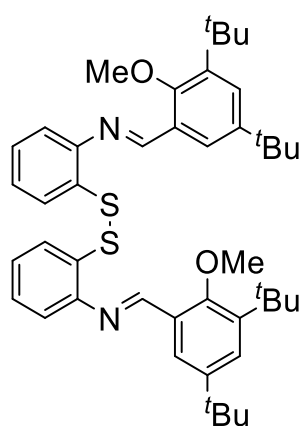
All commercial compounds were used as provided. All ^1H NMR, ^{19}F NMR, ^{11}B NMR and ^{13}C NMR spectra were recorded on 400 MHz or 500 MHz Bruker Ascend NMR machines. Chemical shift values are expressed in δ units relative to tetramethylsilane (TMS) signal as an internal reference in CD_2Cl_2 , CDCl_3 , CD_3CN or d_6 -DMSO. All solvents were purchased from commercial sources and used without further purification. Wherever necessary the solvents were dried by standard literature procedures.¹¹¹ Silica gel (60 Å pore size, 40–63 μm technical grade) was used for chromatography. All TLC plates were visualised using KMnO_4 as a stain. Mass spectrometry was run by University of Sussex using low resolution electron-ionisation or low resolution electrospray ionisation techniques. Elemental analysis was obtained from London Metropolitan University.

2.1 Synthesis of disulfide-linked, aryl-substituted imines

General procedure A

2-Aminothiophenol (1 eq.) and substituted benzaldehyde (1 eq.) were dissolved in ethanol. Air was bubbled through the reaction for 48 hours to afford a solid. The solid was recovered by filtration and washed with ethanol.

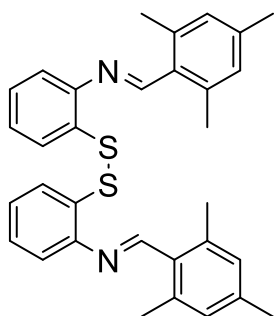
2,2'-Dithiobis{*N*-[(3,5-di-*tert*-butyl-2-methoxyphenyl)methylene]benzenamine}, DSI1



3,5-Di-*tert*-butyl-2-methoxybenzaldehyde (1.10 g, 4.4 mmol) and 2-aminothiophenol (0.46 mL, 4.4 mmol) were dissolved in ethanol (30 mL) and air was bubbled through the reaction. After 2 h a white precipitate had formed which was recovered by filtration and washed with ethanol. This yielded a white solid (0.92 g, 59%). m.p. 155–156 °C. Found: C, 74.35; H, 8.20; N, 4.05. $\text{C}_{44}\text{H}_{56}\text{N}_2\text{O}_2\text{S}_2$ requires C, 74.53; H, 7.96; N, 3.95%. ^1H NMR (500 MHz, CD_2Cl_2) 7.82 (2H, d, $J = 2.5$ Hz, $\text{N}=\text{CH}$), 7.34 (2H, d, $J = 2.5$ Hz, Ar-H), 7.04 (2H, dd, $J = 7.5, 1.3$ Hz, Ar-H), 6.94 (2H, td, $J = 7.7, 1.3$ Hz, Ar-H), 6.78 (2H, d, $J = 3.5$ Hz, Ar-H), 6.74 (2H, td, $J = 7.5, 1.3$ Hz, Ar-H), 6.67 (2H, dd, $J = 7.7, 0.8$ Hz, Ar-H), 3.80 (6H, s, O- CH_3), 1.39 (18H, s, $^t\text{Bu-H}$), 1.26 (18H, s, $^t\text{Bu-H}$). ^{13}C NMR (125

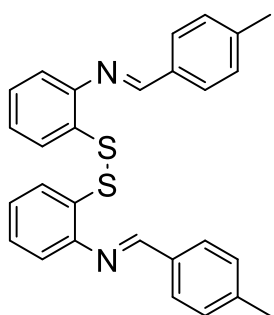
MHz, CD₂Cl₂) 147.3, 142.4, 134.7, 127.3, 125.5, 123.9, 121.1, 110.3, 63.8, 58.8, 35.8, 31.7, 31.4, 18.8. *m/z*: [M]⁺ Calcd for C₄₄H₅₆O₂N₂S₂, 709, found 709. [M/2]⁺ Calcd 355, found 355.

2,2'-Dithiobis[*N*-[(mesityl)methylene]benzenamine], DS12



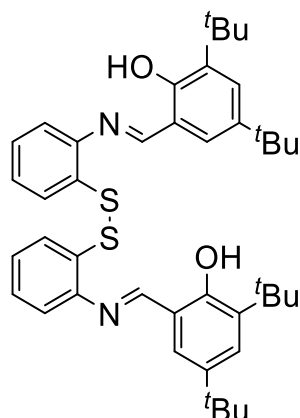
Following general procedure A, 2-aminothiophenol (0.5 mL, 5.0 mmol) and mesitaldehyde (0.7 mL, 5 mmol) dissolved in ethanol (30 mL). This yielded a white solid (0.22 g, 17%). m.p. 203–206 °C. ¹H NMR (500 MHz, CD₂Cl₂) 8.92 (2H, s, N=CH), 7.64 (2H, dd, *J* = 7.9, 1.3 Hz, Ar-*H*), 7.23 (2H, td, *J* = 7.2, 1.3 Hz, Ar-*H*), 7.15 (2H, td, *J* = 7.6, 1.4 Hz, Ar-*H*), 7.06 (2H, dd, *J* = 7.9, 1.3 Hz, Ar-*H*), 6.97 (4H, s, Ar-*H*), 2.65 (12H, s, *o*-CH₃), 2.33 (6H, s, *p*-CH₃). ¹³C NMR (125 MHz, CD₂Cl₂) 161.3, 150.7, 141.3, 140.2, 132.2, 130.6, 130.3, 127.6, 127.0, 126.1, 117.8, 22.1, 21.6. *m/z*: [M]⁺ Calcd for C₃₂H₃₂N₂S₂, 509, found 509. [M/2]⁺ Calcd 254, found 254.

2,2'-Dithiobis[*N*-[(4-tolyl)methylene]benzenamine], DS13



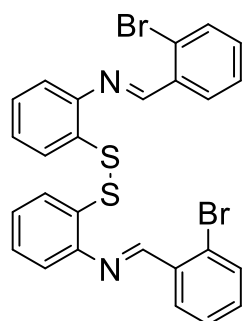
2-Aminothiophenol (1.0 mL, 10 mmol) and *p*-tolualdehyde (1.2 mL, 10 mmol) were dissolved in ethanol (20 mL) and air was bubbled through reaction. After 5 h the pale yellow precipitate formed was recovered by filtration and washed with ethanol. This yielded a pale yellow solid (0.23 g, 10%). m.p. 172–176 °C. ¹H NMR (500 MHz, CD₂Cl₂) 8.48 (2H, s, N=CH), 7.86–7.90 (4H, m, Ar-*H*), 7.64 (2H, dd, *J* = 7.9, 1.3 Hz, Ar-*H*), 7.33 (4H, d, *J* = 8.2 Hz, Ar-*H*), 7.22 (2H, td, *J* = 7.5, 1.9 Hz, Ar-*H*), 7.15 (2H, td, *J* = 7.9, 1.3 Hz, Ar-*H*), 7.08 (2H, dd, *J* = 7.7, 1.4 Hz, Ar-*H*), 2.44 (6H, s, *p*-CH₃). ¹³C NMR (125 MHz, CD₂Cl₂) 160.6, 149.7, 143.1, 134.1, 132.5, 130.1, 129.6, 127.6, 127.2, 126.3, 117.8, 22.0. *m/z*: [M]⁺ Calcd for C₂₈H₂₄N₂S₂, 452, found 452. *m/z*: [M/2]⁺ Calcd 226, found 226.

2,2'-Dithiobis{N-[(3, 5-di-*tert*-butyl-2-hydroxyphenyl)methylene]benzenamine}, DS14



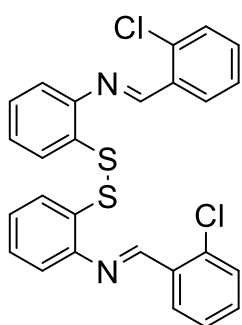
3,5-Di-*tert*-butyl-2-hydroxybenzaldehyde (2.34 g, 10 mmol) and 2-aminothiophenol (1 mL, 10 mmol) were dissolved in ethanol (20 mL) and air was bubbled through the reaction for 16 h. The pale peach precipitate formed was recovered by filtration and washed with ethanol. This yielded an off-white solid (1.04 g, 30%). m.p. 204–205 °C. Found: C, 74.29; H, 7.62; N, 4.68. $C_{42}H_{52}O_2N_2S_2$ requires C, 74.08; H, 7.70; N, 4.11%. 1H NMR (500 MHz, CD_2Cl_2) 13.23 (2H, s, O-H), 8.70 (2H, s, N=CH), 7.67–7.69 (2H, m, Ar-H), 7.51 (2H, d, $J = 2.5$ Hz, Ar-H), 7.26–7.30 (4H, m, Ar-H), 7.20–7.23 (4H, m, Ar-H), 1.49 (18H, s, *t*Bu-H), 1.35 (18H, s, *t*Bu-H). ^{13}C NMR (125 MHz, CD_2Cl_2) 164.8, 158.8, 147.1, 141.5, 137.6, 132.0, 129.3, 128.2, 128.0, 127.9, 127.4, 118.9, 118.3, 35.6, 34.7, 31.7, 29.7. m/z : $[M]^+$ Calcd for $C_{42}H_{52}O_2N_2S_2$, 681, found 681. $[M/2]^+$ Calcd 340, found 340.

2,2'-Dithiobis{N-[(2-bromophenyl)methylene]benzenamine}, DS15



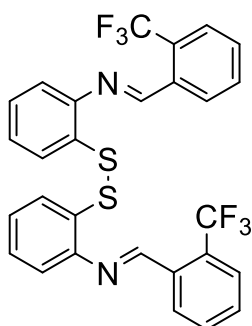
2-Bromobenzaldehyde (1.1 mL, 9.6 mmol) and 2-aminothiophenol (9.6 mmol, 1 mL) were dissolved in ethanol (20 mL) and air was bubbled through the reaction for 16 h. The pale yellow precipitate formed was recovered by filtration and washed with ethanol. This yielded a pale yellow solid (0.83 g, 30%). m.p. 151–154 °C. Found: C, 53.67; H, 2.94; N, 5.06. $C_{26}H_{18}Br_2N_2S_2$ requires C, 53.62; H, 3.12; N, 4.81%. 1H NMR (500 MHz, CD_2Cl_2) 8.91 (2H, s, N=CH), 8.35 (2H, dd, $J = 7.7, 1.7$ Hz, Ar-H), 7.65–7.69 (4H, m, Ar-H), 7.45–7.49 (2H, m, Ar-H), 7.36–7.41 (2H, m, Ar-H), 7.25 (2H, td, $J = 7.5, 1.6$ Hz, Ar-H), 7.20 (2H, td, $J = 7.5, 1.6$ Hz, Ar-H), 7.14 (2H, dd, $J = 7.5, 1.6$ Hz, Ar-H). ^{13}C NMR (125 MHz, CD_2Cl_2) 159.5, 149.2, 135.0, 133.9, 133.4, 132.8, 130.0, 128.5, 127.9, 127.8, 126.6, 118.1. m/z : $[M]^+$ Calcd for $C_{26}H_{18}Br_2N_2S_2$, 582, found 582. $[M/2]^+$ Calcd 291, found 291.

2,2'-Dithiobis{*N*-[(2-chlorophenyl)methylene]benzenamine}, DS16



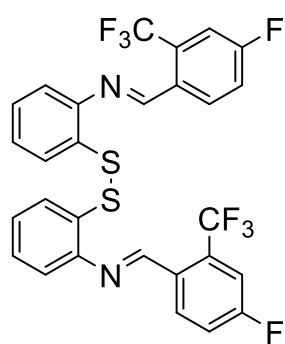
Following general procedure A, 2-chlorobenzaldehyde (1.1 mL, 9.6 mmol) and 2-aminothiophenol (1 mL, 9.6 mmol) were dissolved in ethanol (20 mL). This yielded a pale yellow solid (0.18 g, 8%). m.p. 174–178 °C. Found: C, 63.18; H, 3.59; N, 6.02. $C_{26}H_{18}Cl_2N_2S_2$ requires C, 63.28; H, 3.68; N, 5.68%. 1H NMR (500 MHz, CD_2Cl_2) 8.98 (2H, s, N=CH), 8.35–8.38 (2H, m, Ar-H), 7.66 (2H, dd, $J = 8.0, 1.4$ Hz, Ar-H), 7.46–7.48 (4H, m, Ar-H), 7.40–7.45 (4H, m, Ar-H), 7.25 (2H, td, $J = 7.5, 1.3$ Hz, Ar-H), 7.20 (2H, td, $J = 7.9, 1.6$ Hz, Ar-H), 7.14 (2H, dd, $J = 7.7, 1.4$ Hz, Ar-H). ^{13}C NMR (125 MHz, CD_2Cl_2) 157.2, 149.4, 136.7, 133.6, 133.2, 132.8, 130.6, 129.5, 127.9, 127.8, 126.5, 118.1. m/z : $[M]^+$ Calcd for $C_{26}H_{18}Cl_2N_2S_2$, 493, found 493. $[M/2]^+$ Calcd 246, found 246.

2,2'-Dithiobis{*N*-[(2-(trifluoromethyl)phenyl)methylene]benzenamine}, DS17



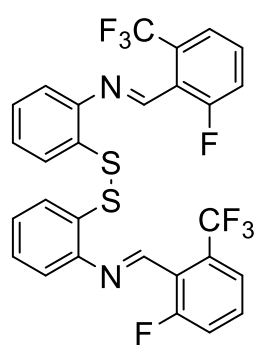
Following general procedure A, 2-(trifluoromethyl)benzaldehyde (2.7 mL, 20 mmol) and 2-aminothiophenol (2.1 mL, 20 mmol) were dissolved in ethanol (25 mL). This yielded a white solid (0.58 g, 10%). m.p. 171–172 °C. Found: C, 60.36; H, 3.11; N, 4.77. $C_{28}H_{18}F_6N_2S_2$ requires C, 59.99; H, 3.24; N, 5.00%. 1H NMR (500 MHz, CD_2Cl_2) 8.87 (2H, q, $J = 2.2$ Hz, N=CH), 8.58 (2H, d, $J = 7.5$ Hz, Ar-H), 7.78 (2H, d, $J = 7.8$ Hz, Ar-H), 7.73 (2H, t, $J = 7.7$ Hz, Ar-H), 7.68 (2H, dd, $J = 7.8, 1.3$ Hz, Ar-H), 7.64 (2H, t, $J = 7.8$ Hz, Ar-H), 7.19–7.28 (4H, m, Ar-H), 7.11 (2H, dd, $J = 7.7, 1.4$ Hz, Ar-H). ^{13}C NMR (125 MHz, CD_2Cl_2) 156.6, 149.1, 134.3, 132.2, 131.7, 129.7, 129.4, 128.1, 127.9, 127.8, 126.6, 118.5, 118.0, 115.7, 58.7, 18.8. ^{19}F NMR (376 MHz, CD_2Cl_2) -57.07 (6F, d, $J = 2.7$ Hz, CF_3). m/z : $[M]^+$ Calcd for $C_{28}H_{18}F_6N_2S_2$, 560, found 560. $[M/2]^+$ Calcd 280, found 280.

2,2'-Dithiobis{N-[(4-fluoro-2-(trifluoromethyl)phenyl)methylene]benzenamine}, DS18



4-Fluoro-2-(trifluoromethyl)benzaldehyde (2.7 mL, 20 mmol) and 2-aminothiophenol (2.1 mL, 20 mmol) were dissolved in ethanol (25 mL) and air was bubbled through the reaction for 16 h. The white precipitate formed was recovered by filtration and washed with ethanol. This yielded a white solid (0.50 g, 8%). m.p. 158–162 °C. ¹H NMR (500 MHz, CD₂Cl₂) 8.80 (2H, q, *J* = 2.2 Hz, N=CH), 8.62 (2H, dd, *J* = 8.6, 5.8 Hz, Ar-H), 7.67 (2H, dd, *J* = 7.7, 1.4 Hz, Ar-H), 7.49 (2H, dd, *J* = 8.8, 2.5 Hz, Ar-H), 7.43 (2H, td, *J* = 8.2, 2.7 Hz, Ar-H), 7.19–7.28 (4H, m, Ar-H), 7.10 (2H, dd, *J* = 7.5, 1.6 Hz, Ar-H). ¹³C NMR (125 MHz, CD₂Cl₂) 155.2, 148.9, 132.9, 132.3, 128.2, 127.9, 126.7, 117.9. ¹⁹F NMR (376 MHz, CD₂Cl₂) -57.56 (6F, d, *J* = 2.0 Hz, CF₃), -107.08 (2F, td, *J* = 8.3, 5.8 Hz, *p*-F). *m/z*: [M]⁺ Calcd for C₂₈H₁₆F₈N₂S₂, 596, found 596. [M/2]⁺ Calcd 298, found 298.

2,2'-Dithiobis{N-[(2-fluoro-6-(trifluoromethyl)phenyl)methylene]benzenamine}, DS19



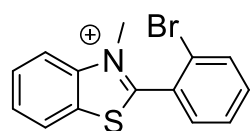
Following general procedure A, 2-fluoro-6-(trifluoromethyl)benzaldehyde (2.7 mL, 20 mmol) and 2-aminothiophenol (2.1 mL, 20 mmol) were dissolved in ethanol (25 mL). This yielded a pale yellow solid (0.60 g, 10%). m.p. 150–151 °C. ¹H NMR (500 MHz, CD₂Cl₂) 8.75 (2H, q, *J* = 2.2 Hz, N=CH), 7.68 (2H, dd, *J* = 7.8, 1.9 Hz, Ar-H), 7.57–7.64 (4H, m, Ar-H), 7.44–7.49 (2H, m, Ar-H), 7.20–7.28 (4H, m, Ar-H), 7.06 (2H, dd, *J* = 7.2, 1.9 Hz, Ar-H). ¹³C NMR (125 MHz, CD₂Cl₂) 163.0, 149.5, 132.4, 128.3, 127.8, 126.6, 117.8. ¹⁹F NMR (376 MHz, CD₂Cl₂) -57.79 (6F, d, *J* = 2.0 Hz, CF₃), -110.82–-110.76 (2F, m, *o*-F). *m/z*: [M]⁺ Calcd for C₂₈H₁₆F₈N₂S₂, 596, found 596. [M/2]⁺ Calcd 298, found 298.

2.2 Synthesis of [*N*-methyl-2-(aryl)benzothiazolium] tetrachlorozincate

General procedure B

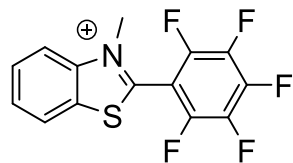
N-Methylaminothiophenol (1 eq.) and substituted benzaldehyde (1 eq.) were dissolved in ethanol. Zinc acetate (0.1 eq.) and 10 drops of hydrochloric acid (37%) were added. Air was bubbled through the reaction for 48 hours. The solid formed was recovered by filtration and washed with ethanol.

2[*N*-Methyl-2-(2-bromophenyl)benzothiazolium][zinc tetrachloride], BNZS1



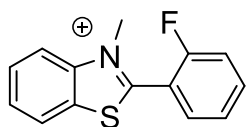
2,2'-Disulfanediybis(*N*-methylaniline) (0.5 g, 1.81 mmol), 2-bromobenzaldehyde (0.4 mL, 3.62 mmol) and zinc acetate (66.4 mg, 0.362 mmol) were dissolved in ethanol (15 mL). Nitrogen was bubbled through the reaction for 16 h. The solvent volume had fallen, and so ethanol (15 mL) and 10 drops of hydrochloric acid (37%) were added. Nitrogen was bubbled through the solution for 16 h, after which time a solid had formed. The solid was recovered by filtration and washed with ethanol to yield an off-white solid (0.17 g, 23%). ¹H NMR (500 MHz, CD₃CN) 8.39–8.42 (1H, m, Ar-*H*), 8.25–8.27 (1H, m, Ar-*H*), 8.03 (1H, ddd, *J* = 8.5, 7.2, 1.3 Hz, Ar-*H*), 7.92–7.97 (2H, m, Ar-*H*), 7.72–7.77 (3H, m, Ar-*H*), 4.11 (3H, s, N-CH₃).

2[*N*-Methyl-2-(pentafluorophenyl)benzothiazolium][zinc tetrachloride], BNZS2



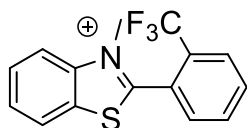
N-Methylaminothiophenol (0.5 g, 3.6 mmol) dissolved in ethanol (30 mL). Pentafluorobenzaldehyde (0.45 mL, 3.6 mmol), zinc acetate (0.066 g, 0.36 mmol) and 10 drops of hydrochloric acid (37%) were added and air was bubbled through the reaction. After 7 hours the white precipitate formed was recovered by filtration and washed with ethanol. This yielded a white solid (0.16 g, 23%). ¹H NMR (500 MHz, CD₃CN) 8.46–8.48 (1H, m, Ar-*H*), 8.31 (1H, dt, *J* = 8.7, 0.8 Hz, Ar-*H*), 8.06 (1H, m, Ar-*H*), 7.96 (1H, ddd, *J* = 8.4, 7.3, 0.9 Hz, Ar-*H*), 4.26 (3H, t, *J* = 1.3 Hz, N-CH₃). ¹⁹F NMR (376 MHz, CD₃CN) -135.17–-135.04 (2F, m, *o*-Ar-*F*), -145.39–-145.24 (1F, m, *p*-Ar-*F*), -160.34–-160.17 (2F, m, *m*-Ar-*F*).

2[*N*-Methyl-2-(2-fluorophenyl)benzothiazolium][zinc tetrachloride], BNZS3



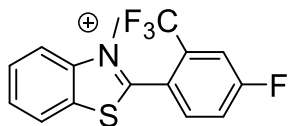
N-Methylaminothiophenol (0.5 g, 3.6 mmol) dissolved in ethanol (20 mL). 2-Fluorobenzaldehyde (0.40 mL, 3.6 mmol), zinc acetate (0.066 g, 0.36 mmol) and 10 drops of hydrochloric acid (37%) were added and air was bubbled through the reaction. After 7 hours the white precipitate formed was recovered by filtration and washed with ethanol. This yielded a white solid (0.26 g, 21%) ¹H NMR (400 MHz, CD₃CN) 8.38–8.41 (1H, m, Ar-*H*), 8.23–8.26 (1H, m, Ar-*H*), 7.99–8.03 (1H, m, Ar-*H*), 7.88–7.99 (2H, m, Ar-*H*), 7.80–7.84 (1H, m, Ar-*H*), 7.58 (1H, td, *J* = 7.78, 1.00 Hz, Ar-*H*), 7.51–7.56 (1H, m, Ar-*H*), 4.20 (3H, d, *J* = 1.76 Hz, N-CH₃). ¹⁹F NMR (376 MHz, CD₃CN) -110.48–-110.55 (1F, m, *o*-F).

2[*N*-Methyl-2-(2-(trifluoromethyl)phenyl)benzothiazolium][zinc tetrachloride], BNZS4



Following general procedure B, *N*-methylaminothiophenol (1.0 g, 7.2 mmol) was dissolved in ethanol (15 mL). 2-(trifluoromethyl)benzaldehyde (0.95 mL, 7.2 mmol), zinc acetate (0.132 g, 0.72 mmol) and hydrochloric acid (37%) were added. This yielded a pale yellow solid (0.52 g, 18%). ¹H NMR (500 MHz, CD₃CN) 8.38–8.41 (1H, m, Ar-*H*), 8.24 (1H, dt, *J* = 8.5, 0.9 Hz, Ar-*H*), 8.08–8.11 (1H, m, Ar-*H*), 8.04 (2H, ddd, *J* = 8.5, 7.5, 1.3 Hz, Ar-*H*), 7.97–8.01 (1H, m, Ar-*H*), 7.94 (1H, ddd, *J* = 8.2, 7.3, 1.1 Hz, Ar-*H*), 7.85 (1H, dd, *J* = 7.4, 1.4 Hz, Ar-*H*), 4.06 (3H, s, N-CH₃). ¹⁹F NMR (376 MHz, CD₃CN) -59.22 (3F, s, CF₃).

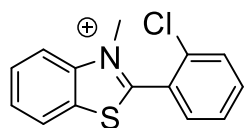
2[*N*-Methyl-2-(4-fluoro-2-(trifluoromethyl)phenyl)benzothiazolium][zinc tetrachloride], BNZS5



Following general procedure B, *N*-methylaminothiophenol (1.0 g, 7.2 mmol) was dissolved in ethanol (20 mL). 4-fluoro-2-(trifluoromethyl)benzaldehyde (0.98 mL, 7.2 mmol), zinc acetate (0.132 g, 0.72 mmol) and hydrochloric acid (37%) were added. This yielded a pale yellow solid (0.26 g, 9%). m.p. 178–180 °C. ¹H NMR (500 MHz, CD₃CN) 8.43–8.46 (1H, m, Ar-*H*), 8.40–8.43 (1H, m, Ar-*H*), 8.26–8.30 (2H, m, Ar-*H*), 8.07–8.11 (1H, m, Ar-*H*), 8.01–8.06 (3H, m, Ar-*H*), 7.86–7.96 (5H, m, Ar-*H*), 7.73–7.78 (1H, m, Ar-*H*), 4.23 (3H, d, *J* = 1.6 Hz, N-CH₃), 4.10 (3H, s,

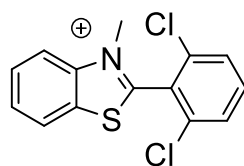
$N-CH_3$). ^{19}F NMR (376 MHz, CD_3CN) -59.64 (3F, s, CF_3), -63.93 (3F, s, CF_3), -104.52 (1F, td, $J = 8.3, 5.1$ Hz, $o-F$), -107.99 (1F, t, $J = 7.8$ Hz, $o-F$).

2[*N*-Methyl-2-(2-chlorophenyl)benzothiazolium][zinc tetrachloride], BNZS6



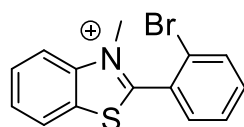
Following general procedure B, *N*-methylaminothiophenol (1.0 g, 7.2 mmol) was dissolved in ethanol (20 mL). 2-chlorobenzaldehyde (0.81 mL, 7.2 mmol), zinc acetate (0.132 g, 0.72 mmol) and hydrochloric acid (37%) were added. This yielded a pale yellow solid (0.51 g, 19%). m.p. 247–248 °C. 1H NMR (500 MHz, CD_3CN) 8.38–8.41 (1H, m, Ar-*H*), 8.24–8.27 (1H, m, Ar-*H*), 8.02 (1H, ddd, $J = 8.4, 7.5, 1.3$ Hz, Ar-*H*), 7.93 (1H, ddd, $J = 8.4, 7.5, 1.1$ Hz, Ar-*H*), 7.76–7.84 (3H, m, Ar-*H*), 7.67–7.71 (1H, m, Ar-*H*), 4.12 (3H, s, $N-CH_3$).

2[*N*-methyl-2-(2,6-dichlorophenyl)benzothiazolium][zinc tetrachloride], BNZS7



Following general procedure B, *N*-methylaminothiophenol (1.0 g, 7.2 mmol) was dissolved in ethanol (20 mL). 2,6-dichlorobenzaldehyde (1.26 g, 7.2 mmol), zinc acetate (0.132 g, 0.72 mmol) and hydrochloric acid (37%) were added. This yielded a pale yellow solid (0.61 g, 21%). MP 216 °C (decomp).

2[*N*-Methyl-2-(2-bromophenyl)benzothiazolium][zinc tetrachloride], BNZS8



Following general procedure B, *N*-methylaminothiophenol (1.0 g, 7.2 mmol) was dissolved in ethanol (20 mL). 2-bromobenzaldehyde (0.83 mL, 7.2 mmol), zinc acetate (0.132 g, 0.72 mmol) and hydrochloric acid (37%) were added. This yielded an off-white solid (0.56 g, 19%). m.p. 246–248 °C. 1H NMR (500 MHz, CD_3CN) 8.38–8.41 (1H, m, Ar-*H*), 8.25 (1H, dt, $J = 8.5, 0.9$ Hz, Ar-*H*), 8.03 (1H, ddd, $J = 8.5, 7.4, 1.3$ Hz, Ar-*H*), 7.92–7.97 (2H, m, Ar-*H*), 7.73–7.75 (2H, m, Ar-*H*), 4.10 (3H, s, $N-CH_3$).

2.3 Synthesis of *N*-Methyl-2-(aryl)benzothiazoline

General procedure C

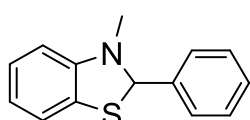
N-Methylaminothiophenol (1 eq.) and substituted benzaldehyde (1 eq.) were dissolved in ethanol. Air was bubbled through the reaction for 48 hours. The solid formed was recovered by filtration and washed with ethanol.

General procedure D

[*N*-Methyl-2-(aryl)benzothiazolium] $\frac{1}{2}$ [zinc tetrachloride] (1 eq.) was dissolved in toluene (or acetonitrile). Sodium triethylborohydride (1M in toluene) (1.1 eq) was added and the reaction stirred for 16 hours to afford a solution and white precipitate. The solution was transferred via cannula and the solvent removed under reduced pressure to produce a solid.

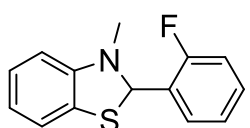
The starting materials for the synthesis of BNZ1 and BNZ2 were received from Prof. Michael Ingleson.

N-Methyl-2-phenylbenzothiazoline, BNZ1



N-Methyl-2-phenylbenzothiazolium iodide (74.4 mg, 0.21 mmol) dissolved in toluene (4 mL). Sodium triethylborohydride (0.3 mL, 0.3 mmol) was added and reaction stirred for 1 h. The solution was filtered and dried *in vacuo* to produce a pale yellow solid (22.9 mg, 48%). ^1H NMR (500 MHz, CD_2Cl_2) 7.54 (2H, dd, $J = 7.8, 1.6$ Hz, Ar-*H*), 7.38–7.41 (3H, m, Ar-*H*), 6.98–7.03 (2H, m, Ar-*H*), 6.69 (1H, td, $J = 7.5, 1.3$ Hz, Ar-*H*), 6.82 (1H, d, $J = 8.2$ Hz, Ar-*H*), 6.00 (1H, s, C2-*H*), 2.63 (3H, s, N- CH_3).

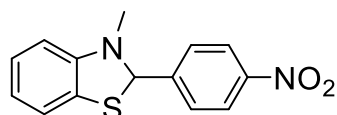
N-Methyl-2-(2-fluorophenyl)benzothiazoline, BNZ2



N-Methyl-2-(*o*-fluorophenyl)benzothiazolium iodide (72 mg, 0.19 mmol) dissolved in toluene (3 mL). Sodium triethylborohydride (0.2 mL, 0.2 mmol) was added and reaction stirred for 1 h. The resulting solution was filtered and dried *in vacuo* to produce a white solid. ^1H NMR (500 MHz, CD_2Cl_2)

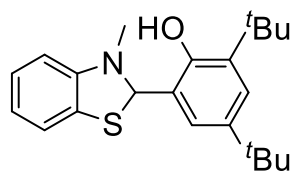
7.68 (1H, t, $J = 7.2$ Hz, Ar-*H*), 7.33 (1H, dt, $J = 7.2, 6.3$ Hz, Ar-*H*), 7.19 (1H, t, $J = 7.4$ Hz, Ar-*H*), 7.09 (1H, t, $J = 9.3$ Hz, Ar-*H*), 7.02 (2H, q, $J = 6.9$ Hz, Ar-*H*), 6.70 (1H, t, $J = 7.4$ Hz, Ar-*H*), 6.45 (1H, d, $J = 7.8$ Hz, Ar-*H*), 6.37 (1H, s, C2-*H*), 2.71 (3H, s, N- CH_3). ^{19}F NMR (470 MHz, CD_2Cl_2) -120.45 (1F, quint, $J = 4.7$ Hz).

***N*-Methyl-2-(4-nitrophenyl)benzothiazoline, BNZ3**



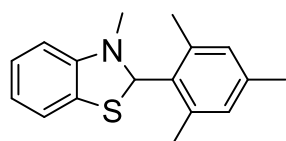
N-Methylaminothiophenol (1.00 g, 7.2 mmol) dissolved in ethanol (30 mL). Added 4-nitrobenzaldehyde (1.084 g, 7.2 mmol) and air was bubbled through reaction. After 10 min an orange precipitate formed which was recovered by filtration and washed with ethanol. This yielded an orange solid (1.04 g, 53%). ^1H NMR (500 MHz, CD_2Cl_2) 8.21–8.24 (2H, m, Ar-*H*), 7.70–7.73 (2H, m, Ar-*H*), 7.05 (1H, td, $J = 7.7, 1.3$ Hz, Ar-*H*), 7.01 (1H, dd, $J = 7.5, 1.3$ Hz, Ar-*H*), 6.73 (1H, td, $J = 7.5, 0.9$ Hz, Ar-*H*), 6.47 (1H, dd, $J = 8.0, 1.1$ Hz, Ar-*H*), 6.10 (1H, s, C2-*H*), 2.67 (3H, s, N- CH_3).

***N*-Methyl-2-(3,5-di-*tert*-butyl-2-hydroxyphenyl)benzothiazoline, BNZ4**



N-Methylaminothiophenol (1.00 g, 7.2 mmol) dissolved in ethanol (30 mL). 3,5-di-*tert*-butyl-2-hydroxybenzaldehyde (1.687 g, 7.2 mmol) was added and air was bubbled through reaction. After 2 h, a white ppt had formed which was recovered by filtration and washed with ethanol. This yielded a white solid (1.397 g, 55%). m.p. 167 °C (decomp). ^1H NMR (500 MHz, CD_2Cl_2) 9.10 (1H, s, OH), 7.37 (1H, d, $J = 2.2$ Hz, Ar-*H*), 7.13 (1H, dd, $J = 7.5, 0.9$ Hz, Ar-*H*), 7.10 (1H, td, $J = 7.8, 1.4$ Hz, Ar-*H*), 6.93 (1H, d, $J = 2.5$ Hz, Ar-*H*), 6.89 (1H, td, $J = 7.6, 1.1$ Hz, Ar-*H*), 6.69 (1H, d, $J = 7.8$ Hz, Ar-*H*), 5.91 (1H, s, C2-*H*), 2.72 (3H, s, N- CH_3), 1.44 (9H, s, *t*Bu-*H*), 1.31 (9H, s, *t*Bu-*H*). m/z : $[\text{M}]^+$ Calcd for $\text{C}_{22}\text{H}_{29}\text{NOS}$, 355, found 355.

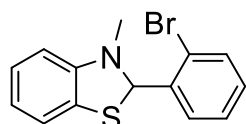
***N*-Methyl-2-(mesityl)benzothiazoline, BNZ5**



Magnesium turnings (0.635 g, 26 mmol) were suspended in dry THF (20 mL) and cooled to 0 °C. 2-bromomesitylene (3.9 mL, 25.3 mmol) was added slowly drop wise and the resulting solution was stirred for 2.5 h until only small amount of magnesium remained. *N*-Methylbenzothiazolium

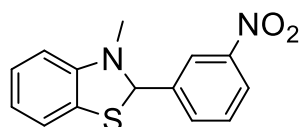
iodide (7.01 g, 25.3 mmol) suspended in THF (20 mL), the Grignard solution transferred over and the reaction stirred at 0 °C for 2 h. This was dried *in vacuo* to produce a dark red solid. The latter was redissolved in minimal CH₂Cl₂ and undissolved solid removed by filtration. The solution run through an alumina plug and colourless filtrate collected. The solvent was removed *in vacuo* to produce a white solid (0.555 g, 8%). m.p. 95–97 °C. Found: C, 75.38; H, 7.13; N, 5.79. C₁₇H₁₉NS requires C, 75.79; H, 7.11; N, 5.20%. ¹H NMR (500 MHz, CD₂Cl₂) 6.96–7.00 (2H, m, Ar-H), 6.87 (2H, br s, Ar-H), 6.65 (1H, td, *J* = 7.5, 1.3 Hz, Ar-H), 6.63 (1H, s, C2-H), 6.35 (1H, d, *J* = 7.8 Hz, Ar-H), 2.54 (3H, s, N-CH₃), 2.43 (6H, br, d, *J* = 534.3 Hz, *o*-CH₃), 2.27 (3H, s, *p*-CH₃). ¹³C NMR (125 MHz, CD₂Cl₂) 149.0, 138.7, 130.1, 126.6, 126.2, 121.9, 119.1, 107.8, 72.6, 33.2, 21.1. *m/z*: [M]⁺ Calcd for C₁₇H₁₉NS, 269, found 269. [M-mesityl]⁺ Calcd 150, found 150.

***N*-Methyl-2-(2-bromophenyl)benzothiazoline, BNZ6**



Following general procedure D, [*N*-methyl-2-(2-bromophenyl)benzothiazolium]^{1/2}[zinc tetrachloride] (0.172 g, 0.42 mmol) was dissolved in toluene (10 mL). Sodium triethylborohydride (0.6 mL, 0.6 mmol) was added. This yielded a yellow solid (0.071 g, 55%). m.p. 99–102 °C. ¹H NMR (500 MHz, CD₂Cl₂) 7.66 (1H, dd, *J* = 7.8, 1.6 Hz, Ar-H), 7.59 (1H, dd, *J* = 8.0, 1.1 Hz, Ar-H), 7.34–7.38 (1H, m, Ar-H), 7.21 (1H, td, *J* = 7.7, 1.6 Hz, Ar-H), 7.03 (1H, td, *J* = 7.7, 1.3 Hz, Ar-H), 6.98 (1H, dd, *J* = 7.5, 1.3 Hz, Ar-H), 6.70 (1H, td, *J* = 7.5, 1.3 Hz, Ar-H), 6.48 (1H, dd, *J* = 8.0, 0.8 Hz, Ar-H), 6.43 (1H, s, C2-H), 2.77 (3H, s, N-CH₃). ¹³C NMR (125 MHz, CD₂Cl₂) 133.6, 130.4, 128.8, 128.7, 126.3, 125.6, 122.9, 122.0, 119.7, 108.0, 75.2, 34.9. *m/z*: [M]⁺ Calcd for C₁₄H₁₂BrNS, 306, found 306.

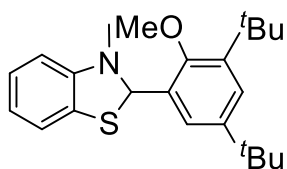
***N*-Methyl-2-(3-nitrophenyl)benzothiazoline, BNZ7**



Following general procedure C, *N*-methylaminothiophenol (0.50 g, 3.6 mmol) and 3-nitrobenzaldehyde (0.544 g, 3.6 mmol) were dissolved in ethanol (25 mL). This yielded a yellow solid (0.60 g, 62%). m.p. 113–116 °C. Found: C, 62.07; H, 4.42; N, 10.33. C₁₄H₁₂N₂O₂S requires C, 61.75; H, 4.44; N, 10.29%. ¹H NMR (500 MHz, CD₂Cl₂) 8.40–8.41 (1H, m, Ar-H), 8.21 (1H, ddd, *J* = 8.2, 2.4, 1.1 Hz, Ar-H), 7.91 (1H, ddt, *J* = 7.7, 1.7, 0.8, 0.8 Hz, Ar-H), 7.59 (1H, t, *J* = 7.9 Hz, Ar-H), 7.05 (1H, td, *J* = 7.8, 1.3 Hz, Ar-H), 7.01 (1H, dd, *J* = 7.5, 0.9 Hz, Ar-H), 6.74 (1H, td, *J* = 7.5, 0.9

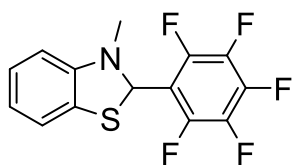
Hz, Ar-H), 6.48 (1H, dd, $J = 8.0, 1.1$ Hz, Ar-H), 6.11 (1H, s, C2-H), 2.67 (3H, s, N-CH₃). m/z : [M]⁺
Calcd for C₁₄H₁₂N₂O₂S, 272, found 272.

***N*-Methyl-2-(3,5-di-*tert*-butyl-2-methoxyphenyl)benzothiazoline, BNZ8**



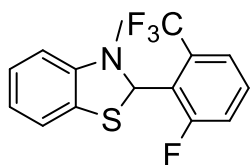
3,5-di-*tert*-butyl-2-methoxybenzaldehyde (0.71 g, 2.86 mmol) and *N*-methylaminothiophenol (0.399 g, 2.86 mmol) were dissolved in ethanol (20 mL) and air was bubbled through the reaction. After 10 min a white precipitate had formed which was recovered by filtration and washed with ethanol. This yielded a white solid (0.517 g, 49%). m.p. 125–126 °C. Found: C, 74.62; H, 8.58; N, 3.99. C₂₃H₃₁NOS requires C, 74.75; H, 8.46; N, 3.79%. ¹H NMR (500 MHz, CD₂Cl₂) 7.76 (1H, d, $J = 2.8$ Hz, Ar-H), 7.34 (1H, d, $J = 2.5$ Hz, Ar-H), 6.98–7.04 (2H, m, Ar-H), 6.70 (1H, td, $J = 7.5, 1.3$ Hz, Ar-H), 6.42 (1H, dd, $J = 7.9, 0.6$ Hz, Ar-H), 6.39 (1H, s, C2-H), 3.78 (3H, s, O-CH₃), 2.54 (3H, s, N-CH₃), 1.40 (9H, s, ^{*t*}Bu-H), 1.27 (9H, s, ^{*t*}Bu-H). ¹³C NMR (125 MHz, CD₂Cl₂) 142.4, 132.5, 126.3, 126.0, 125.4, 124.3, 121.9, 119.6, 107.9, 71.3, 63.9, 35.8, 35.1, 34.0, 31.7, 31.5. m/z : [M]⁺ Calcd for C₂₃H₃₁NOS, 369, found 369.

***N*-Methyl-2-(pentafluorophenyl)benzothiazoline, BNZ9**



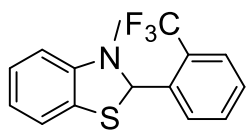
[*N*-methyl-2-(pentafluorophenyl)-benzothiazolium]⁺[zinc tetrachloride]⁻ (0.2 g, 0.48 mmol) was dissolved in toluene (4 mL). Lithium triethylborohydride solution (1M in THF) (0.5 mL, 0.5 mmol) was added and the reaction stirred for 16 hours to form a yellow solution and white precipitate. The solution was filtered and the solvent removed under reduced pressure to produce a yellow solid (22.9 mg, 15%). m.p. 89–90 °C. Found: C, 52.65; H, 2.58; N, 4.46. C₁₄H₈F₅NS requires C, 53.00; H, 2.64; N, 4.41%. ¹H NMR (500 MHz, CD₂Cl₂) 7.00–7.06 (2H, m, Ar-H), 6.70 (1H, t, $J = 7.4$ Hz, Ar-H), 6.55 (1H, s, C2-H), 6.40 (1H, d, $J = 7.8$ Hz, Ar-H), 2.75 (3H, s, N-CH₃). ¹³C NMR (125 MHz, CD₂Cl₂) 159.8, 125.9, 120.9, 118.8, 107.1, 64.1, 33.3. ¹⁹F NMR (376 MHz, CD₂Cl₂) -142.36 (2F, d, $J = 18.4$ Hz, *o*-Ar-F), -154.48 (1F, tt, $J = 21.1, 2.0$ Hz, *p*-Ar-F), -162.24–-162.07 (2F, m, *m*-Ar-F). m/z : [M]⁺ Calcd for C₁₄H₈F₅NS, 317, found, 317.

***N*-Methyl-2-(2-fluoro-6-(trifluoromethyl)phenyl)benzothiazoline, BNZ10**



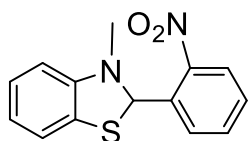
N-Methylaminothiophenol (1.0 g, 7.2 mmol) was dissolved in ethanol (20 mL). 2-fluoro-6-(trifluoromethyl)benzaldehyde (0.96 mL, 7.2 mmol), zinc acetate (0.132 g, 0.72 mmol) and 10 drops of hydrochloric acid (37%) were added and air was bubbled through the reaction for 48 hours. The pale yellow sticky precipitate was isolated by filtration. The solid was redissolved in minimal CH₂Cl₂ and the solvent removed under reduced pressure to afford a pale yellow solid (0.498 g, 22%). m.p. 172–174 °C. ¹H NMR (500 MHz, CD₃CN) 7.54–7.62 (2H, m, Ar-*H*), 7.41–7.46 (1H, m, Ar-*H*), 6.97–7.03 (2H, m, Ar-*H*), 6.62–6.66 (2H, m, Ar-*H*), 6.40 (1H, d, *J* = 7.8 Hz, C2-*H*), 2.69 (3H, s, N-CH₃). ¹³C NMR (125 MHz, CD₃CN) 165.3, 163.3, 148.8, 132.1, 132.0, 129.9, 129.7, 126.9, 126.1, 125.9, 125.8, 123.7, 123.6, 122.8, 122.6, 121.5, 119.2, 107.8, 67.9, 33.6. ¹⁹F NMR (376 MHz, CD₃CN) -57.23 (3F, s, CF₃) -107.15–107.17 (1F, m, *o*-F). *m/z*: [M]⁺ Calcd for C₁₅H₁₁F₄NS, 313, found 313.

***N*-Methyl-2-(2-(trifluoromethyl)phenyl)benzothiazoline, BNZ11**



Following general procedure D, [*N*-methyl-2-(2-(trifluoromethyl)phenyl)benzothiazolium]^{1/2}[zinc tetrachloride] (0.5 g, 1.26 mmol) was dissolved in acetonitrile (10 mL). Sodium triethylborohydride (1.3 mL, 1.3 mmol) was added. This yielded a yellow oil. Purification via alumina plug (5:1 hexane:ethyl acetate) to afford a sticky yellow oil. ¹H NMR (500 MHz, CD₂Cl₂) 8.10 (1H, d, *J* = 7.8 Hz, Ar-*H*), 7.69 (1H, d, *J* = 7.8 Hz, Ar-*H*), 7.63 (1H, t, *J* = 7.5 Hz, Ar-*H*), 7.47 (1H, t, *J* = 7.8 Hz, Ar-*H*), 7.06 (1H, td, *J* = 7.7, 1.3 Hz, Ar-*H*), 7.00 (1H, dd, *J* = 7.2, 0.9 Hz, Ar-*H*), 6.73 (1H, td, *J* = 7.5, 0.9 Hz, Ar-*H*), 6.47 (1H, t, *J* = 3.8 Hz, C2-*H*), 2.68 (3H, s, N-CH₃). ¹³C NMR (125 MHz, CD₂Cl₂) 148.6, 140.0, 133.3, 129.6, 129.2, 126.5, 126.1, 125.6, 121.8, 119.8, 107.8, 71.4, 34.2. ¹⁹F NMR (376 MHz, CD₂Cl₂) -57.93 (3F, s, CF₃).

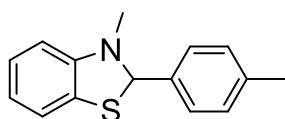
***N*-Methyl-2-(2-nitrophenyl)benzothiazoline, BNZ12**



Following general procedure C, *N*-methylaminothiophenol (1.0 g, 7.2 mmol) was dissolved in ethanol (20 mL). 2-nitrobenzaldehyde (1.088 g, 7.2 mmol) was added. This yielded an orange solid (0.98 g, 50%). m.p. 132–136 °C. ¹H NMR (500 MHz, CD₂Cl₂) 8.04 (1H, dd, *J* = 8.2, 1.3

Hz, Ar-H), 7.81, (1H, dd, $J = 7.8, 1.6$ Hz, Ar-H), 7.67 (1H, td, $J = 7.4, 1.3$ Hz, Ar-H), 7.49 (1H, td, $J = 7.8, 1.4$ Hz, Ar-H), 7.04 (1H, td, $J = 7.7, 1.3$ Hz, Ar-H), 6.98 (1H, dd, $J = 7.5, 0.9$ Hz, Ar-H), 6.70 (1H, td, $J = 7.5, 1.3$ Hz, Ar-H), 6.53 (1H, s, C2-H), 6.50 (1H, dd, $J = 7.8, 0.6$ Hz, Ar-H), 2.79 (3H, s, N-CH₃). ¹³C NMR (125 MHz, CD₂Cl₂) 134.9, 129.6, 128.8, 125.6, 121.8, 119.8, 107.8, 71.2, 35.1. m/z : [M]⁺ Calcd for C₁₄H₁₂N₂O₂S, 272, found 272, [M-C₆H₄NO₂]⁺ Calcd 150, found 150.

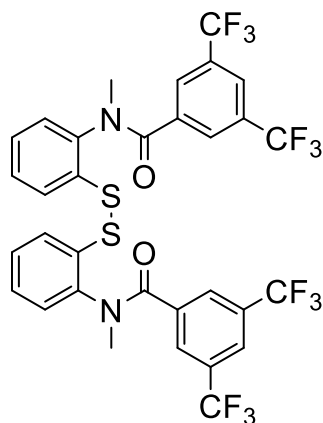
***N*-Methyl-2-(4-tolyl)benzothiazoline, BNZ13**



Following general procedure C, *N*-methylaminothiophenol (1.0 g, 7.2 mmol) was dissolved in ethanol (20 mL) and *p*-tolualdehyde (0.85 mL, 7.2 mmol) was added. This yielded a white solid (0.60 g, 35 %). m.p. 98–100 °C. Found: C, 74.10; H, 5.88; N, 5.40. C₁₅H₁₅NS requires C, 74.65; H, 6.26; N, 5.80%. ¹H NMR (500 MHz, CD₂Cl₂) 7.42 (2H, d, $J = 8.2$ Hz, Ar-H), 7.20 (2H, d, $J = 7.8$ Hz, Ar-H), 6.97–7.02 (2H, m, Ar-H), 6.68 (1H, td, $J = 7.5, 0.9$ Hz, Ar-H), 6.41 (1H, dd, $J = 7.8, 0.9$ Hz, Ar-H), 5.97 (1H, s, C2-H), 2.61 (3H, s, N-CH₃), 2.36 (3H, s, Ar-CH₃). ¹³C NMR (125 MHz, CD₂Cl₂) 148.9, 136.9, 129.9, 129.0, 128.0, 126.3, 121.7, 119.6, 107.9, 77.1, 34.0, 21.5. m/z : [M]⁺ Calcd for C₁₅H₁₅NS, 241, found 241, [M-tolyl]⁺ Calcd 152, found 152.

2.4 Other syntheses

N,N-(Dithiodi-2,1-phenylene)bis[3,5-bis(trifluoromethyl)-*N*-methyl]benzamide, DSA1

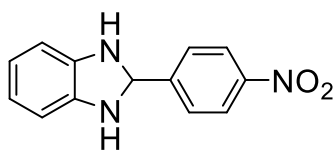


N-Methylaminothiophenol (1.0 g, 7.2 mmol) was dissolved in ethanol (25 mL). 3,5-Bis(trifluoromethyl)benzaldehyde (1.2 mL, 7.2 mmol), zinc acetate (0.132 g, 0.72 mmol) and 10 drops hydrochloric acid (37%) were added and the solution heated (40 °C) for 30 mins with air bubbled through the reaction. After heating the solution was stirred with bubbling for a further 96 hours. The white precipitate formed was recovered by filtration and washed with ethanol. This yielded a white solid (0.122 g, 22%). m.p. 159–161 °C. ¹H NMR (500 MHz, CD₃CN) 7.93 (2H, d, *J* = 12.2 Hz, Ar-*H*), 7.85 (4H, d, *J* = 10.7 Hz, Ar-*H*), 7.42 (2H, t, *J* = 7.8 Hz, Ar-*H*), 7.26 (2H, t, *J* = 7.5 Hz, Ar-*H*), 7.14 (2H, q, *J* = 8.5 Hz, Ar-*H*), 6.95 (2H, q, *J* = 7.8 Hz, Ar-*H*), 3.39 (3H, s, N-CH₃), 3.34 (3H, s, N-CH₃). ¹³C NMR (125 MHz, CD₃CN) 168.1, 142.2, 139.1, 134.9, 131.7, 131.4, 130.7, 130.6, 129.7, 128.0, 127.9, 125.2, 37.7. ¹⁹F NMR (376 MHz, CD₃CN) -63.59 (6F, s, CF₃), -63.65 (6F, s, CF₃). *m/z*: [M]⁺ Calcd for C₃₂H₂₀F₁₂N₂O₂S₂, 756, found 756. [M/2]⁺ Calcd 378, found 378. [M-F¹⁹]⁺ Calcd, 737, found 737.

tert-Butyl-(2-aminophenyl)carbamate

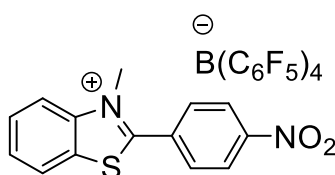
Synthesis was adapted from reference 112. *o*-Phenylenediamine (2.02 g, 18.7 mmol) was dissolved in CH₂Cl₂ (20 mL) and cooled to 0 °C. Triethylamine (2.6 mL, 18.7 mmol) and di-*tert*-butyl dicarbonate (4.077 g, 18.7 mmol) and the reaction stirred at 0 °C for 4 hours. Distilled water (25 mL) was added and the product extracted with ethyl acetate (2 × 50 mL). Organic layer was dried over sodium sulfate and dried *in vacuo*. The pale brown solid was purified by column chromatography (hexane/ethyl acetate 4:1) to produce a white solid (2.706 g, 69%). *R_f* 0.14. ¹H NMR (500 MHz, CDCl₃) 7.27 (1H, d, *J* = 7.8 Hz, Ar-*H*), 6.99 (1H, td, *J* = 7.8, 1.5 Hz, Ar-*H*), 6.74–6.82 (2H, m, Ar-*H*), 6.29 (1H, br s, N-*H*), 3.76 (2H, br. s, N-*H*₂), 1.51 (9H, s, ^tBu-*H*).

2-(4-Nitrophenyl)benzimidazole



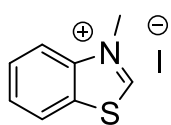
o-Phenylenediamine (1.618 g, 15 mmol) and 4-nitrobenzaldehyde (2.269 g, 15 mmol) were dissolved in ethanol (30 mL) and air was bubbled through the reaction for 16 h. A dark red precipitate had formed which was isolated by filtration and washed with ethanol. This yielded a dark red solid (3.184 g, 88%). ¹H NMR (500 MHz, CD₂Cl₂) 8.66 (1H, s, C2-*H*) 8.29–8.33 (2H, m, Ar-*H*), 8.08–8.12 (2H, m, Ar-*H*), 7.15 (1H, dd, *J* = 7.9, 1.3 Hz, Ar-*H*), 7.09–7.13 (1H, m, Ar-*H*), 6.79 (1H, dd, *J* = 7.9, 1.3 Hz, Ar-*H*), 6.72–6.76 (1H, m, Ar-*H*), 4.38 (2H, br. s, N-*H*).

[*N*-Methyl-2-(4-nitrophenyl)benzothiazolium][tetrakis(pentafluorophenyl)borate]



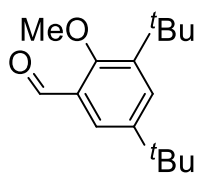
N-Methyl-2-(4-nitrophenyl)benzothiazoline (0.0551 g, 0.2 mmol) and trityl tetrakis(pentafluorophenyl)borate (0.1856 g, 0.2 mmol) were dissolved in dry CH₂Cl₂ (10 mL) and stirred for 4 h. The solvent volume reduced by half *in vacuo* and dry petroleum ethers (5 mL) was added and the reaction stirred. The volume was reduced *in vacuo* until precipitate started to form, and the solution cooled to -25 °C for 16 h. More pale yellow precipitate formed which was isolated by filtration and the solid dried *in vacuo* (0.114 g, 60%). ¹H NMR (500 MHz, CD₂Cl₂) 8.59–8.64 (2H, m, Ar-*H*), 8.29 (1H, d, *J* = 8.0 Hz, Ar-*H*), 8.07–8.15 (2H, m, Ar-*H*), 7.99–8.04 (1H, m, Ar-*H*), 7.92–7.97 (2H, m, Ar-*H*), 4.32 (3H, s, N-CH₃). ¹¹B NMR (160 MHz, CD₂Cl₂) -16.69 (s). ¹⁹F NMR (376 MHz, CD₂Cl₂) -133.11 (8F, d, *J* = 11.6 Hz, *o*-Ar-F), -163.53 (4F, t, *J* = 19.8 Hz, *p*-Ar-F), -167.48 (8F, t, *J* = 17.4 Hz, *m*-Ar-F).

N-Methylbenzothiazolium iodide



Synthesis undertaken following literature preparation,¹¹⁹ using benzothiazole (0.9 mL, 8 mmol) and 6 eq. iodomethane (3.0 mL, 48 mmol) in DMF (3 mL) (1.112 g, 50%). ¹H NMR (500 MHz, DMSO-*d*₆) 10.52 (1H, s, C2-*H*), 8.49–8.51 (1H, m, Ar-*H*), 8.32 (1H, dt, *J* = 8.3, 0.9 Hz, Ar-*H*), 7.95 (1H, ddd, *J* = 8.5, 7.2, 1.3 Hz, Ar-*H*), 7.87 (1H, ddd, *J* = 8.2, 7.2, 0.9, Ar-*H*), 4.40 (3H, d, N-CH₃). This is consistent with the data in the literature.¹¹⁹

3,5-Di-*tert*-butyl-2-methoxybenzaldehyde



3,5-Di-*tert*-butyl-2-hydroxybenzaldehyde (1.005 g, 4.27 mmol) dissolved in dry acetonitrile (50 mL). Anhydrous potassium carbonate (5.899 g, 42.7 mmol) and iodomethane (2.7 mL, 43.3 mmol) were added and reaction stirred for 16 h. The solution was filtered and dried *in vacuo* to produce a yellow oil and white solid. This was redissolved in minimal CH_2Cl_2 and filtered. The solution was dried *in vacuo* to produce a yellow oil (1.085 g, 100%). ^1H NMR (500 MHz, CD_2Cl_2) 10.32 (1H, s, CHO), 7.69 (1H, d, $J = 2.5$ Hz, Ar-H), 7.63 (1H, d, $J = 2.8$ Hz, Ar-H), 3.92 (3H, s, O- CH_3), 1.43 (9H, s, $^t\text{Bu-H}$), 1.33 (9H, s, $^t\text{Bu-H}$).

$[\text{Bu}_4\text{N}][\text{HB}(\text{C}_6\text{F}_5)_3]$

$\text{B}(\text{C}_6\text{F}_5)_3$ (2.04 g, 3.98 mmol) dissolved in dry toluene (50 mL). Sodium triethylborohydride (4.4 mL, 4.4 mmol) was added and the reaction stirred for 2 h. The white solid formed was washed with petroleum ethers (10 mL) and then toluene (10 mL) and dried *in vacuo* to give the intermediate $\text{Na}[\text{HBArF}_{15}]$ (0.688 g, 32%). ^{11}B NMR (160 MHz, CD_2Cl_2) -24.98 (d, $J = 82.2$ Hz). ^{19}F NMR (376 MHz, CD_2Cl_2) -137.45 (6F, *o*-Ar-F), -161.34 (3H, *p*-Ar-F), -165.28 (6F, *m*-Ar-F).

Sodium tris(pentafluorophenyl)borohydride (0.688 g, 1.28 mmol) was dissolved in dry CH_2Cl_2 (10 mL). Tetrabutylammonium chloride (0.358 g, 1.28 mmol) was dissolved in dry CH_2Cl_2 (40 mL) and added to the solution of borohydride. The reaction was stirred for 16 h under an argon atmosphere. The solution was filtered and the solvent reduced *in vacuo* until it became turbid. This was then layered with an equal amount of dry petroleum ethers and the solution cooled for 16 h (-25 °C). The resulting white solid was isolated by filtration and dried *in vacuo* (0.655 g, 68%). ^1H NMR (500 MHz, CD_2Cl_2) 3.33–3.87 (1H, m, B-H), 3.06–3.10 (8H, m, $\text{N-CH}_2\text{CH}_2\text{CH}_2\text{CH}_3$), 1.59 (8H, p, $J = 7.9$ Hz, $\text{NCH}_2\text{-CH}_2\text{CH}_2\text{CH}_3$), 1.38 (8H, sextet, $J = 7.4$ Hz, $\text{NCH}_2\text{CH}_2\text{-CH}_2\text{CH}_3$), 0.97 (12H, t, $J = 7.4$ Hz, $\text{NCH}_2\text{CH}_2\text{CH}_2\text{-CH}_3$). ^{11}B NMR (160 MHz, CD_2Cl_2) -25.33 (d, $J = 90.0$ Hz). ^{19}F NMR (376 MHz, CD_2Cl_2) -133.89 (6F, d, $J = 23.7$ Hz, *o*-Ar-F), -164.55 (3F, t, $J = 19.9$ Hz, *p*-Ar-F), -167.51 (6F, td, $J = 17.0, 6.8$ Hz, *m*-Ar-F).

$[\text{Trityl}][\text{tetrakis}(\text{pentafluorophenyl})\text{borate}]$

Synthesis was adapted from reference 113. $\text{Li}(\text{OEt}_2)_n\text{BArF}_{20}$ (3.005 g, 3.31 mmol) was dissolved in dry CH_2Cl_2 (40 mL). Trityl chloride (1.114 g, 4 mmol) was dissolved in dry CH_2Cl_2

(20 mL) and the solution added to the solution of $\text{Li}(\text{OEt})_n\text{BARF}_{20}$. The reaction was stirred for 2 hours before drying *in vacuo*. The solid was redissolved in minimal CH_2Cl_2 and filtered to remove to the precipitate formed. The solution was layered with dry petroleum ethers and cooled to $-25\text{ }^\circ\text{C}$. The solution was filtered and the solvent removed *in vacuo* to produce a dark yellow solid (0.938 g, 31%). ^1H NMR (500 MHz, CD_2Cl_2) 8.28 (3H, t, $J = 7.5\text{ Hz}$, *p*-Ar-H), 7.88 (6H, t, $J = 8.0\text{ Hz}$, *m*-Ar-H), 7.66 (6H, d, $J = 7.2\text{ Hz}$, *o*-Ar-H). ^{11}B NMR (160 MHz, CD_2Cl_2) -16.68 (s). ^{19}F NMR (376 MHz, CD_2Cl_2) -133.10 (8F, s, *o*-Ar-F), -163.71 (4F, t, $J = 21.2\text{ Hz}$, *p*-Ar-F), -167.56 (8F, t, $J = 18.2\text{ Hz}$, *m*-Ar-F).

N-Methylaminothiophenol

Synthesis undertaken following literature preparation,¹¹⁴ using lithium aluminium hydride (5.6922 g, 0.15 mol) and benzothiazole (22 mL, 0.20 mol) (11.965 g, 43%). ^1H NMR (500 MHz, CD_2Cl_2) 7.68 (1H, dd, $J = 7.7, 1.4\text{ Hz}$, Ar-H), 7.52 (1H, dd, $J = 7.8, 1.6\text{ Hz}$, Ar-H), 7.32 (1H, td, $J = 7.5, 1.6\text{ Hz}$, Ar-H), 7.28 (1H, td, $J = 7.5, 1.9\text{ Hz}$, Ar-H), 3.08 (3H, s, N- CH_3). This is consistent with the data in the literature.¹¹⁴

N-Methyl-2-phenylbenzothiazolium iodide

Synthesis undertaken following literature procedure.¹¹⁰ 2-Phenylbenzothiazole (0.300 g, 1.42 mmol) in a Schlenk tube fitted with Youngs' tape. Iodomethane (10 eq., 0.9 mL) was added. (0.286 g, 34%). ^1H NMR (500 MHz, CD_2Cl_2) 8.42 (1H, d, $J = 8.2\text{ Hz}$, Ar-H), 8.21 (1H, d, $J = 8.5\text{ Hz}$, Ar-H), 8.00 (2H, d, $J = 7.2\text{ Hz}$, Ar-H), 7.96 (1H, d, $J = 8.5\text{ Hz}$, Ar-H) 7.82–7.88 (2H, m, Ar-H), 7.75 (2H, t, $J = 7.5\text{ Hz}$, Ar-H), 4.46 (3H, s, N- CH_3). This is consistent with the data in the literature.¹¹⁰

2.5 X-ray crystallographic data

For each sample, crystals were suspended in oil and one was mounted on a loop and fixed into the cold stream of the diffractometer. Data were collected using either Mo-K α radiation ($\lambda = 0.71073 \text{ \AA}$) or Cu-K α radiation ($\lambda = 1.54184 \text{ \AA}$) using a Rigaku Synergy diffractometer equipped with confocal mirrors. Data were processed with CrysAlisPro,¹¹⁵ structures solved using SHELXT-2018¹¹⁶ and refined on F^2 using SHELXL-2018.¹¹⁷ Non-hydrogen atoms were refined with anisotropic thermal parameters. Hydrogen atoms bound to carbon were included in idealised positions and the U_{iso} values set to ride on the U_{eq} values of the parent atom. In **DSA1**, the two CF₃ groups were disordered and were both modelled using two components related by rotation about the carbon-carbon bond and with similarity restraints applied between the parts.

	DSI3	DSI5	DSI9	DSA1
Formula	$C_{28}H_{24}N_2S_2$	$C_{26}H_{18}Br_2N_2S_2$	$C_{28}H_{16}F_8N_2S_2$	$C_{32}H_{20}F_{12}N_2O_2S_2$
Formula weight	452.61	582.36	596.55	756.62
Crystal system	Monoclinic	Monoclinic	Triclinic	Monoclinic
Space group	$C2/c$	$C2/c$	$P\bar{1}$	$C2/c$
$a/\text{\AA}$	12.12970(10)	8.3740(2)	7.81480(10)	28.4645(16)
$b/\text{\AA}$	8.49800(10)	13.3667(3)	8.01560(10)	7.1927(4)
$c/\text{\AA}$	22.6459(2)	20.6333(5)	20.2031(2)	15.5746(12)
$\alpha/^\circ$	90	90	100.3470(10)	90
$\beta/^\circ$	102.9640(10)	97.306(2)	102.8430(10)	100.623(6)
$\gamma/^\circ$	90	90	102.8430(10)	90
$V/\text{\AA}^3$	2274.80(4)	97.306(2)	1204.38(3)	3134.0(4)
Z	4	4	2	4
T/K	100.00(10)	100.00(10)	100.00(10)	100.00(10)
Crystal size/mm	$0.128 \times 0.129 \times 0.140$	$0.042 \times 0.067 \times 0.074$	$0.090 \times 0.110 \times 0.145$	$0.039 \times 0.070 \times 0.075$
$\lambda/\text{\AA}$	1.54184	0.71073	1.54184	0.71073
$\theta/^\circ$	67.684	25.242	67.684	25.242
Reflections measured	33 594	14 141	27 449	14 625
Unique reflections	2423	3232	4912	3727
Reflections with $I > 2\sigma I$	2404	2805	4819	3008
R_{int}	0.0351	0.0698	0.0328	0.0498
No. parameters	146	145	361	283
$R_1 (I > 2\sigma I)$	0.0286	0.0290	0.0337	0.0847
wR_2 (all data)	0.0766	0.0714	0.0855	0.2385

	BNZ4	BNZ5	BNZ7	BNZ8	BNZ13
Formula	C ₂₂ H ₂₉ NOS		C ₁₄ H ₁₂ N ₂ O ₂ S		C ₁₅ H ₁₅ NS
Formula weight	355.52		272.32		241.34
Crystal system	Monoclinic		Orthorhombic		Monoclinic
Space group	<i>P</i> 2 ₁ / <i>c</i>		<i>Pbca</i>		<i>P</i> 2 ₁ / <i>c</i>
<i>a</i> /Å	13.0038(3)		7.2254(2)		8.09270(10)
<i>b</i> /Å	12.7258(3)		15.3815(4)		11.28440(10)
<i>c</i> /Å	12.1572(3)		22.3181(6)		13.78090(10)
α /°	90		90		90
β /°	92.974(2)		90		98.9960(10)
γ /°	90		90		90
<i>V</i> /Å ³	2009.11(8)		2480.39(12)		1243.01(2)
<i>Z</i>	4		8		4
<i>T</i> /K	118(20)		100.00(10)		100.1(6)
Crystal size/mm	0.060 × 0.070 × 0.112	0. × 0. × 0.	0. × 0. × 0.	0. × 0. × 0.	0.057 × 0.079 × 0.217
λ /Å	1.54184		1.54184		1.54184
θ /°	67.684		67.684		67.684
Reflections measured	25758		18609		27825
Unique reflections	4173		2613		2594
Reflections with $I > 2\sigma_I$	4003		2296		2466
R_{int}	0.0560		0.0851		0.0529
No. parameters	237		173		156
R_1 ($I > 2\sigma_I$)	0.0431		0.0501		0.0378
wR_2 (all data)	0.1194		0.1515		0.0994

	BNZS3	BNZS6 · MeCN	BNZS7	BNZS8
Formula	$2(\text{C}_{14}\text{H}_{11}\text{ClINS}), \text{ZnCl}_4$	$2(\text{C}_{14}\text{H}_{11}\text{FNS}), \text{Cl}_4\text{Zn}, \text{C}_2\text{H}_3\text{N}$	$2(\text{C}_{14}\text{H}_{10}\text{Cl}_2\text{NS}), \text{Cl}_4\text{Zn}$	$2(\text{C}_{14}\text{H}_{11}\text{BrNS}), \text{Cl}_4\text{Zn}$
Formula weight	728.66	736.82	797.55	817.58
Crystal system	Monoclinic	Monoclinic	Tetragonal	Monoclinic
Space group	$P2_1/c$	$P2_1/m$	$P4_32_12$	$P2_1/c$
$a/\text{Å}$	9.97140(10)	8.40750(10)	10.8996(3)	10.0890(4)
$b/\text{Å}$	8.73440(10)	19.7801(3)	10.8996(3)	8.7194(3)
$c/\text{Å}$	18.2837(2)	9.76190(10)	28.2128(12)	18.2561(6)
$\alpha/^\circ$	90	90	90	90
$\beta/^\circ$	93.5220(10)	96.9540(10)	90	93.326(3)
$\gamma/^\circ$	90	90	90	90
$V/\text{Å}^3$	1589.40(3)	1611.47(4)	3351.7(2)	1603.29(9)
Z	2	2	4	2
T/K	100.00(10)	126(30)	100.00(10)	100.01(10)
Crystal size/mm	$0.030 \times 0.065 \times 0.080$	$0.12 \times 0.15 \times 0.25$	$0.046 \times 0.055 \times 0.098$	$0.076 \times 0.088 \times 0.129$
$\lambda/\text{Å}$	1.54184	1.54184	1.54184	25.242
$\theta/^\circ$	67.684	67.684	67.684	0.71073
Reflections measured	25965	12395	11502	11972
Unique reflections	3328	3281	3428	3848
Reflections with $I > 2\sigma_I$	3204	2923	3232	3142
R_{int}	0.0603	0.0589	0.0298	0.0339
No. parameters	188	201	187	178
$R_1 (I > 2\sigma_I)$	0.0290	0.0472	0.0308	0.0336
wR_2 (all data)	0.1141	0.1378	0.1041	0.0887

3. Synthesis: Results and Discussion

3.1 Background

In recent years, 2-(substituted-aryl)benzothiazoles (Structure A, Figure 3.1.1) and their corresponding *N*-methyl-2-(substituted-aryl)benzothiazolines (Structure B, Figure 3.1.1) have been examined for many different synthetic applications. These include acting as protecting groups for aldehydes and ketones,¹¹⁸⁻¹¹⁹ hydride donors¹²⁰ (discussed further in Section 5.1), and amine oxidants.¹²¹ Additionally, these compounds have been investigated for their antifungal,¹²² antimicrobial and antispermatogenic activity,¹²³ and used as non-steroidal anti-inflammatory¹²⁴ and anti-tumour agents.¹²⁵⁻¹²⁷ There have been several synthetic routes reported for the formation of these molecules which will be discussed later in this chapter. *N*-methylbenzothiazolium salts are of particular interest. Specifically, Thioflavin T (Figure 3.1.2), has been used as a fluorescent dye in aggregation assays for amyloid fibril formation, which is associated with Alzheimer's disease,¹²⁸ and previously shown to have anthelmintic properties.¹²⁹ Many of their uses have been observed within nature. In 2017, Ingleson and co-workers reported the use of *N*-methyl-2-(aryl)benzothiazolium salts (Structure C, Figure 3.1.1) as carbon Lewis acids for the activation of Si-H σ -bonds¹¹⁰ (discussed further in Section 5.1).

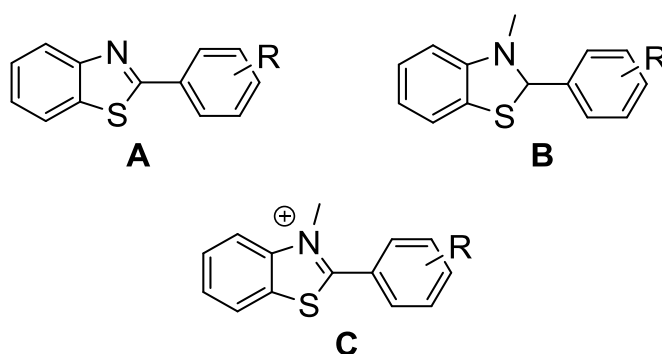


Figure 3.1.1 – General structure for 2-(aryl)benzothiazole (A), *N*-methyl-2-(aryl)benzothiazoline (B), and *N*-methyl-2-(aryl)benzothiazolium cation (C)

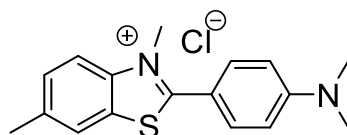
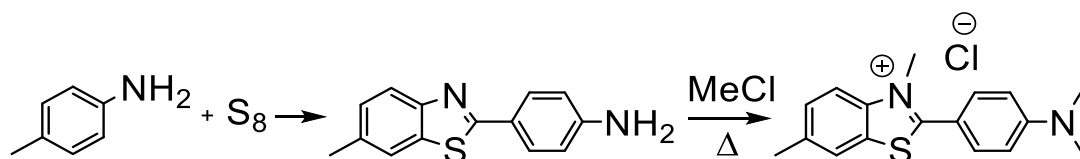


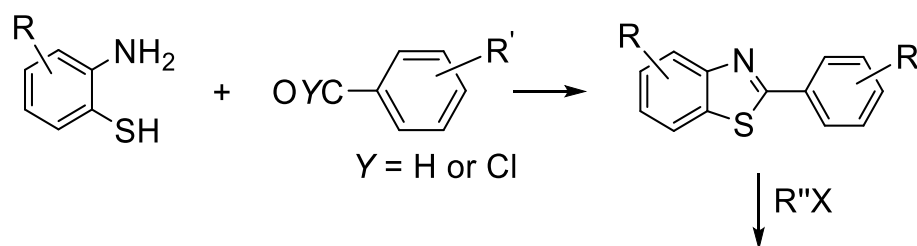
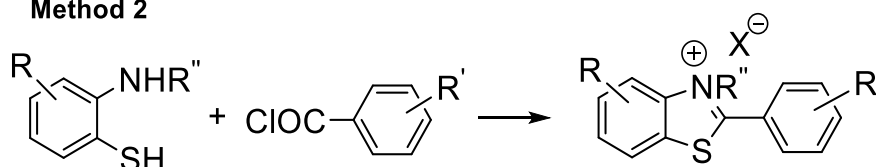
Figure 3.1.2 - The structure of Thioflavin T, used as a fluorescent dye¹²⁸

In 1889, the original synthetic method for Thioflavin T was reported.¹³⁰ This involved the condensation of sulfur with 4-methylaniline and the subsequent addition of methyl chloride at high temperatures to produce the chloride salt (Scheme 3.1.1).



Scheme 3.1.1 - The synthetic route for the synthesis of Thioflavin T¹³⁰

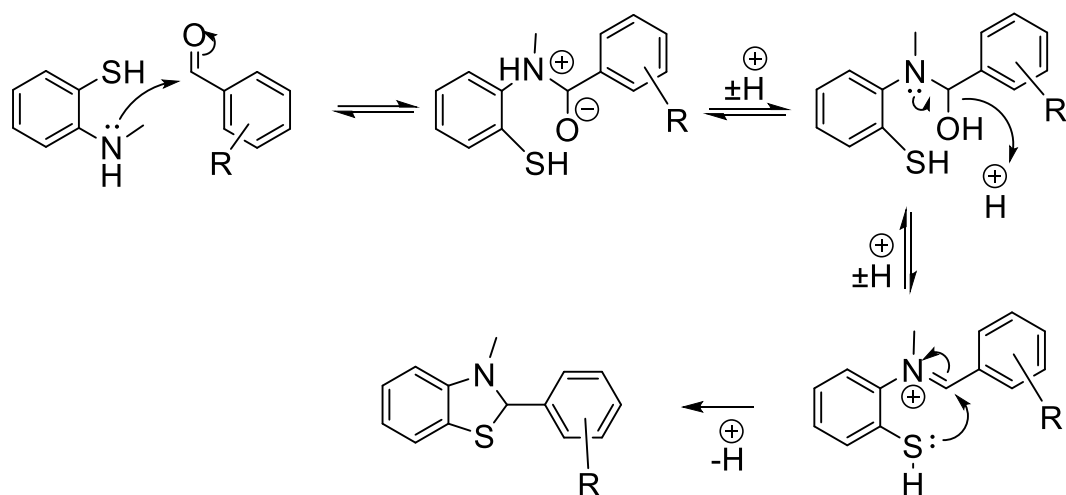
It is notable that the synthesis was conducted at high temperatures and as such probably afforded decomposition products. In 1889, chemists did not have the same spectroscopic equipment that is available today i.e. NMR, so the proposed synthesis of this product is questionable. This was also corroborated by the reported difficulty in reproducing this compound and its analogues.¹²⁹ In 1969, Garmaise and co-workers reported 2 new synthetic routes for benzothiazolium salts to overcome this limitation, using 2-aminothiophenol or an *N*-alkylaminothiophenol as reactants (Scheme 3.1.2), with a range of different R groups including methyl, ethyl and chloro groups, R' as 4-dimethylamino, R'' as a methyl group and X as a halogen. Again, it should be noted that the only data supporting the assignment of these compounds was the melting point and elemental analysis.

Method 1**Method 2**

Scheme 3.1.2 - The synthetic routes for the formation of the benzothiazolium salt¹²⁹

In the procedure (Scheme 3.1.2, Method 1), a condensation reaction between the substituted 2-aminothiophenol and a substituted benzaldehyde or benzoyl chloride gave the desired benzothiazole; subsequently the intermediate underwent alkylation of the endocyclic nitrogen to form the desired *N*-alkylbenzothiazolium salt. However, a second proposed synthetic pathway prepared the product directly via a condensation reaction of a substituted *N*-methylaminothiophenol and a substituted acid chloride (Scheme 3.1.2, Method 2) to form the *N*-alkylbenzothiazolium salt. It can be noted that the starting materials differ; when a primary amine was used (Method 1), it was reacted with either an aldehyde or an acid chloride, but in the case of a secondary amine (Method 2), the amine was reacted with an acid chloride. It is not stated whether the use of an acid chloride is significant for the reaction with a secondary amine.

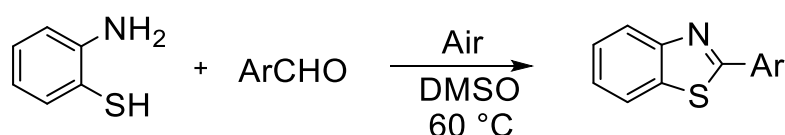
In 2008, Tang and co-workers outlined a synthetic route for *N*-methyl-2-(aryl)benzothiazolines, using *N*-methylaminothiophenol and substituted benzaldehydes or ketones (Scheme 3.1.3). The reactions were undertaken in ethanol at room temperature, or under reflux with catalytic amounts of concentrated hydrochloric acid.¹³¹



Scheme 3.1.3 – Mechanism for the synthesis of *N*-methyl-2-(aryl)benzothiazolines, from *N*-methylaminothiophenol and a substituted benzaldehyde

Akiyama and co-workers have since reported a similar route for the synthesis of 2-(aryl)benzothiazolines, from the reaction of 2-aminothiophenol with 2-naphthaldehyde or benzaldehyde in ethanol at room temperature.¹³² Around this time, several other methods were reported, which used catalysts such as ZnO nanoparticles,¹³³ nano-CeO₂¹³⁴ and ABM (Animal Bone Meal).¹³⁵

In 2016, Hu and co-workers reported a catalyst-free route for benzothiazole synthesis; optimal conditions included a slight excess of aldehyde in DMSO at 60 °C¹³⁶ (Scheme 3.1.4).

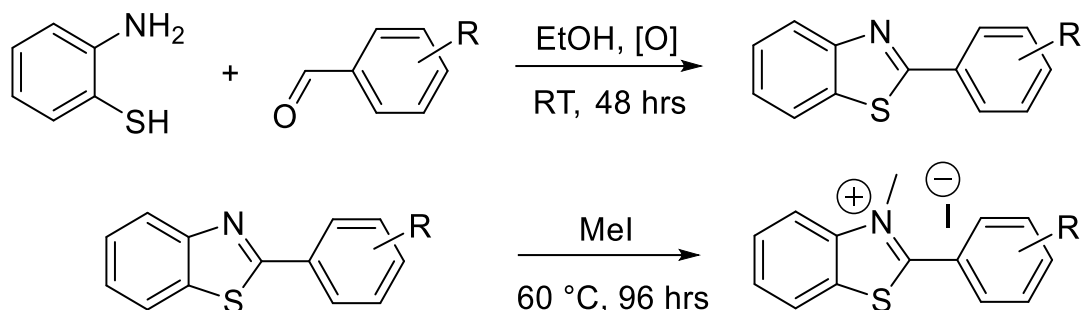


Scheme 3.1.4 – The synthesis of a 2-substituted-benzothiazole, from 2-aminothiophenol and a substituted benzaldehyde, using air as the oxidant¹³⁶

DMSO is an aprotic solvent that has been used in organic synthesis^{137–138} and has previously played a cooperative role with other oxidants.^{139–142} It was reported that under a nitrogen atmosphere there was no formation of 2-phenylbenzothiazole and so it was assumed that the oxygen is key for the final oxidation.¹³⁶

Soon after, in 2017, Ingleson and co-workers reported a different route for the synthesis (Scheme 3.1.5), similar to those reported by Garmaise *et al.* and Akiyama *et al.*, with respect

to the starting point of 2-aminothiophenol, but also similar to the detailed route of Tang *et al.* with regards to reaction conditions.



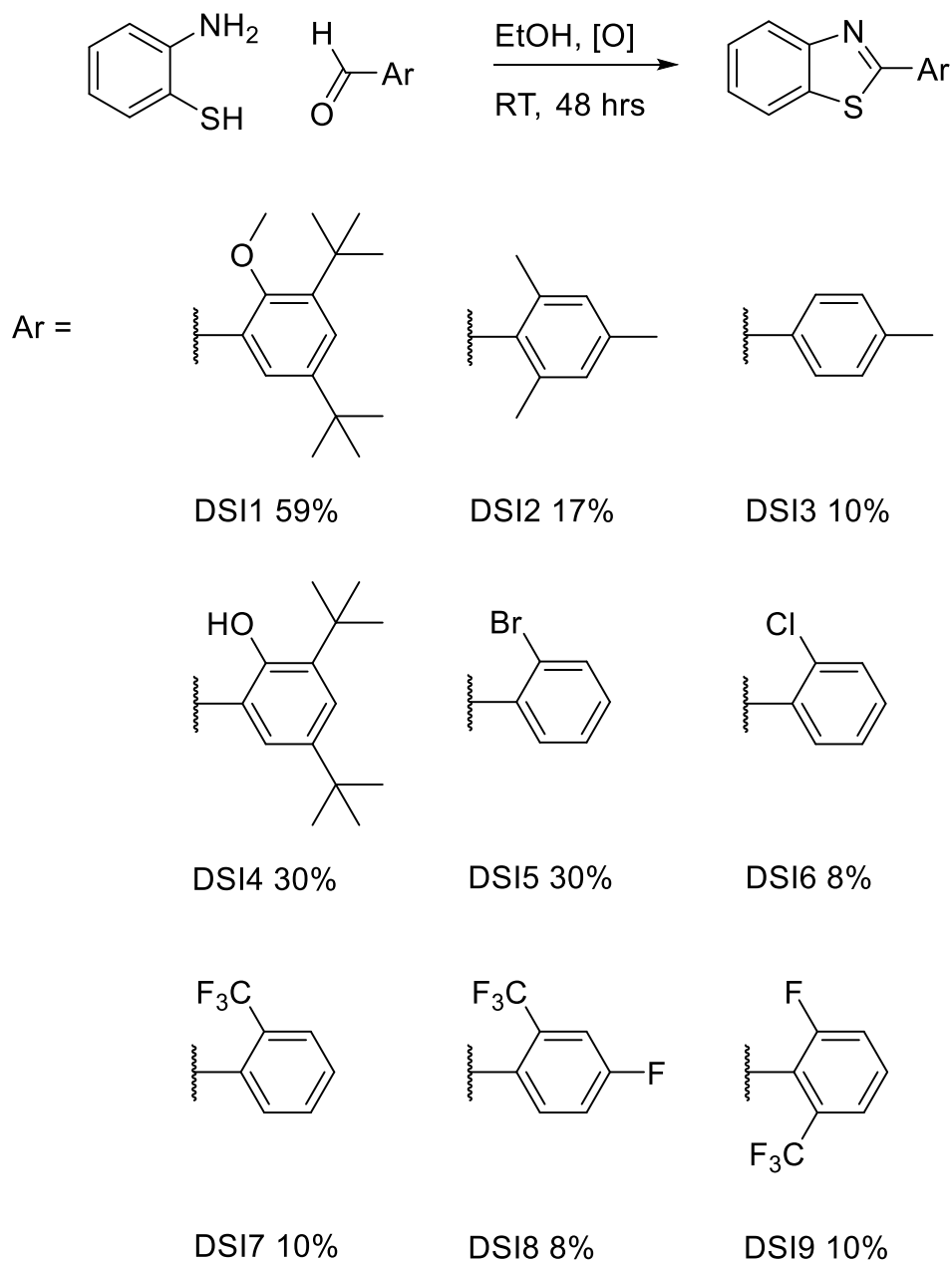
Scheme 3.1.5 – The synthetic route for the formation of 2-(aryl)benzothiazoles, and subsequent formation of *N*-methyl-2-(aryl)benzothiazolium salts, after the addition of methyl iodide¹¹⁰

Garmaise and co-workers reported moderate to high yields (30–86%) working on a multi-gram scale (17–170 g). Akiyama and co-workers worked on a much smaller, relatively dilute conditions (mmol in 16 mL of ethanol) and produced moderate yields (42–71%). Tang and co-workers produced results with a moderate to high yield (43–97%) with a molar ratio of 1:1 with respect to *N*-methylaminothiophenol and benzaldehyde, but did not report the scale of the reactions. Ingleson and co-workers reported the successful synthesis of multiple benzothiazoles, in relatively dilute conditions (mmol in 30 mL ethanol) with moderate reported yields. Although the yields reported by Garmaise were good, it would not be financially viable to do such synthesis on such a big scale. It was deemed unnecessary to carry out these experiments on a scale that big as those quantities weren't needed for this work.

Following the general procedure reported by Ingleson *et al.*, and modifying it where required, my aim was to synthesise several novel *N*-methyl-2-(aryl)benzothiazolines and their corresponding *N*-methyl-2-(aryl)benzothiazolium salts to see if they could be used as hydride shuttles in conjunction with an FLP system for electrocatalytic hydrogen oxidation.

3.2 Synthesis of dithiol-linked, aryl-substituted compounds

Following the procedure by Ingleson *et al.*, 2-aminothiophenol was reacted with a variety of substituted benzaldehydes (Scheme 3.2.1) but the expected benzothiazole was not formed.



Scheme 3.2.1 – Synthetic route for the synthesis of 2-(aryl)benzothiazoles, from 2-aminothiophenol and substituted benzaldehydes

The synthesis was undertaken using ethanol as the solvent and under oxidative conditions (air was bubbled through the reaction for 48 h).¹¹⁰ A condensation reaction occurred between the nitrogen of the 2-aminothiophenol and the carbonyl group of the substituted benzaldehyde. The oxidative conditions were needed in order to form the benzothiazole instead of the benzothiazoline.¹³⁶ A benzothiazole was necessary in order for the nitrogen to be methylated using methyl iodide.¹¹⁰ Methylation of the nitrogen increased the electrophilicity of the C2 position, and it was this position which was the intended target for fine-tuning with the addition of electron-donating or electron-withdrawing groups on the C2 aromatic ring. However, the oxidative conditions used in these reactions were found to potentially aid the formation of a disulfide bridge, which caused the dimer to precipitate. Table 3.2.1 shows the different disulfide imines formed and their yields. Table 3.2.2 shows the proton NMR shift for the C2 proton, specifically examining the imine or benzothiazoline, the most reliable diagnostic for the NMR confirmation of the desired products. The C2-*H* position in the benzothiazoline (Structure A, Figure 3.2.1) and the di-thiol-linked, substituted-aryl compounds (Structure B, Figure 3.2.1) have been labelled.

Table 3.2.1 - The ¹H NMR shift, in ppm, of the C2 proton for the different substituted-aryl rings; showing the shift for the five-membered ring, the imine and the synthesised product. Data taken from website nmrd.org

Substituted aryl ring	Predicted NMR shift of C2- <i>H</i> (ppm)		C2- <i>H</i> NMR shift for synthesised molecule (ppm)
	Benzothiazoline	Imine	
Mesityl	6.12	8.88	8.92
4-tolyl	6.12	8.83	8.48
3,5-di- <i>tert</i> -butyl-2-hydroxy	5.89	8.91	8.70
2-bromo	6.20	8.91	8.92
3,5-di- <i>tert</i> -butyl-2-methoxy	5.84	8.90	7.82
2-chloro	6.18	8.93	8.98
2-(trifluoromethyl)	6.36	8.91	8.87
4-fluoro-2-(trifluoromethyl)	6.25	8.87	8.80
6-fluoro-2-(trifluoromethyl)	6.35	8.98	8.75

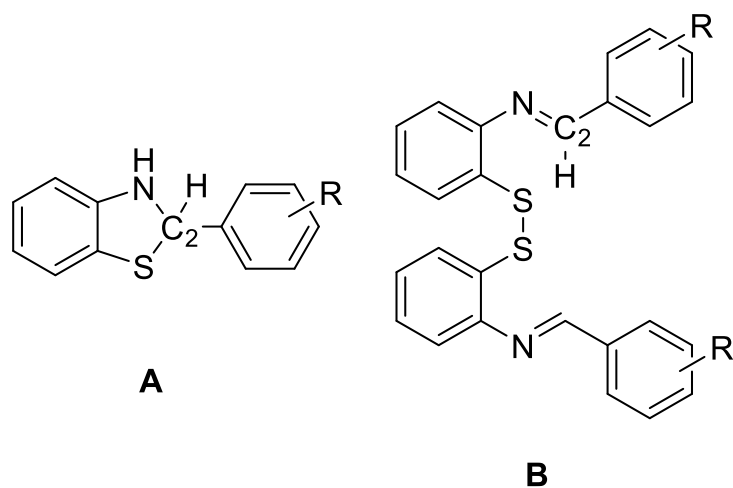


Figure 3.2.1 – General structure for 2-(aryl)benzothiazoline (A) and di-thiol-linked, substituted-aryl compounds (B), showing the C2-*H*

It can be noted that the chemical NMR shift for the synthesised molecules closely matched those of the calculated chemical shifts for imines. While the NMR shifts in Table 3.2.1 were calculated using computational analysis (molecules were drawn and proton shifts were predicted by the software from the website nmrdb.org), this data and interpretation was confirmed by X-ray analysis for **DSI3**, **DSI5** and **DSI9** (4-tolyl, 2-bromo and 6-fluoro-2-(trifluoromethyl) respectively) (Figures 3.2.2, 3.2.3 and 3.2.4).

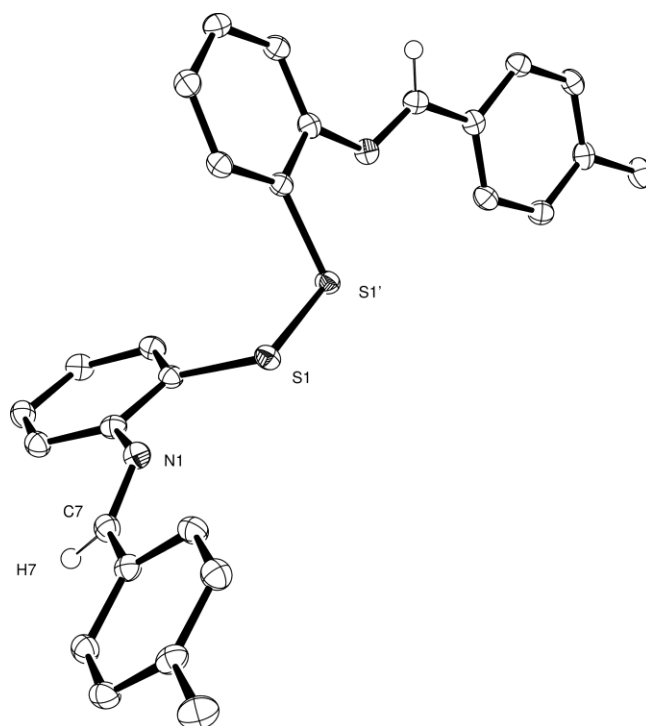


Figure 3.2.2 - ORTEP representation of the structure of **DS13** showing 50% probability ellipsoids; hydrogen atoms other than H(7) (hydrogen attached to the C7 carbon) have been omitted for clarity.

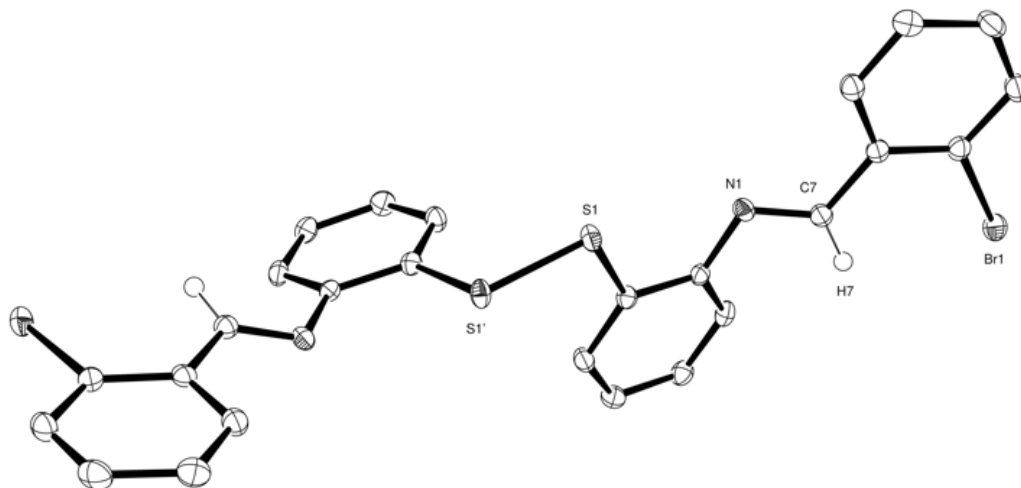


Figure 3.2.3 - ORTEP representation of the structure of **DS15** showing 50% probability ellipsoids; hydrogen atoms other than H(7) (hydrogen attached to the C7 carbon) have been omitted for clarity.

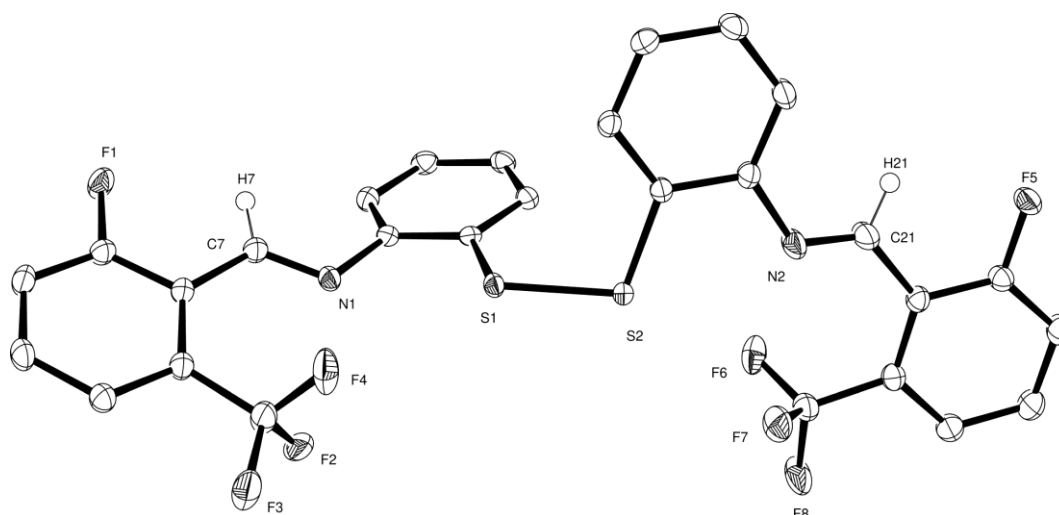


Figure 3.2.4 - ORTEP representation of the structure of **DSI9** showing 50% probability ellipsoids; hydrogen atoms other than H(7) (hydrogen attached to the C7 carbon) have been omitted for clarity.

This indicates that the published method for the synthesis of 2-(aryl)benzothiazole molecules¹¹⁰ was not successful for these analogues. This could be due to the electron-withdrawing ability of many of the benzaldehydes and their inherent loss of electrophilicity and/or steric hinderance surrounding the C2 position, which may be inaccessible for the incoming sulfur nucleophile. The stability of the disulfide may also have contributed to the alternative reaction pathway. As oxygen was bubbled through the reaction mixture for 48 h, the sulfur would have been oxidised to the more stable disulfide. Additionally, oxidation to a disulfide is an uncatalysed reaction and can happen spontaneously over time. Once the oxidation occurred the resulting compound was stable, and it precipitated out of solution. This precipitation would have driven the equilibrium to favour the undesired disulfide product. As the imine was lacking in solution, it would not have been possible for cyclisation and benzothiazoline formation to occur from a sulfur nucleophilic attack of the C2 carbon. Another possibility is that the starting material was, in fact, the disulfide and not the 2-aminothiophenol it was thought to be. This would need to be proven by NMR and would be indicated by the loss of the *S-H* peak. This would mean that although the condensation reaction could take place, the resulting stable compound would precipitate out of solution.

Table 3.2.2 shows the important bond lengths in these set of molecules taken from the x-ray crystallographic data. The disulfide bond in all three imine structures and the amide compound are in accordance with the literature which describes an average S–S bond of 2.05 Å.¹⁴³ The carbon-nitrogen bond length for all three imine compounds lies close to the typical bond length for a carbon-nitrogen double bond of 1.27 Å.¹⁴⁴ The carbon-carbon bond of all three imine compounds lies between the average bond length of a carbon-carbon single

bond and a carbon-carbon double bond (1.541 Å and 1.337 Å respectively).¹⁴⁴ However the data is closer to that of a carbon-carbon single bond and so the structure in Figure 3.2.6 is seen to be correct. In contrast, the data for the carbon-carbon bond for the amide compound (**DSA1**) is much closer to the literature value for a carbon-carbon single bond. However, the carbon-nitrogen bond for this compound lies between that of a carbon-nitrogen single bond and a carbon-nitrogen double bond (1.27 Å and 1.49 Å respectively).¹⁴⁴ This is likely due to resonance (Figure 3.2.5). The carbon-oxygen bond in the amide compound compares well with the literature (1.215(5) Å and 1.23 Å respectively)¹⁴⁴ but is shorter than the average carbon-oxygen double bond. This could be due to the electron-withdrawing effect of the two trifluoromethyl groups on the aryl ring (Figure 3.2.7). The N-C-C bond angles for the three imine compounds are close to that of an sp²-hybridised carbon (120°) and therefore have trigonal planar geometry.

Table 3.2.2 – The S-S, C-N and C-C bond lengths of the various disulfide-linked, aryl-substituted imine compounds (**DSI3**, **DSI5** and **DSI9**) and the dithiol-linked aryl-substituted amide compound (**DSA1**)

Compound	S-S disulfide bond length (Å)	C7-N (C21-N) imine double bond length (Å)	C7-C8 (C21-C22) bond length (Å)	N-C7-C8 (N-C21-C22) angle (°)
DSI3	2.0430(5)	1.277(2)	1.462(2)	123.2(1)
DSI5	2.0425(8)	1.281(2)	1.465(2)	123.01(16)
DSI9	2.0389(5)	1.270(2) (1.211(2))	1.475(2) (1.479(2))	124.91(14) (127.64(16))
DSA1	2.0294	1.373(5)	1.511(5)	-

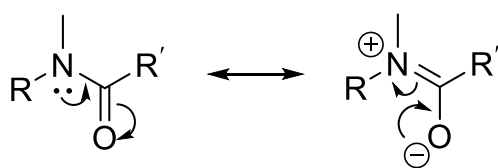


Figure 3.2.5 – The resonance forms of the amide compound, **DSA1**

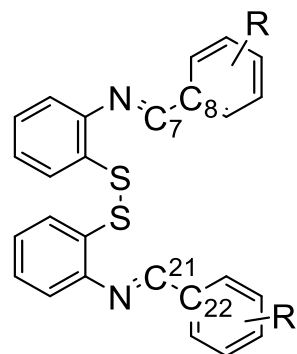
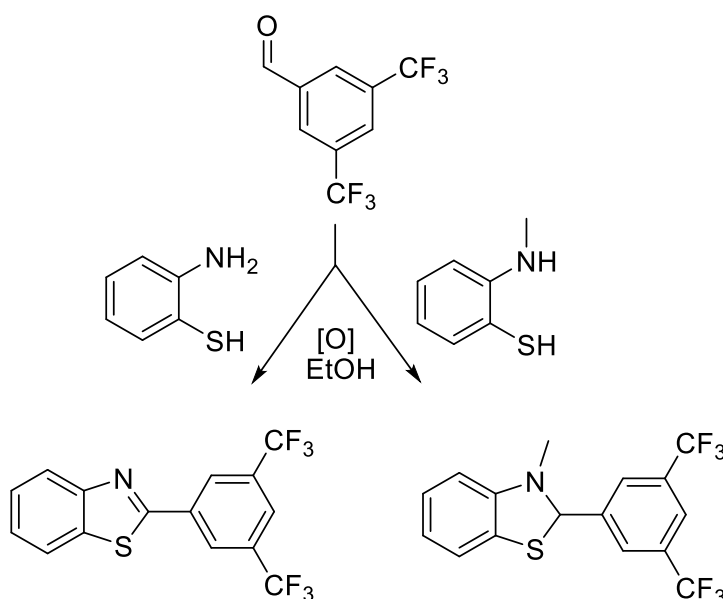


Figure 3.2.6 – The generic molecular drawing for the disulfide-linked, substituted-aryl imine compounds, highlighting the important carbon atoms

The synthesis of 2-(3,5-bis(trifluoromethyl)phenyl)benzothiazole and *N*-methyl-2-bis(3,5-(trifluoromethyl)phenyl)benzothiazoline were attempted using 2-aminothiophenol and *N*-methylaminothiophenol respectively, with 3,5-bis(trifluoromethyl)benzaldehyde under oxidative conditions (see Scheme 3.2.2).



Scheme 3.2.2 - Planned synthetic route to 2-(3,5-bis(trifluoromethyl)phenyl)benzothiazole (left) and *N*-methyl-2-bis(3,5-bis(trifluoromethyl)phenyl)benzothiazoline (right).

The addition of zinc acetate and a few drops of hydrochloric acid have previously been shown to aid the formation of benzothiazolium salts (discussed in Section 3.4) when using electron-withdrawing substituents on the benzaldehyde. However, when similar conditions were used for the synthesis of the 3,5-(trifluoromethyl)phenyl, the solution turned black overnight and no precipitation was observed. The synthesis was repeated, with initial heating. Overnight, a precipitate started to form but again the solution darkened in colour. ^1H NMR spectroscopic

observations suggested that the benzothiazolium zinc salt had formed (no C2-H peak present in ^1H NMR spectrum). However, after single crystal growth, it was confirmed to be *N,N*-(dithiodi-2,1-phenylene)bis[3,5-bis(trifluoromethyl)-*N*-methyl]benzamide (**DSA1**) (Figure 3.2.7). This could have been due to the initial heating as the relative rate of amide formation is faster than that of the corresponding benzothiazoline. Again, starting from a secondary amine meant that imine formation was not possible in this instance. In the cases of no reaction occurring, it is most likely that the substituted benzaldehyde was oxidised overnight to form the substituted benzoic acid,¹⁴⁵ which is far less reactive than the corresponding aldehyde. This means that the carbon is far less electrophilic in the benzoic acid than the benzaldehyde, meaning that attack from the nucleophilic nitrogen was far less likely, no intended product was noted and the solution turned black under the oxidative conditions.

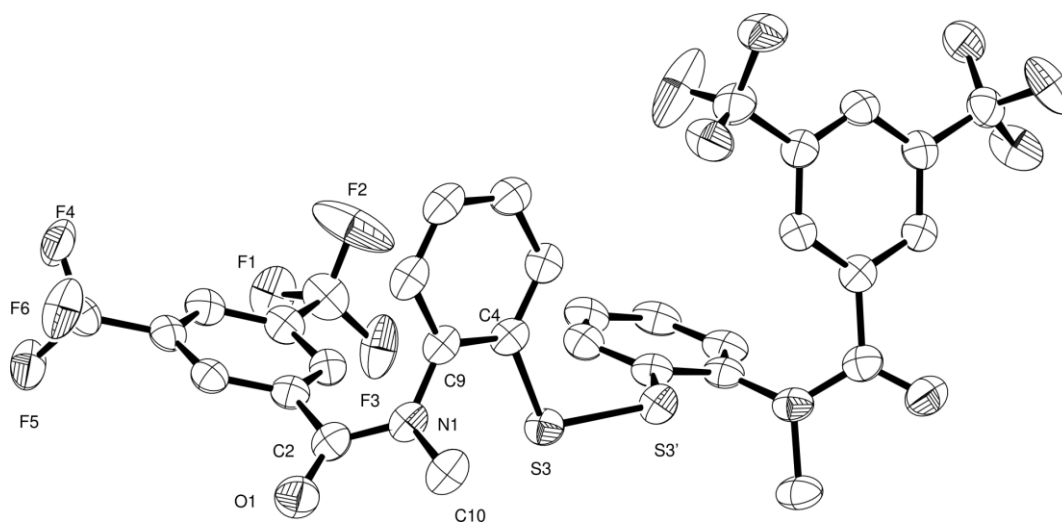


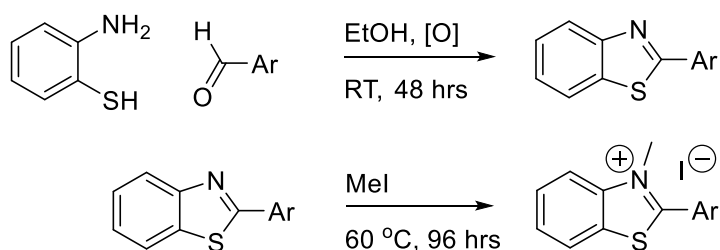
Figure 3.2.7 - ORTEP representation of the structure of **DSA1** showing 50% probability ellipsoids; hydrogen atoms have been omitted for clarity.

An alternative preparative scheme, avoiding the use of secondary amines would be to form the 2-(aryl)benzothiazole, followed by a methylation step. Preparation of 2-(4-nitrophenyl)benzothiazole was successful, however the subsequent methylation step was not feasible. This was possibly due to the electron-withdrawing ability of the nitro group on the substituted aryl ring. While using a stronger methylating agent, such as methyl triflate or trimethyloxonium tetrafluoroborate, could have been considered as an alternative, a different strategy was adopted. The methylation was fine-tuned by starting with *N*-methylaminothiophenol and reacting this with different benzaldehydes to form the desired *N*-methyl-2-(aryl)benzothiazolines.

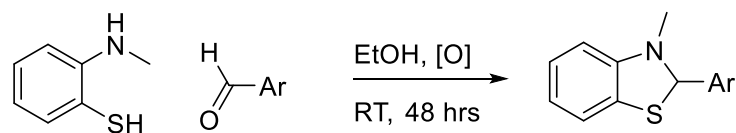
3.3 Synthesis of *N*-methyl-2-(aryl)benzothiazolines

The preparation published by Ingleson and co-workers used 2-aminothiophenol as the starting material, and required a subsequent methylation step to produce *N*-methyl-2-(aryl)benzothiazolium iodide salts (Scheme 3.3.1).¹¹⁰ These salts would then need to undergo reduction in order to form the corresponding *N*-methyl-2-(aryl)benzothiazoline. Starting from *N*-methylaminothiophenol meant that no further methylation was required (Scheme 3.3.2).

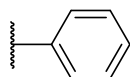
Synthesis of *N*-methylaminothiophenol involved a condensation reaction with 2-aminothiophenol and formaldehyde to form benzothiazole as a colourless oil after distillation. Reduction of the benzothiazole using lithium aluminium hydride afforded the yellow solid product of *N*-methylaminothiophenol.¹¹⁴ However, it was very difficult working with a viscous, yellow oil, and the distillation afforded a very low yield of a colourless oil. As such, this step was skipped and commercially available benzothiazole was used as a starting material.



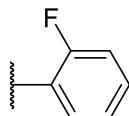
Scheme 3.3.1 – Two step reaction scheme: 1) 2-aminothiophenol and a substituted benzaldehyde to produce 2-(aryl)benzothiazole; 2) methylation to produce *N*-methyl-2-(aryl)benzothiazolium iodide salt¹¹⁰



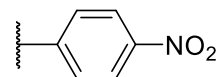
Ar =



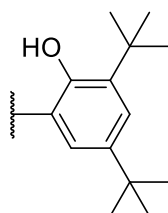
BNZ1 48%



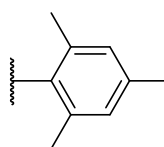
BNZ2



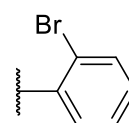
BNZ3 53%



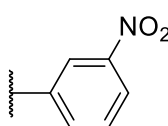
BNZ4 55%



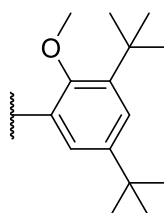
BNZ5 8%



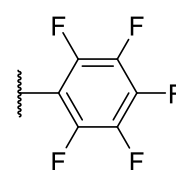
BNZ6 55%



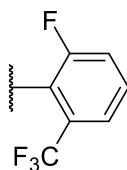
BNZ7 62%



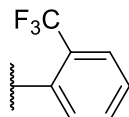
BNZ8 49%



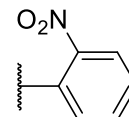
BNZ9 15%



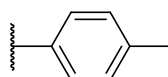
BNZ10 22%



BNZ11



BNZ12 50%



BNZ13 35%

Scheme 3.3.2 – Reaction scheme of *N*-methylaminothiophenol and a substituted benzaldehyde to produce *N*-methyl-2-(aryl)benzothiazoline

N-methylaminothiophenol was synthesised from benzothiazole following a literature procedure¹¹⁴ and then reacted with a variety of substituted benzaldehydes to form the *N*-methyl-2-(aryl)benzothiazoline (see Scheme 3.3.2). These condensation reactions were successful, forming the five-membered ring of the *N*-methyl-2-(aryl)benzothiazoline rather than the imine formed previously, due to the use of a secondary amine. Instead of a hydrogen, the nitrogen is bonded to a methyl group and cannot undergo further oxidation. This synthetic route was successful, and in most cases very quick, resulting in electron-donating substituents (3,5-di-*tert*-butyl-2-hydroxy, **BNZ4** (Figure 3.3.1), and 3,5-di-*tert*-butyl-2-methoxy, **BNZ8** (Figure 3.3.2)) and various nitro groups substituents, **BNZ3** (Figure 3.3.3), **BNZ7** (Figure 3.3.4) and **BNZ12** (Figure 3.3.5). All the compounds gave satisfactory ¹H NMR spectroscopic data with the presence of the indicative C2 proton and *N*-methyl proton peaks in accordance with the literature, where the C2-*H* ranges from 2.64–3.52 ppm and the *N*-methyl protons range from 5.95–6.90 ppm.¹⁴⁶ The different substituents will have a slightly different effect on the C2 proton, which can be seen in Table 3.3.2, with a shift of 5.91–6.53 ppm. This is due to the electron-withdrawing/electron-donating ability of the substituents, and their proximity to the proton. This can be seen with the difference in the C2 proton shift between the different-positioned nitro groups. The proximity of the 2-nitro significantly increased the proton chemical shift. The 2-nitro substituent has a greater effect; being strongly electron withdrawing, and in closer proximity to the proton, the proton is more deshielded, and hence the observed chemical shift is further downfield.

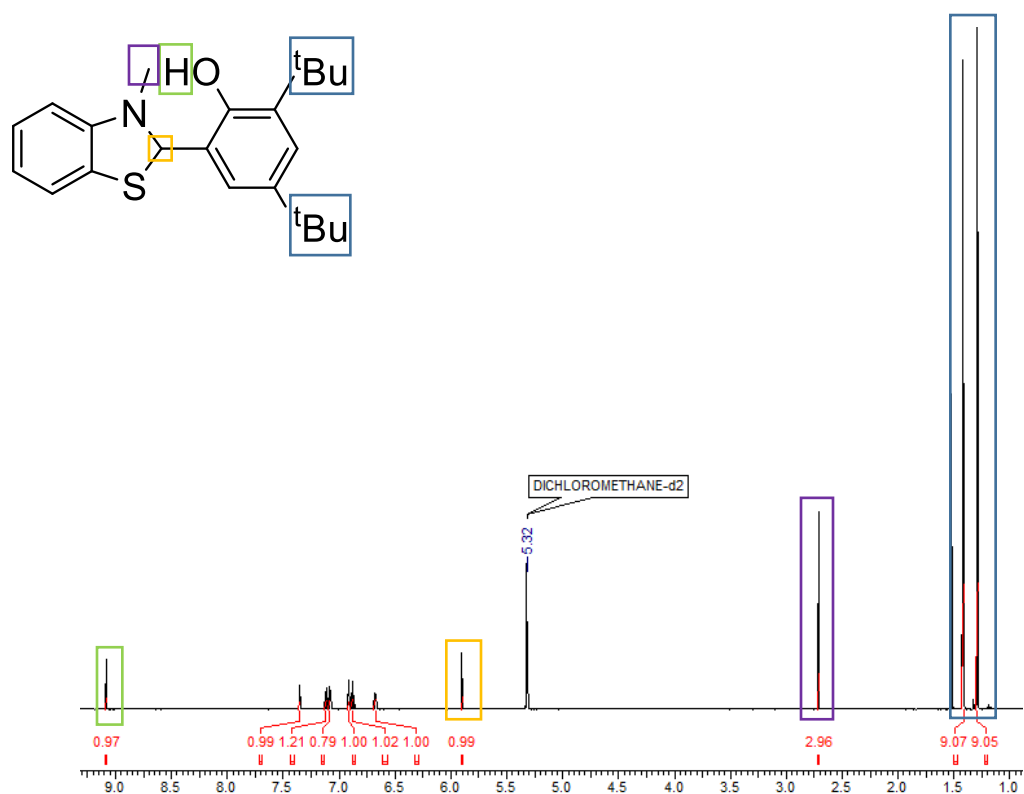


Figure 3.3.1 - The ¹H NMR spectrum of *N*-methyl-2-(3,5-di-*tert*-butyl-2-hydroxyphenyl)benzothiazoline, **BNZ4**

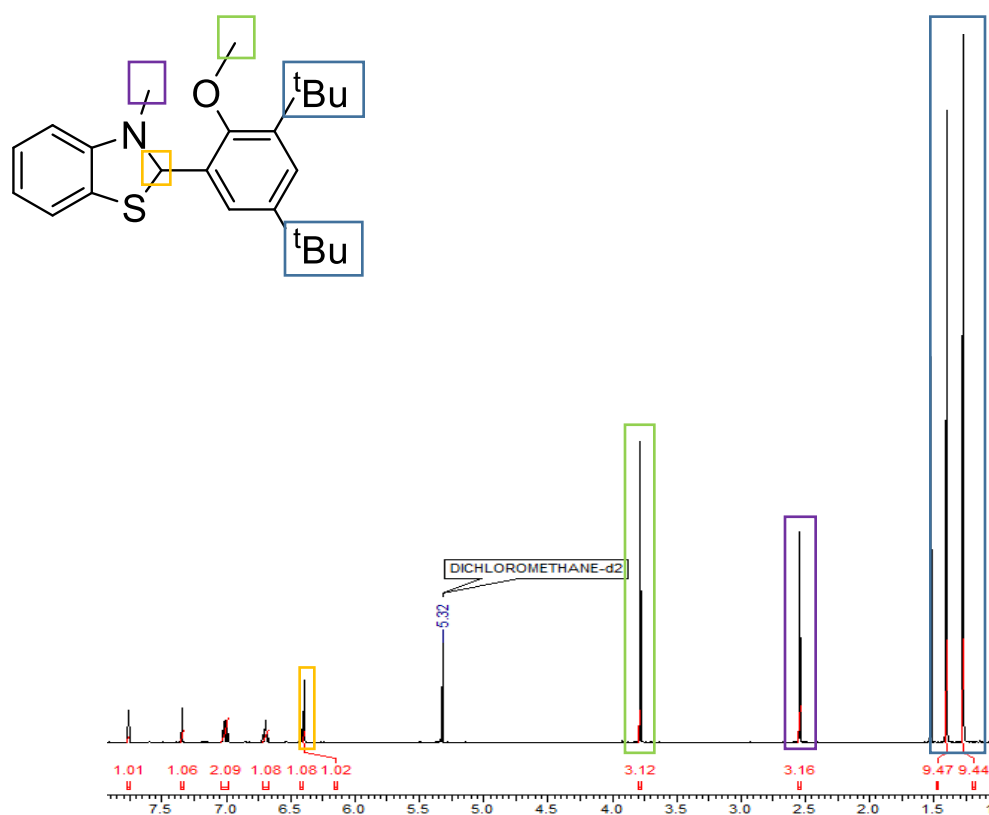


Figure 3.3.2 – The ¹H NMR spectrum of *N*-methyl-2-(3,5-di-*tert*-butyl-2-methoxyphenyl)benzothiazoline, **BNZ8**

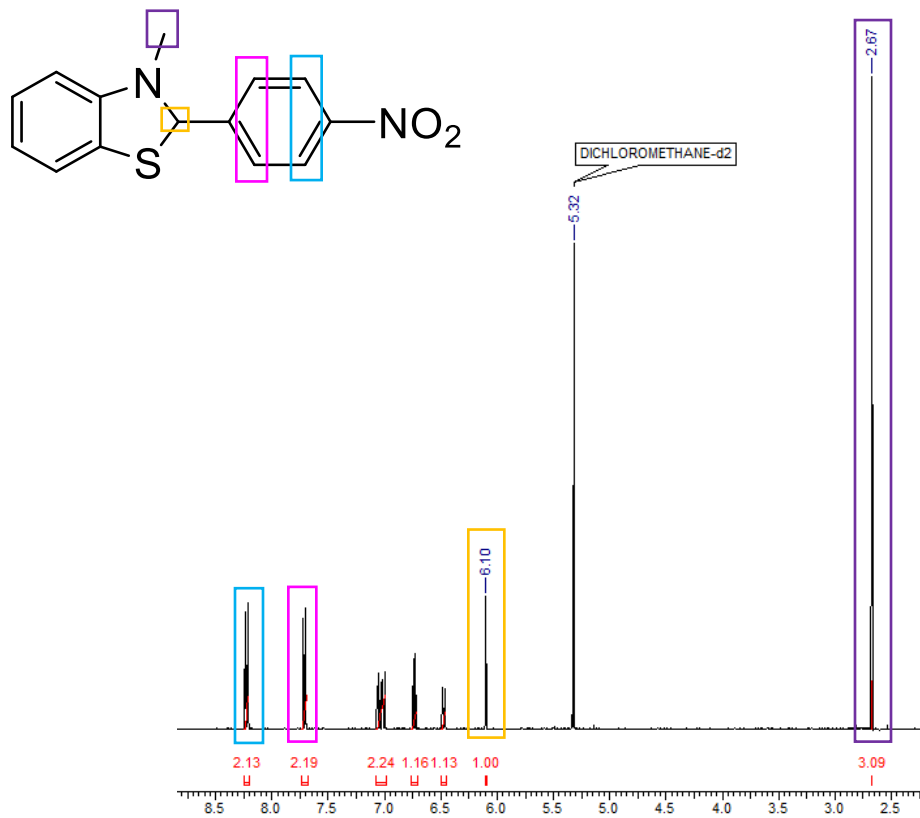


Figure 3.3.3 – The ¹H NMR spectrum of *N*-methyl-2-(4-nitrophenyl)benzothiazoline, **BNZ3**

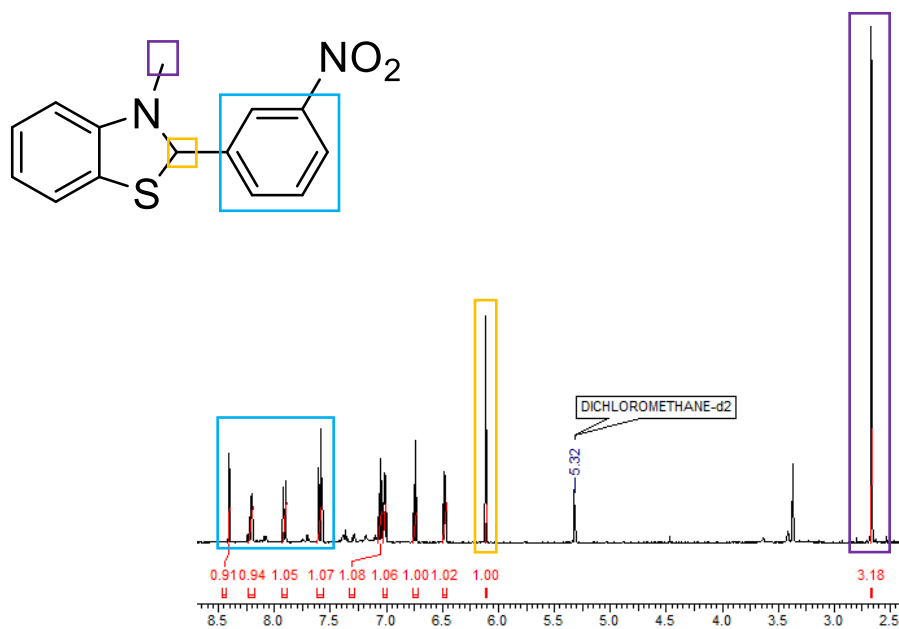


Figure 3.3.4 – The ¹H NMR spectrum of *N*-methyl-2-(3-nitrophenyl)benzothiazoline, **BNZ7**

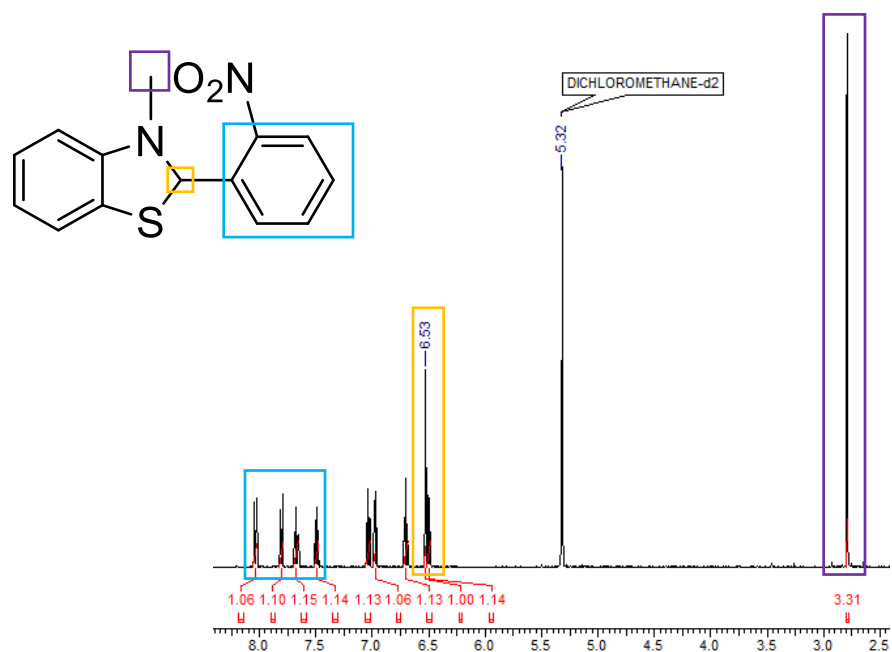


Figure 3.3.5 - The ^1H NMR spectrum of *N*-methyl-2-(2-nitrophenyl)benzothiazoline, **BNZ12**

Table 3.3.1 - ^1H NMR shifts for the C2 proton and *N*-methyl protons of the various synthesised *N*-methyl-2-(aryl)benzothiazolines

Phenyl substituent	^1H NMR shift of C2-H (ppm)	^1H NMR shift of N-CH ₃ (ppm)
3,5-di- <i>tert</i> -butyl-2-hydroxy, BNZ4	5.91	2.72
3,5-di- <i>tert</i> -butyl-2-methoxy, BNZ8	6.39	2.54
4-nitro, BNZ3	6.10	2.67
3-nitro, BNZ7	6.11	2.67
2-nitro, BNZ12	6.53	2.79

X-ray quality crystals were obtained for various *N*-methyl-2-(aryl)benzothiazoline compounds (Figures 3.3.6 to 3.3.10).

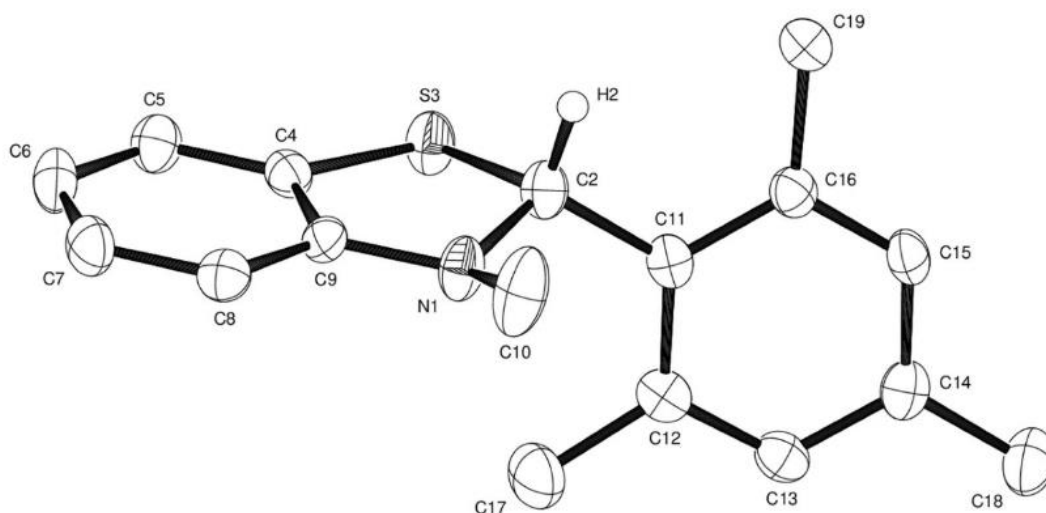


Figure 3.3.6 - ORTEP representation of the structure of **BNZ5** showing 50% probability ellipsoids; hydrogen atoms other than H(2) have been omitted for clarity.

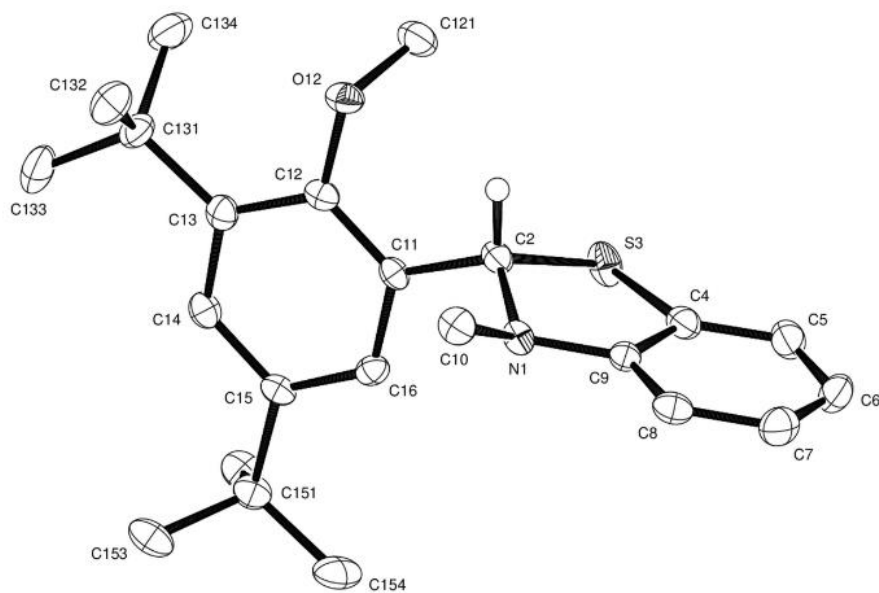


Figure 3.3.7 - ORTEP representation of the structure of **BNZ8** showing 50% probability ellipsoids; hydrogen atoms have been omitted for clarity.

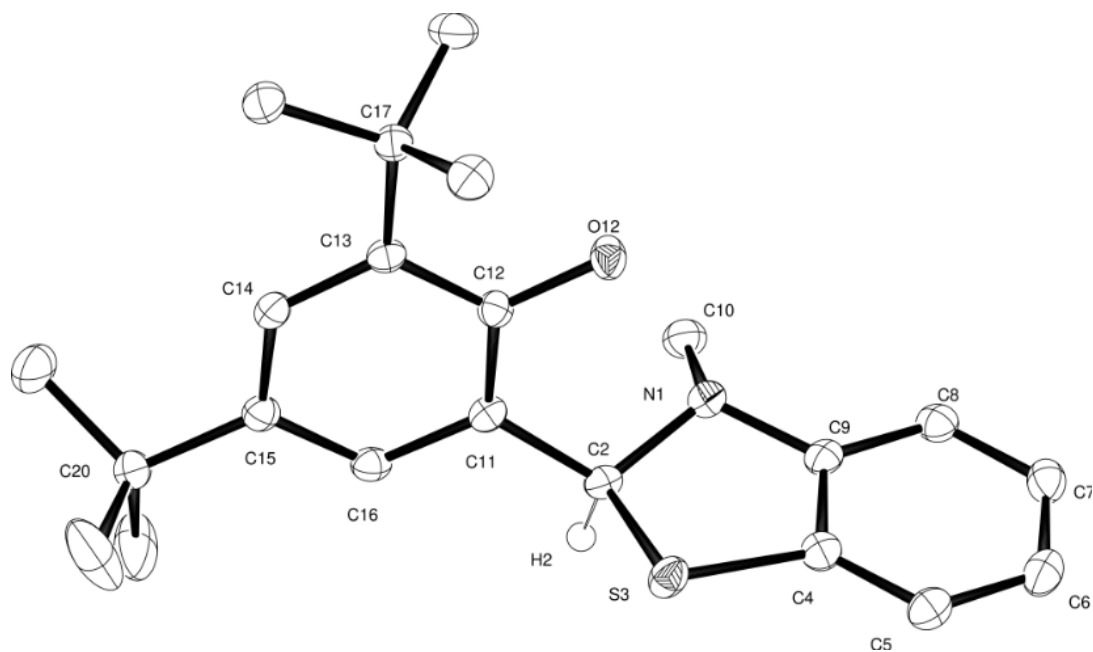


Figure 3.3.8 - ORTEP representation of the structure of **BNZ4** showing 50% probability ellipsoids; hydrogen atoms other than H(2) have been omitted for clarity.

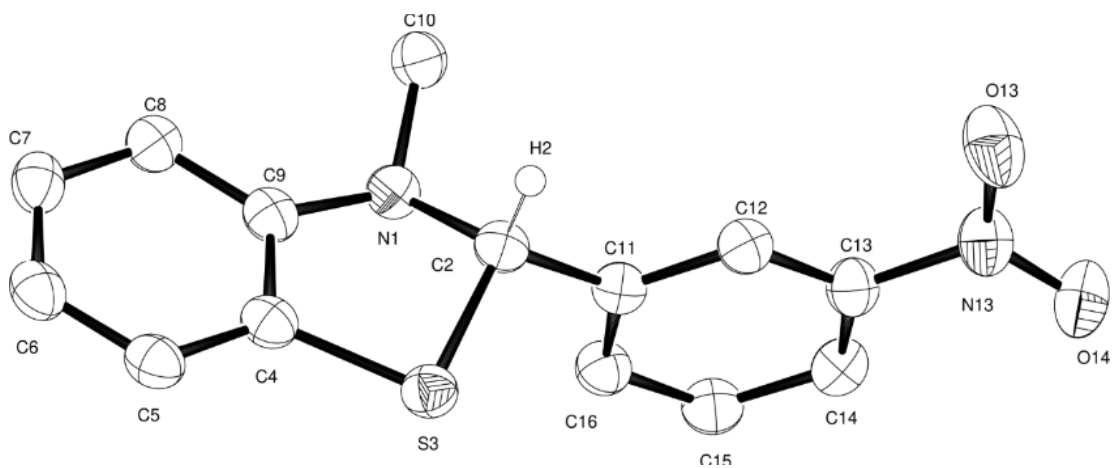


Figure 3.3.9 - ORTEP representation of the structure of **BNZ7** showing 50% probability ellipsoids; hydrogen atoms other than H(2) have been omitted for clarity.

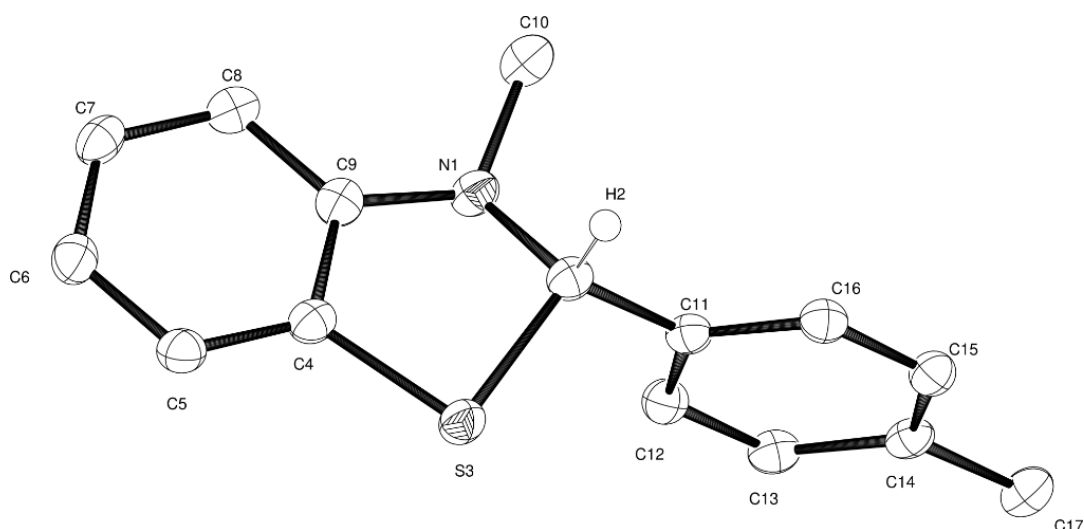


Figure 3.3.80 - ORTEP representation of the structure of **BNZ13** showing 50% probability ellipsoids; hydrogen atoms other than H(2) have been omitted for clarity.

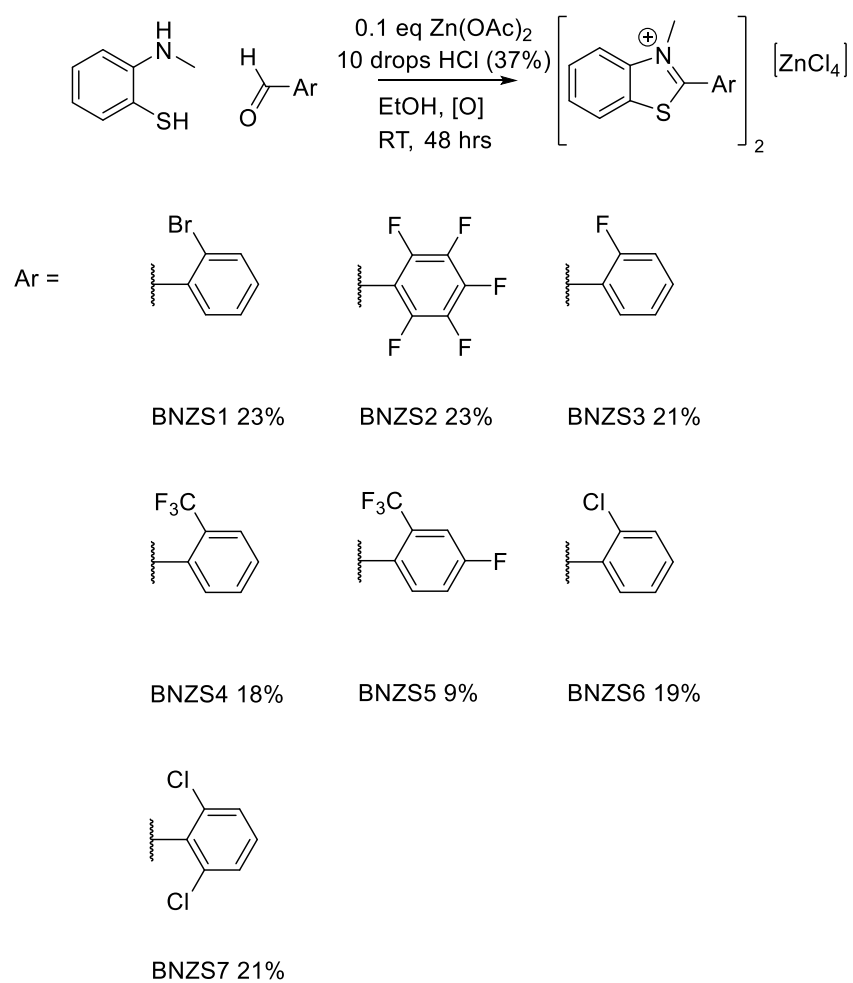
Crystallographic data for the (methyl)carbon-nitrogen bond and (C2) carbon-nitrogen bond are indicative of carbon-nitrogen single bonds (literature value of average carbon-nitrogen single bond is 1.49 Å).¹⁴⁴ However, the (methyl)carbon-nitrogen bond of the compounds with purely electron-donating substituents (BNZ5 and BNZ13) are significantly shorter than the (methyl)carbon-nitrogen bond for the compounds that have a mixture of electron-donating and electron-withdrawing substituents (BNZ4 and BNZ8) or purely electron-withdrawing substituents (BNZ7). The carbon-carbon bonds for these compounds also closely match that found for a carbon-carbon single bond (1.541 Å).¹⁴⁴ This carbon-carbon bond lengths do not vary much between the molecules, from electron-donating substituents (BNZ5 and BNZ13 in Table 3.3.3), to a mixture of substituents (BNZ8 and BNZ4 in Table 3.3.3), to electron-withdrawing substituents (BNZ7 in Table 3.3.3).

Table 3.3.2 – The important N–C and C–C bonds in the various *N*-methyl-2-(substituted-phenyl)benzothiazolines compounds.

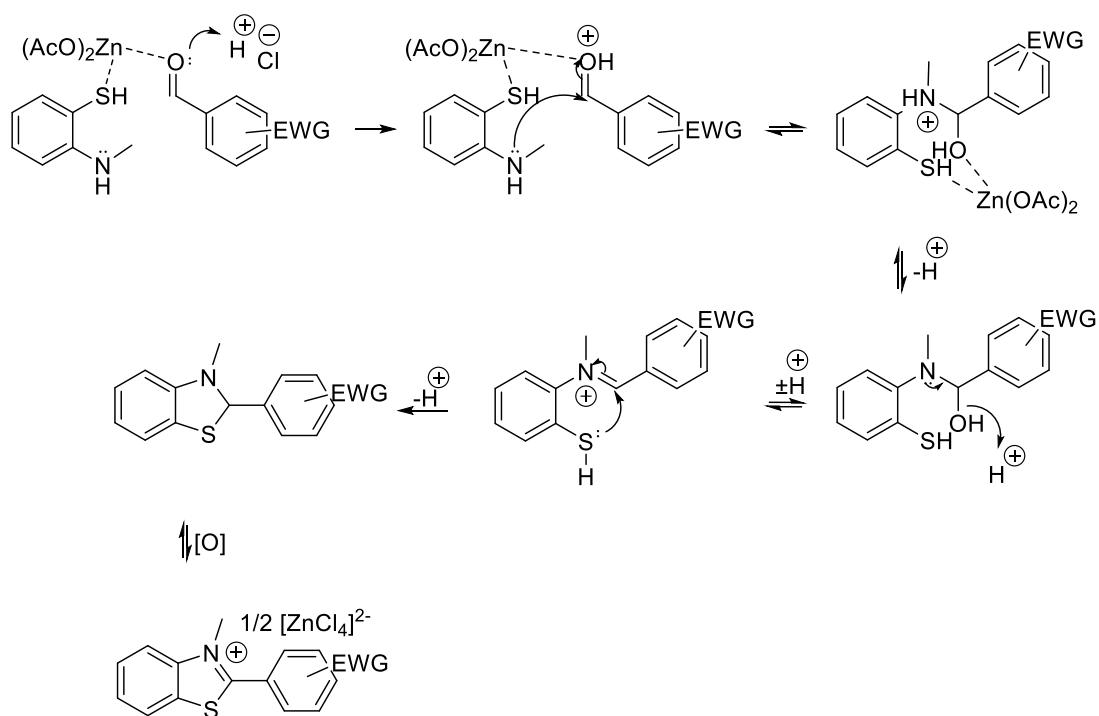
Compound	N–C (methyl) bond length (Å)	N–C2 bond length (Å)	C2–C(aryl) bond length (Å)
BNZ5	1.414(3)	1.460(3)	1.514(3)
BNZ13	1.431(2)	1.470(2)	1.511(2)
BNZ8	1.457(6)	1.466(6)	1.516(7)
BNZ4	1.457(2)	1.477(2)	1.512(2)
BNZ7	1.453(3)	1.461(2)	1.512(2)

3.4 Synthesis of [*N*-methyl-2-(aryl)benzothiazolium] tetrachlorozincate

An alternative synthetic route to synthesise *N*-methyl-2-(aryl)benzothiazolines via an [*N*-methyl-2-(aryl)benzothiazolium] tetrachlorozincate salt was undertaken using zinc acetate as a soft Lewis acid and hydrochloric acid to help initiate the reaction (Scheme 3.4.1). This was due to difficulties with some electron-withdrawing substituted benzaldehydes not undergoing the condensation reaction to form the required product. The mechanism for the reaction involving zinc acetate and hydrochloric acid is shown in Scheme 3.4.2. The salt was then treated with a hydride source, usually sodium triethylborohydride, to reduce the benzothiazolium to the benzothiazoline. An anion exchange reaction between the initial zinc salts formed and Li[BArF₂₀] was uncomplicated and would have afforded the desired [*N*-methyl-2-(aryl)benzothiazolium][BArF₂₀] salts. This approach was preferable to the reduction to the benzothiazoline and oxidation to the BArF₂₀ salt using trityl BArF₂₀.



Scheme 3.4.1 – Reaction scheme of *N*-methylaminothiophenol with an electron-withdrawing substituted benzaldehyde to produce *N*-methyl-2-arylbenzothiazolium tetrachlorozincate salt



Scheme 3.4.2 – Mechanism for the formation of the [N-methyl-2-(aryl)benzothiazolium] tetrachlorozincate salt, from *N*-methylaminothiophenol and electron-withdrawing-substituted benzaldehyde, initiated by hydrochloric acid and the addition of zinc acetate

X-ray quality crystals were obtained for various [N-methyl-2-(aryl)benzothiazolium] tetrachlorozincate salts (Figures 3.4.1 to 3.4.4).

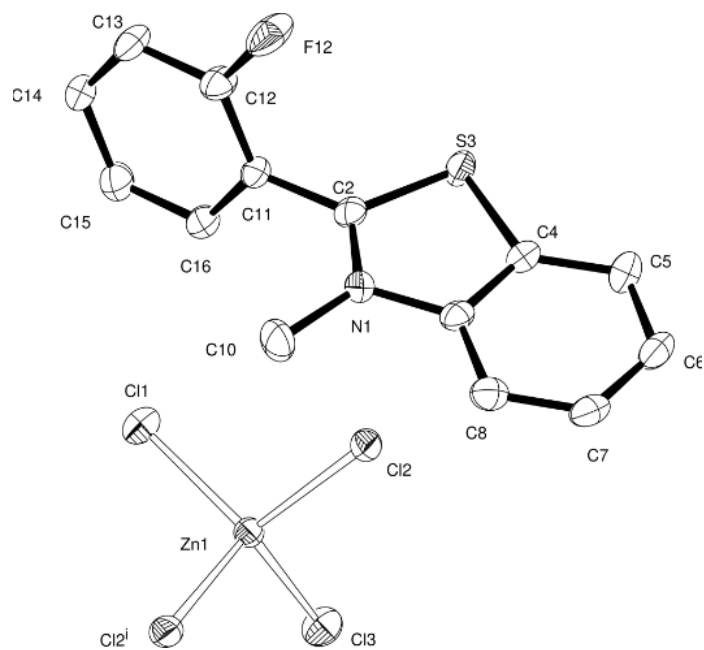


Figure 3.4.1 - ORTEP representation of the structure of **BNZS3** showing 50% probability ellipsoids; hydrogen atoms have been omitted for clarity.

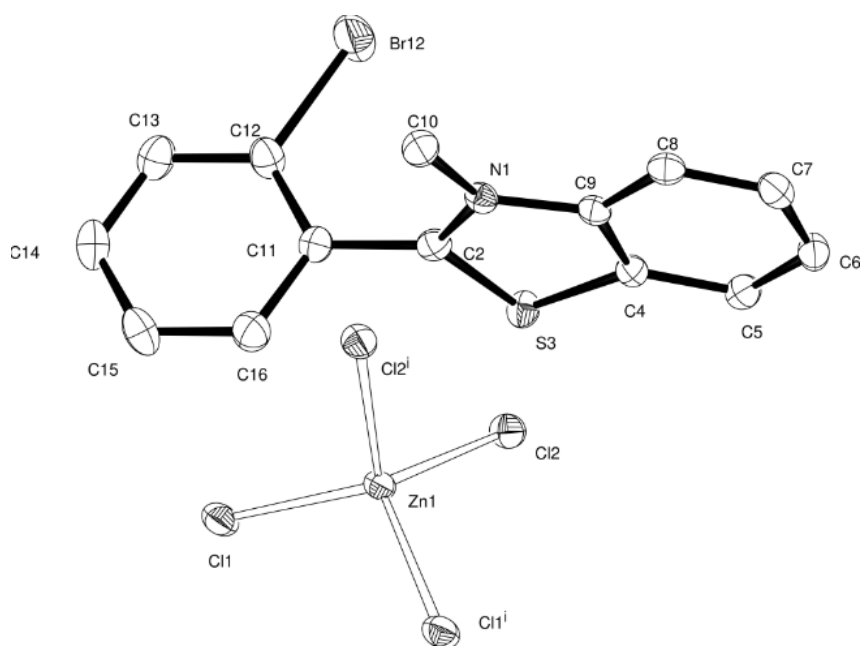


Figure 3.4.2 - ORTEP representation of the structure of **BNZS8** showing 50% probability ellipsoids; hydrogen atoms have been omitted for clarity.

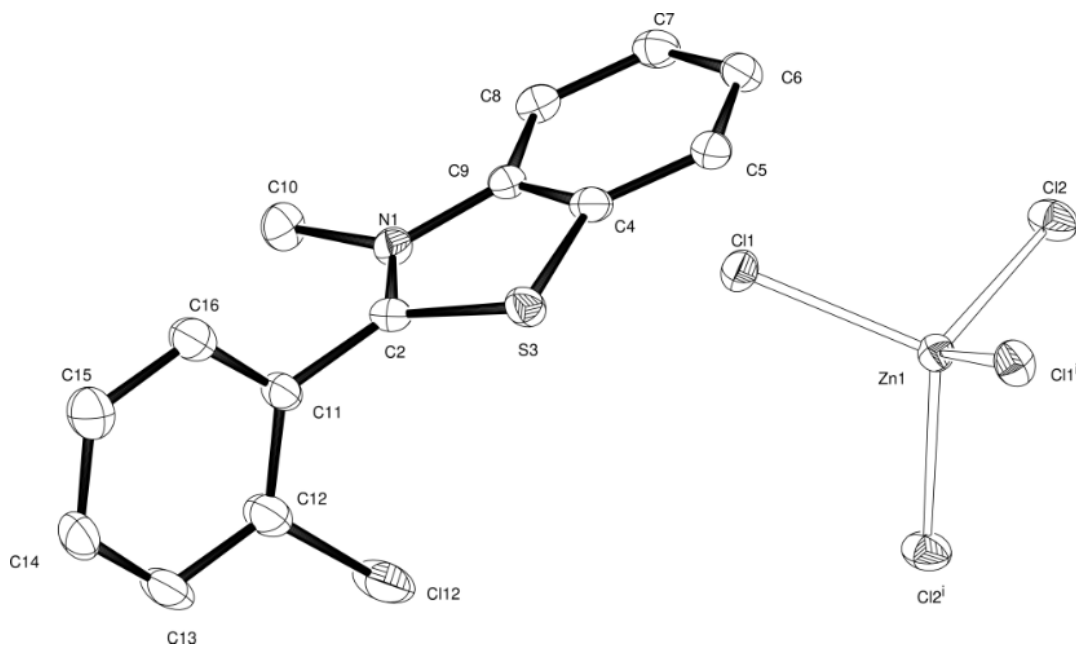


Figure 3.4.3 - ORTEP representation of the structure of **BNZS6** showing 50% probability ellipsoids; hydrogen atoms have been omitted for clarity.

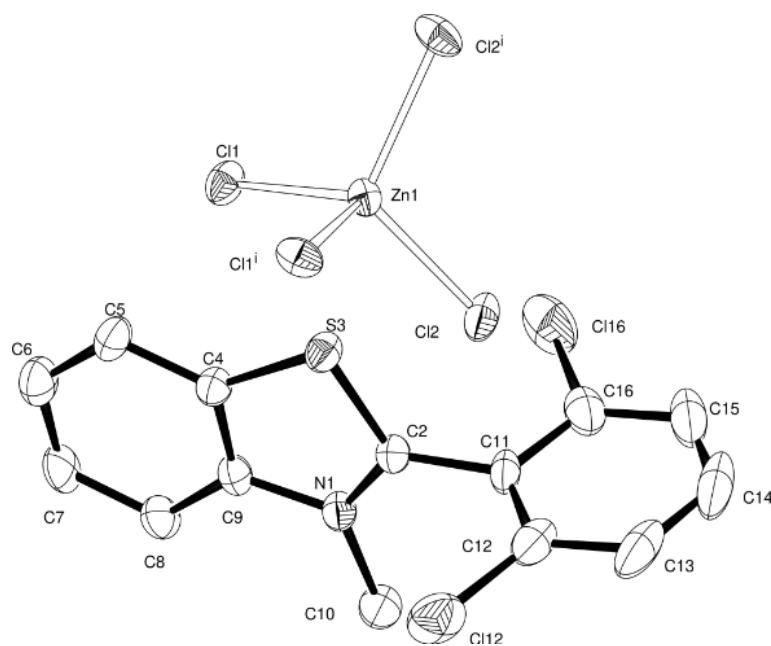


Figure 3.4.4 - ORTEP representation of the structure of **BNZS7** showing 50% probability ellipsoids; hydrogen atoms have been omitted for clarity.

The (C10) carbon-nitrogen bond length is close to that of an average carbon-nitrogen single bond (1.49 Å).¹⁴⁴ The (C2) carbon-nitrogen bond is closer to that of a carbon-nitrogen double bond (1.27 Å).¹⁴⁴ This would suggest that the positive charge is held on the nitrogen, generating the iminium ion and a carbocation is not formed (see Figure 3.4.5).

Table 3.4.1 – The important N–C and C–C bond lengths for the different [*N*-methyl-2-(aryl)benzothiazolium] $\frac{1}{2}$ [zinc tetrachloride] salts

Compound	N–C10 bond length (Å)	N–C2 bond length (Å)	C2–C11 bond length (Å)
BNZS3	1.461(4)	1.319(4)	1.482(3)
BNZS8	1.471(3)	1.324(3)	1.480(3)
BNZS6	1.472(2)	1.315(2)	1.483(2)
BNZS7	1.470(5)	1.320(5)	1.478(5)

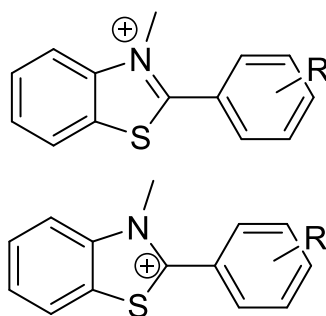


Figure 3.4.5 – Iminium formation (top) and carbocation formation (bottom) in the formation of the *N*-methyl-2-(substituted-phenyl)benzothiazolium cation

Table 3.4.2 also shows the carbon-carbon bond lengths for these molecules lie between the average carbon-carbon single bond and carbon-carbon double bond (1.541 Å and 1.337 Å respectively)¹⁴⁴ but more towards the single bond length. This is consistent with the formation of the iminium cation (Figure 3.4.5 – Top).

3.5 Synthesis of [*N*-methyl-2-(aryl)benzothiazolium][BARF₂₀] salts

As a model for the electrochemical investigations, the introduction of a BARF anion was explored. This was achieved for *N*-methyl-2-(4-nitrophenyl)benzothiazoline with the addition of trityl BARF₂₀. The trityl cation was a strong enough oxidant to abstract the hydride from the C2 position, forming [*N*-methyl-2-(4-nitrophenyl)benzothiazolium][BARF₂₀] and trityl hydride. This was evidenced by the loss of the proton signal at 6.10 ppm, and the shift of the *N*-methyl signal from 2.67 ppm to 4.32 ppm in the ¹H NMR spectrum. This downfield shift of the methyl signal is due to the nitrogen forming a double bond with the C2 position, as the cation is formed.

The electron-withdrawing effect of the nitro group made the abstraction of the hydride using trityl BARF₂₀ possible. The nitro group withdraws electron density from the benzene ring, which in turn withdraws electron density away from the C2 carbon. This allowed for the abstraction of the hydride, due to the change in polarity of the C–H bond. It could be proposed that this method of forming the benzothiazolium salt would work for any of the electron-withdrawing benzothiazolines. This avenue requires further exploration.

It was found that trityl was not a strong enough hydride abstractor when trying to oxidise *N*-methylbenzothiazolines with electron-donating substituents. The donation of electron density generated insufficient polarisation of the C2–H bond and was therefore too strong a bond to break. Also, the compounds *N*-methyl-2-(3,5-di-*tert*-butyl-2-hydroxyphenyl)benzothiazoline (**BNZ4**) and *N*-methyl-2-(3,5-di-*tert*-butyl-2-methoxyphenyl)benzothiazoline (**BNZ8**) include an oxy *ortho*-substituent which may have helped stabilise the molecule through resonance and therefore these molecules are unlikely to oxidise to form the benzothiazolium. Potentially, a stronger hydride abstractor would need to be used in this case to form the benzothiazolium salt.

Due to the above challenges associated with synthesising the benzothiazolium with electron-donating groups, an alternate strategy attempting to synthesise the [*N*-methyl-2-(aryl)benzothiazolium] tetrachlorozincate salts was explored. These products could undergo an anion exchange reaction to form the desired [*N*-methyl-2-(aryl)benzothiazolium][BARF₂₀] that was needed to execute the hydrogen experiments. However, the formation of the benzothiazoline was kinetically favourable and formed quickly – in preference to the benzothiazolium formation.

4. Electrochemistry

In cyclic voltammetry an applied potential at the working electrode is swept from a start potential to an upper potential and back to a stop potential, at a constant scan rate. The measured flow of current is plotted against the applied potential to produce the resulting cyclic voltammogram (Figure 4.1).

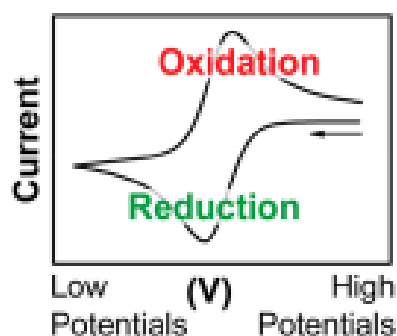


Figure 4.1 – IUPAC convention for electrochemistry. (Taken from reference 146)

Figure 4.1 shows reversibility, with reduction and oxidation waves of equal size. The asymmetric-shaped voltammogram is a result of multiple factors which include the concentrations of the redox couple relative to the distance from the electrode surface and the dependence on the applied potential, and how the species move between the electrode surface and bulk solution. As the potential is scanned cathodically (negatively), the oxidised species at the electrode surface is depleted as it is reduced. Where the cathodic peak current is observed, the current is dictated by the diffusion of the oxidised species to the electrode surface from the bulk solution. The volume of solution containing the newly reduced species at the electrode surface is called the diffusion layer, and this continues to grow throughout the scan. This slows the mass transport of oxidised species to the electrode surface. Upon scanning to more negative potentials, the rate of diffusion of the oxidised species to the electrode surface becomes slower which results in a decrease in current as the scan continues. When a switching potential is reached, the direction of the scan is reversed and is scanned in a positive direction (anodically). The concentration of reduced species at the electrode surface is high, and is oxidised back as the potential becomes more positive. In the opposite fashion, where the anodic peak current is observed the current is dictated by the diffusion of the reduced species to the electrode surface from the bulk solution. The mass transport of the reduced species is slowed by the diffusion layer of the newly formed oxidised species. With increasing (more positive) potentials the rate of diffusion of the reduced

species becomes slower which results in a decrease in current. This results in the observed asymmetrical shape of the cyclic voltammogram.¹⁴⁷

4.1 Electrochemical equilibria

Like chemical reactions, the direction of an electrochemical process is also governed by thermodynamics. When a system is in equilibrium, its Gibbs free energy is minimised. When an electrode, such as platinum wire, is put in the system, the solution now has a source of electrons and an electrochemical equilibrium is reached at the surface of the electrode. This equilibrium is responsible for the difference in charge at the electrode surface and the solution. This is known as the electrode potential $(\varphi_m - \varphi_s)_{Pt}$. It is impossible to measure an electrode potential for a single electrode-solution interface and so an additional electrode is required. This is known as a reference electrode $(\varphi_m - \varphi_s)_{Ref} = 0$ V. With the addition of the reference electrode, the electrode potential (E) at the platinum wire-solution interface can be measured, $E = (\varphi_m - \varphi_s)_{Pt} - (\varphi_m - \varphi_s)_{Ref}$. The electrochemical analysis in this project uses a silver wire as a reference electrode. However, the potential difference across the silver wire-solution interface is not constant; the electrode potential can drift slightly due to corrosion, adsorption etc., and so the measured electrode potential must be referenced. The accepted convention is to correct the potentials to the ferrocene/ferrocenium couple ($Cp_2Fe^{0/+}$).¹⁴⁸

The Nernst equation relates the measured reduction potential (E) of an electrochemical process to its standard reduction potential (E^0), in terms of the activities of the oxidised and reduced forms at the electrode surface. The activities, γ_x , of the oxidised and reduced species are used instead of concentrations because of solution non-uniformity due to solvent-ion and ion-ion interactions. However, for ideal solutions the activity coefficient, γ , would approach unity. Below is the Nernst equation for the electrochemical reduction of A to B ($A + e^- \rightleftharpoons B$).¹⁴⁹⁻¹⁵⁰

$$E = E^0 - \frac{RT}{nF} \ln \frac{\gamma_B[B]}{\gamma_A[A]}$$

E = measured electrode potential

E^0 = standard electrode potential

R = gas constant (8.314 V C K⁻¹ mol⁻¹)

T = temperature (K)

n = number of moles of electrons

F = Faraday's constant (96485.3 C mol⁻¹)

[B] = concentration of reduced species at electrode surface

[A] = concentration of oxidised species at electrode surface

The Nernst equation can be derived from the Gibbs free energy equation $\Delta G = \Delta G^0 + RT \ln K$ and $\Delta G^0 = -nFE^0$, relating the change in Gibbs free energy to standard electrode potential.

4.2 Electrode kinetics

The measured current at the surface of the electrode is directly proportional to the area of the electrode (A) and the flux of reactant to the electrode surface (j) given the following equation, $i = nFAj$. The net flux of reactant undergoing oxidation/reduction at the electrode (j) can be expressed in terms of the rates of the forward and backward electrochemical reactions, k_f and k_b respectively. The following equation shows the net flux of A being reduced to form B , $j = k_f[A] - k_b[B]$.

When the rate constants for forward and backward electrochemical reactions are equal i.e. equilibrium is reached and no net flux ($j = 0$), there is simplification of the rate constants to the standard electrochemical rate constant, k^0 . With rearrangement and substitution of the Arrhenius equation we produce the Butler-Volmer equation.

$$i = nFAk^0 \left[[A]e^{\frac{-\alpha\eta}{RT}} - [B]e^{\frac{(1-\alpha)\eta}{RT}} \right]$$

For a reductive electrochemical process ($A + e^- \rightarrow B$) the rate of electron transfer increases as the electrode potential becomes more negative. In this equation, k^0 is a measure of the rate of electron transfer between a redox couple. If k^0 is large then equilibrium is attained quickly. However, if k^0 is small then the electrochemical process is described as irreversible.

4.3 Mass transport – Diffusion, Migration and Convection

Electrons transfer between the electrode surface and the electroactive species.¹⁵⁰ This results in a zone whereby additional electroactive species must diffuse in order to be within a distance for further electron transfer to occur. At any point from the electrode there will be diffusive flux (j), which is described by Fick's first law of diffusion ($j = -D \frac{dc}{dx}$), where D is the diffusion constant.^{151–152} D increases as temperature increases, and decreases as solvent viscosity increases. Larger molecules create more viscous drag and therefore slow down diffusion, compared to smaller molecules.

Migration effects involve the movement of ions due to their interaction with an external electric field. Faradaic current is the electron current that flows during electrolysis.¹⁴⁹ In the absence of electrolysis there is a build up of surface charge at the electrode surface. To prevent this, a supporting electrolyte is added to the solution. This balances the build-up of electrode surface charge by the formation of an adsorption layer of solvated and unsolvated electrolyte ions.¹⁵³ The electrolyte also ensures that the potential drop between the electrode and surrounding solution is compressed (10–20 Å) and in doing so means that the electric field outside this range is zero. This means that diffusion is the only means of mass transport.

Convection involves the movement of molecules from more dense to less dense areas. This maintains the concentration of the bulk solution at a constant value. During electrolysis the concentration of the reactant decreases and the concentration of the product increases at the electrode surface. This causes a change in local densities and creates a density gradient. To overcome this, between experimental runs, the cell is deliberately agitated (swirled or stirred). This is necessary to make sure that all experiments are under diffusion control.

Three electrode setup

- I) Working electrode (glassy carbon or platinum) – Where the flow of current/potential is being measured, across the electrode-solution interface
- II) Reference electrode (Silver wire) – Provides a way of measuring the applied potential at the working electrode and is corrected to the ferrocene/ferrocenium redox couple ($\text{Cp}_2\text{Fe}^{0/+}$)
- III) Counter electrode (Platinum wire) – A source or sink of electrons, to maintain the potential at the working electrode surface

4.4 Supporting electrolyte

Electrochemical experiments in organic solutions are predominantly conducted in acetonitrile, THF or CH_2Cl_2 containing a supporting electrolyte of an ammonium salt of $[\text{BF}_4]^-$ or $[\text{PF}_6]^-$. These types of supporting electrolytes suffer from poor conductivities due to their incomplete dissociation.¹⁵⁴ Another issue is the long belief that the anion component such as $[\text{BF}_4]^-$ was non-coordinating when in fact it is now accepted that this is untrue.¹⁵⁵ The $[\text{BF}_4]^-$ anion has been shown to coordinate to cationic main group metals, and to undergo decomposition through fluoride abstraction reactions.¹⁵⁶ This behaviour has driven the development of new weakly coordinating anions that are weakly nucleophilic.¹⁵⁷

Weakly coordinating anions have a low overall charge which is delocalised, as much as possible, over the whole anion. Two examples of this are $[\text{B}(\text{C}_6\text{F}_5)_4]^-$ ¹⁵⁸ and $[\text{B}(\text{ArF}_2)_4]^-$ (tetrakis[3,5-bis(trifluoromethyl)phenyl]borate)¹⁵⁹ (Figure 4.4.1).

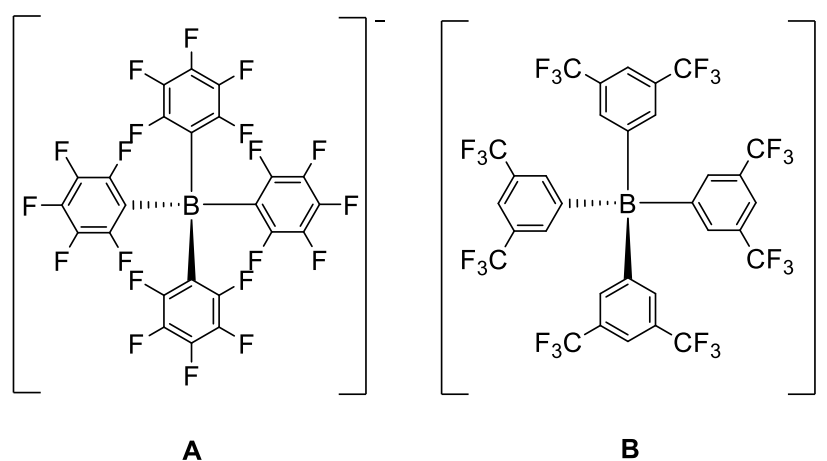


Figure 4.4.1 – Examples of weakly coordinating anions A) tetrakis(pentafluorophenyl)borate (BArF_{20}); and B) tetrakis[3,5-bis(trifluoromethyl)phenyl]borate (BArF_{24})

For electrochemical analysis of Lewis acids such as boranes, it is better to limit the system to non-coordinating solvents such as CH_2Cl_2 , as boranes have a tendency to form classical Lewis adducts with strong donor solvents, such as acetonitrile or THF. Solvents such as 1,2-difluorobenzene have been reported to have electrochemical advantages over CH_2Cl_2 ¹⁶⁰ which is due to its high dielectric constant (13.8 vs. 8.9 for CH_2Cl_2). This allows the dissolution of electrolyte salts and polar/ionic species present. 1,2-difluorobenzene is a weakly-

coordinating and relatively chemically inert solvent but is more expensive than CH_2Cl_2 , which is the reason it wasn't chosen as the solvent for this work.

4.5 Chronoamperometry

In single step chronoamperometry, the potential is stepped from a value where no electrolysis occurs to a value where complete electrolysis occurs at the electrode surface. In double step experiments, the potential is then stepped to a further potential. For experiments of reversible electrochemical reactions this further step is usually set to the original potential. This ensures that products are converted back to reactants. The current response for this process is measured as a function of time.

The current that flows is plotted against the applied potential to give a cyclic voltammogram (CV). In this report a positive current is indicative of an oxidative electrode process and a negative current indicates a reductive electrode process.

For reversible systems, under standard conditions, the average of the peak potentials is equal to the standard reduction potential (E^0), as long as the charge transfer coefficient = 0.5.

$$E_{1/2} = \frac{E_{p, \text{ox}} + E_{p, \text{red}}}{2}$$

Under reversible conditions, the ratio of oxidative and reductive peak currents are equal. In the reversible and irreversible limits, the peak current is directly proportional to the square root of the scan rate, if the electroactive species is dissolved in solution and is under diffusion control. This means that as voltage scan rates increase the peak current also increases and this can be seen in a cyclic voltammogram.

4.6 Electrochemical analysis of various N-methyl-2-arylbenzothiazolines

Cyclic voltammetry was performed on the various N-methyl-2-arylbenzothiazolines in CH₂Cl₂ to analyse the tuning of the C2–H. Figure 4.6.1 shows the cyclic voltammogram of the various N-methyl-2-(aryl)benzothiazolines at a scan rate of 100 mV s⁻¹ in DCM, with [tBu₄N][BARF₂₀] as the supporting electrolyte.

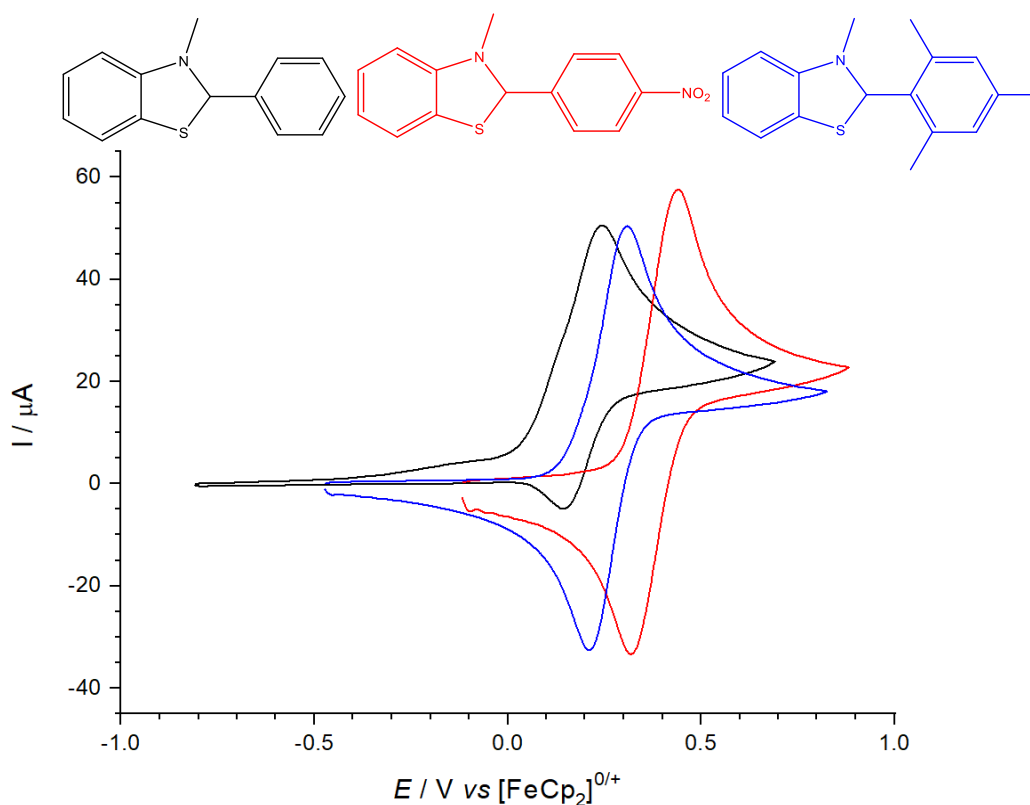


Figure 4.6.1 - The cyclic voltammogram of various benzothiazolines at a scan rate of 100 mV s⁻¹. Black line - N-methyl-2-phenylbenzothiazoline. Red line - N-methyl-2-(4-nitrophenyl)benzothiazoline. Blue line - N-methyl-2-mesitylbenzothiazoline.

From Figure 4.6.1 it can be seen that the oxidation wave shifts with varying the substituents on the aryl ring. The most positive waves (vs. FeCp₂^{0/+}) relate to the nitro substituent (red line - *para*-substituted). This can be related to the Hammett parameters with a nitro substituent having a value of +0.78 (electron-withdrawing).¹⁶¹ This would make the C2–H more difficult to remove. In contrast, the mesityl substituent (blue line) is less positive. This is an electron-donating substituent (σ_p value of -0.17 for a methyl group).¹⁶¹ This would make the C2–H easier to remove. The non-substituted aryl ring is the least positive oxidation wave (black line) which would suggest that it is not purely electronic effects that determines the hydricity of the C2–H position.

Variable scan rate (VSR) cyclic voltammetry was undertaken on all the samples, individually (Figures 4.6.2 to 4.6.4).

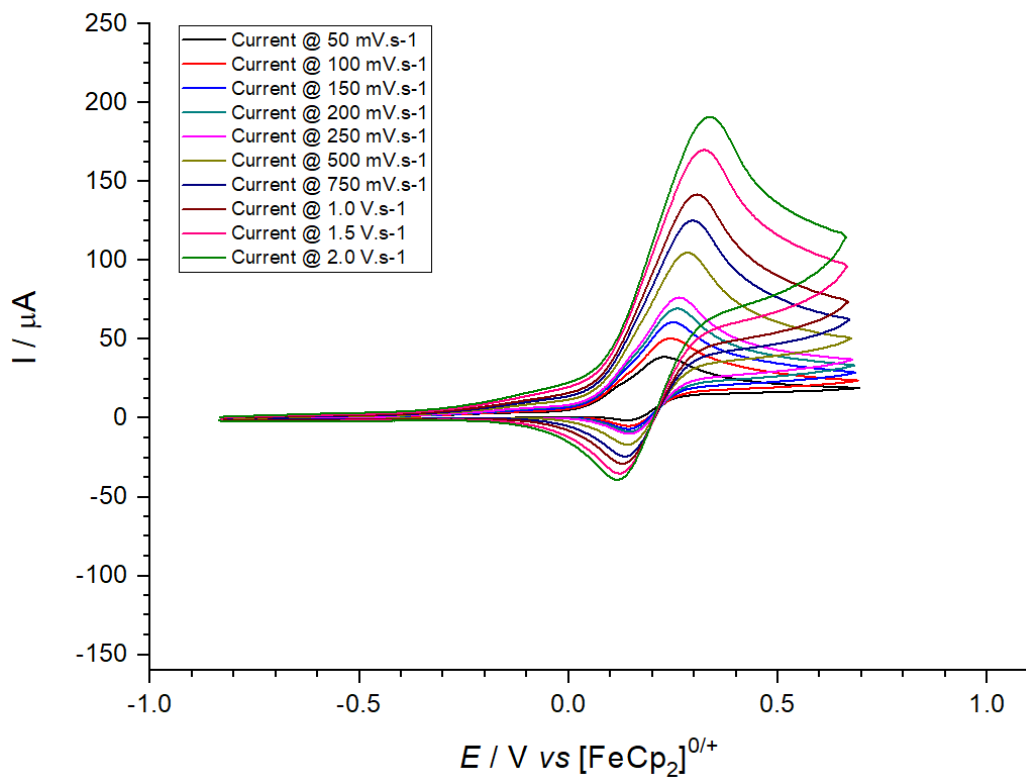


Figure 4.6.2 – VSR cyclic voltammetry for *N*-methyl-2-phenylbenzothiazoline, **BNZ1**

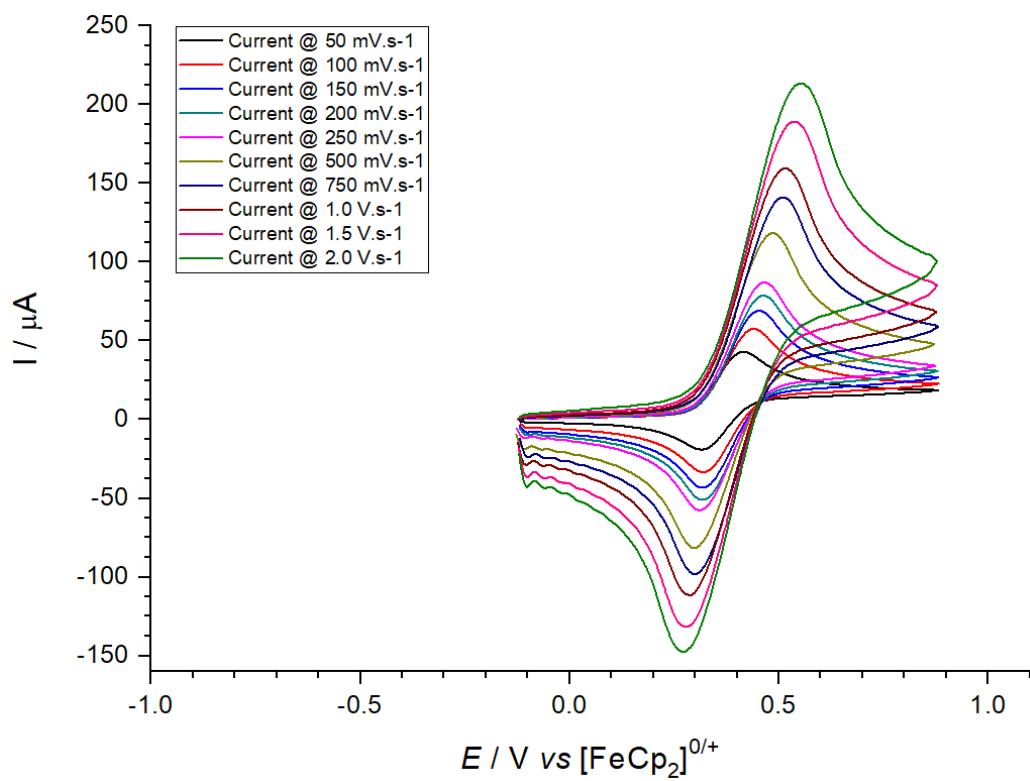


Figure 4.6.3 – VSR cyclic voltammetry for *N*-methyl-2-(4-nitrophenyl)benzothiazoline, **BNZ3**

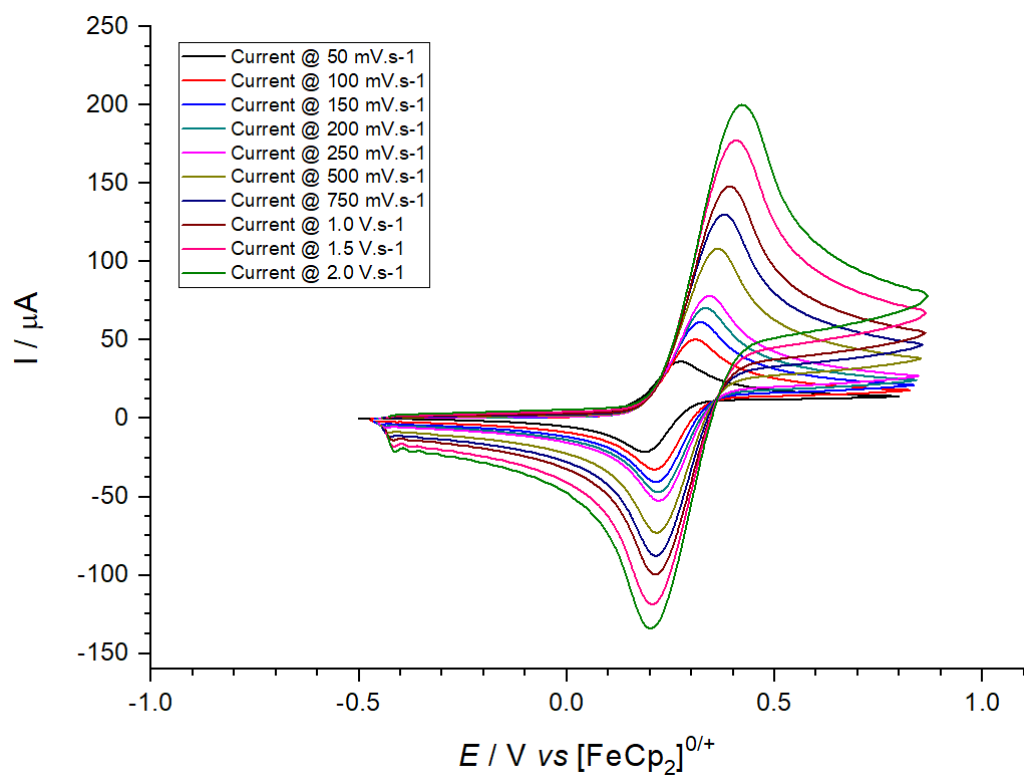


Figure 4.6.4 – VSR cyclic voltammetry of *N*-methyl-2-mesitylbenzothiazoline, **BNZ5**

From Figures 4.6.2 to 4.6.4 it can be seen that as the scan rate is increased, the current also increased. It can also be noted that they seem to appear to get more reversible as the scan rate is increased, especially for *N*-methyl-2-phenylbenzothiazoline (Figure 4.6.2). This suggests an EC process; oxidation followed by an irreversible chemical reaction. As the scan rate is increased, the time scale of the experiment competes with the chemical step, and more oxidised species is left to be reduced back. At faster scan rates, the electrochemical feature regains reversibility as the chemical reaction is outcompeted by reduction. This can be seen in Figure 4.6.2 as the reduction wave increases at higher scan rates.¹⁴⁷

Figures 4.6.5 to 4.6.7 show the Randles-Sevcik plot for each *N*-methyl-2-(aryl)benzothiazoline (peak current vs \sqrt{v} scan rate). These plots show the linear relationship between the peak current and the \sqrt{v} scan rate. However, in all cases, the gradients of the line for both oxidation and reduction are not equal (summarised in Table 4.6.1). This suggests that the electrochemical process is not fully reversible, and can be described as quasi-reversible. However, Figure 4.6.6 and 4.6.7 show the plotted lines for reduction and oxidation to be more symmetrical whereas the line for reduction in Figure 4.6.5 is significantly flatter than the oxidation line. This again suggests that for the phenyl substituent the process is more complicated (EC process).

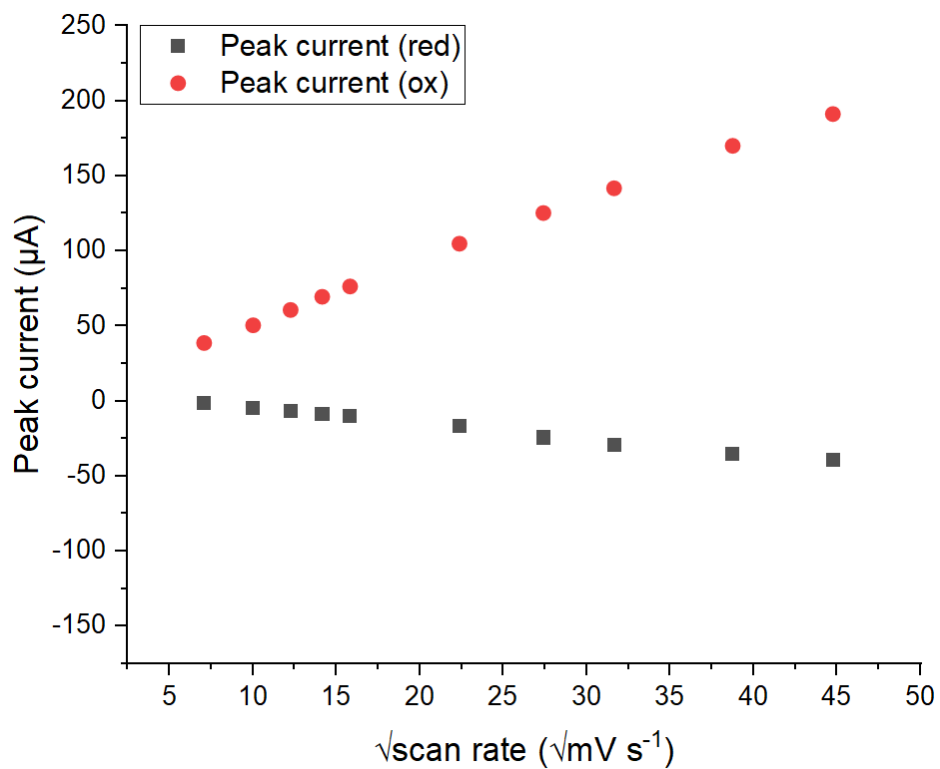


Figure 4.6.5 – Randles-Sevcik plot for *N*-methyl-2-phenylbenzothiazoline, **BNZ1**

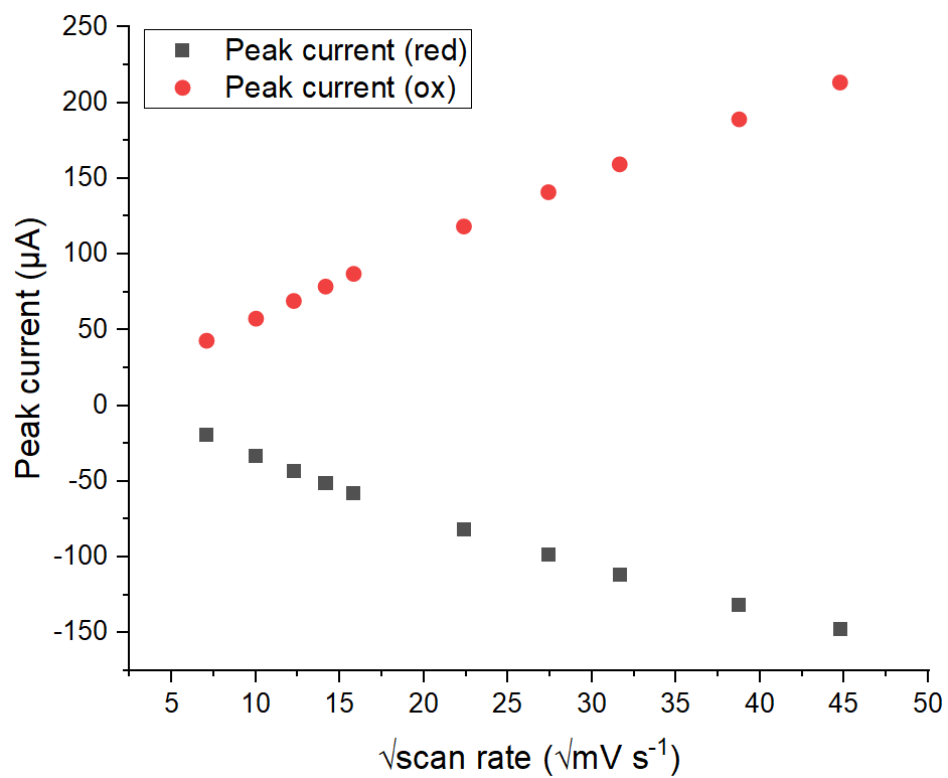


Figure 4.6.6 – Randles-Sevcik plot for *N*-methyl-2-(4-nitrophenyl)benzothiazoline, **BNZ3**

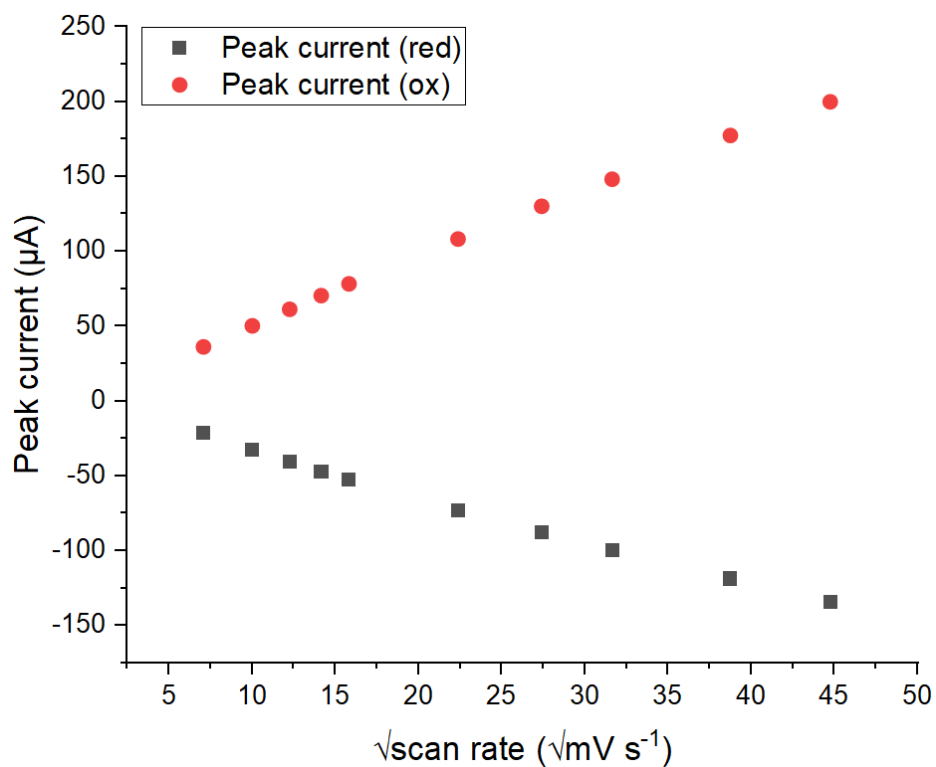


Figure 4.6.7 – Randles-Sevcik plot for *N*-methyl-2-mesitylbenzothiazoline, **BNZ5**

Table 4.6.1 – The gradient of the oxidation and reduction lines from the Randles-Sevcik plot of the different *N*-methyl-2-(aryl)benzothiazolines

Benzothiazoline	Gradient of line from Randles-Sevcik plot ($\times 10^{-6}$)	
	Oxidation	Reduction
Phenyl	4.050	-1.002
2-fluoro	3.287	-1.876
4-nitro	4.526	-3.411
3,5-di- <i>tert</i> -butyl-2-hydroxy	3.599	-2.728
Mesityl	4.345	-2.991
3-nitro	4.613	-3.783
3,5-di- <i>tert</i> -butyl-2-methoxy	2.727	-1.978

Table 4.6.1 shows the gradient of both oxidation and reduction waves from the varying scan rates. It can be noted that there is the greatest difference in the gradients for the phenyl substituent. This is previously been discussed as an EC process.

Table 4.6.1 – The $E_{1/2}$ and peak separation of the different *N*-methyl-2-(aryl)benzothiazolines

Benzothiazoline	$E_{1/2}$ @ 100 mV s⁻¹ (mV)	Peak separation @ 100 mV s⁻¹ (mV)
Phenyl	0.20	102
2-fluoro	0.27	113
4-nitro	0.38	122
3,5-di- <i>tert</i> -butyl-2-hydroxy	0.39	105
Mesityl	0.26	96
3-nitro	0.45	81
3,5-di- <i>tert</i> -butyl-2-methoxy	0.28	93

From Table 4.6.2 it can be seen that it is possible to tune the C2 position, as there is variation in the $E_{1/2}$. However, there is a competing chemical reaction for the phenyl substituent which is overcome at greater scan rates. For most other benzothiazolines the process appears to be much closer to reversibility.

5. Hydride transfer from activated frustrated Lewis pairs to N-methyl-2-arylbenzothiazolium cations

5.1 Background

In 2009, the use of *N*-methyl-2-phenylbenzothiazoline and *N,N*-dimethyl-2-phenylbenzimidazoline (Figure 5.1.1) as hydride donors for the reduction of NAD^+ analogues, acridinium and quinolinium cations was reported.¹²⁰

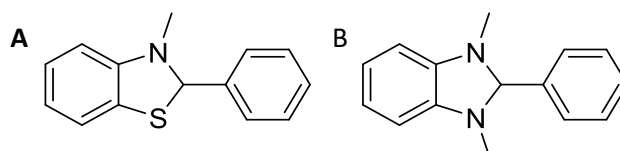
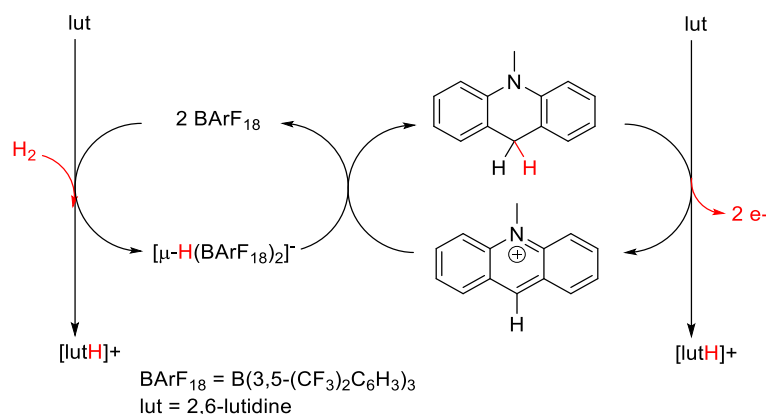


Figure 5.1.1 - Chemical structures of A) *N*-methyl-2-phenylbenzothiazoline and B) *N,N*-dimethyl-2-phenylbenzimidazoline.

It was reported that *N*-methyl-2-phenylbenzothiazoline was less reactive than the corresponding *N,N*-dimethyl-2-phenylbenzimidazoline¹²⁰ which suggested it was a less potent reducing agent. This was most likely due to the increased electron-withdrawing ability of the benzimidazoline, as it has an additional electronegative nitrogen, compared to the benzothiazoline which has a sulfur atom. The benzimidazoline hydride-donating abilities are greater than that of both benzothiazoline, and NADH .¹⁶² They have been found to be one of the strongest neutral C–H hydride donors.¹⁶³ However, the corresponding benzothiazolium salts can be used as hydride acceptors.¹⁶² These characteristics heavily influenced the decision to utilise the benzothiazoline/benzothiazolium couple for its hydride-donating and hydride-accepting capabilities.

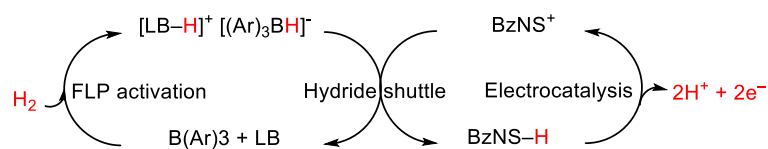
Previous work investigating the first metal-free electrocatalyst for hydrogen activation used *N*-methylacridinium as the hydride shuttle and BARF_{18} and lutidine as the frustrated Lewis pair (FLP) for hydrogen splitting¹⁰⁹ (Scheme 5.1.1). The results were encouraging and so it was decided to explore benzothiazolium salts for electrocatalytic hydrogen activation, and the possibility of the reverse reaction, hydrogen production (Scheme 5.1.2).



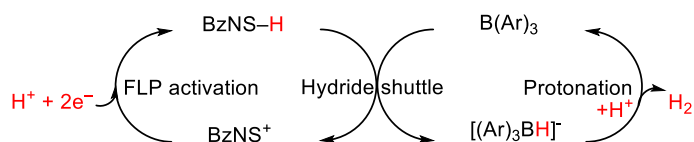
Scheme 5.1.1 - First metal-free electrocatalytic cycle, using BARF_{18} and lutidine as the frustrated Lewis pair (FLP), and *N*-methylacridinium cation as the hydride shuttle¹⁰⁹

In 2017, Ingleson and co-workers reported using *N*-methylbenzothiazolium salts as carbon-based Lewis acids for the activation of Si-H bonds.¹¹⁰ It was reported that the hydride ion affinity of *N*-methyl-2-phenylbenzothiazolium cation ($-45 \text{ kcal mol}^{-1}$) was comparable to the hydride ion affinity of BARF_{15} ($-41 \text{ kcal mol}^{-1}$). The hydride ion affinity of these species are both less than that calculated for the *N*-methylacridinium cation ($-53 \text{ kcal mol}^{-1}$), which was previously used as a hydride shuttle source in the cycle proposed by Wildgoose *et al.* (Scheme 5.1.1). The lower hydride ion affinity value for the *N*-methylbenzothiazolium compared to the *N*-methylacridinium suggests it would be a more applicable Lewis acid for reductions. This was due to the corresponding hydride (*N*-methylbenzothiazoline vs. *N*-methylacridane) having a greater reductive capacity,¹¹⁰ and foregoing hydride loss. Using the information from Ingleson and co-workers and previous work from Zhu and co-workers, the *N*-methylbenzothiazoline/thiazolium couple was explored with the proposed system (Scheme 5.1.2), adapted from the work done by Wildgoose and co-workers.¹⁰⁹

Electrocatalytic H₂ activation



Electrocatalytic H₂ production



Scheme 5.1.2 - The electrocatalytic cycle for hydrogen activation and hydrogen production; using Triaryl boranes and a Lewis base as an FLP and the benzothiazolium as a hydride shuttle.

Scheme 5.1.2 suggested that the use of an FLP system involving a triarylborane and a Lewis base (2,6-lutidine or 2,2,6,6-tetramethylpiperidine) would heterolytically cleave hydrogen; allowing the hydride to be transferred to the benzothiazolium to form the benzothiazoline. At the electrode, the benzothiazolium would be oxidised, giving up the proton and two electrons. Hydrogen production would reduce the benzothiazolium at the electrode, on addition of a proton and two electrons, to form the benzothiazoline. This hydride would be transferred to a triarylborane and, after protonation, would evolve hydrogen. The rest of this chapter concentrated on the activation of hydrogen (electrocatalytic H₂ activation in Scheme 5.1.1).

5.2 Initial hydride transfer experiments

Initial NMR studies were undertaken with two compounds that had been received from Prof. Michael Ingleson. Figure 5.2.1 shows the two compounds.

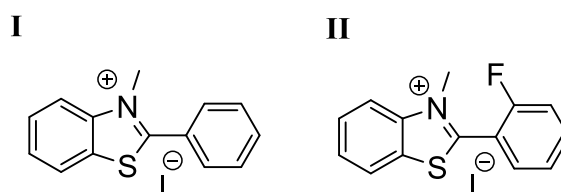


Figure 5.2.1 – Structures of **I** [*N*-methyl-2-phenylbenzothiazolium][iodide] and **II** [*N*-methyl-2-(2-fluorophenyl)benzothiazolium][iodide]

Using [*N*-methyl-2-phenylbenzothiazolium][iodide] (**I**) and [*N*-methyl-2-(2-fluorophenyl)benzothiazolium][iodide] (**II**), initial NMR studies were undertaken with borohydride salts that were readily available in the laboratory. These experiments were assembled under an inert atmosphere (glovebox) in a solution of CD_2Cl_2 containing a 1:1 mixture of **I** or **II** and $[\text{Bu}_4\text{N}][\text{HB}(\text{C}_6\text{F}_5)_3]$ or $[\text{Bu}_4\text{N}][\text{HB}(\text{C}_6\text{H}_5)_3]$ respectively.

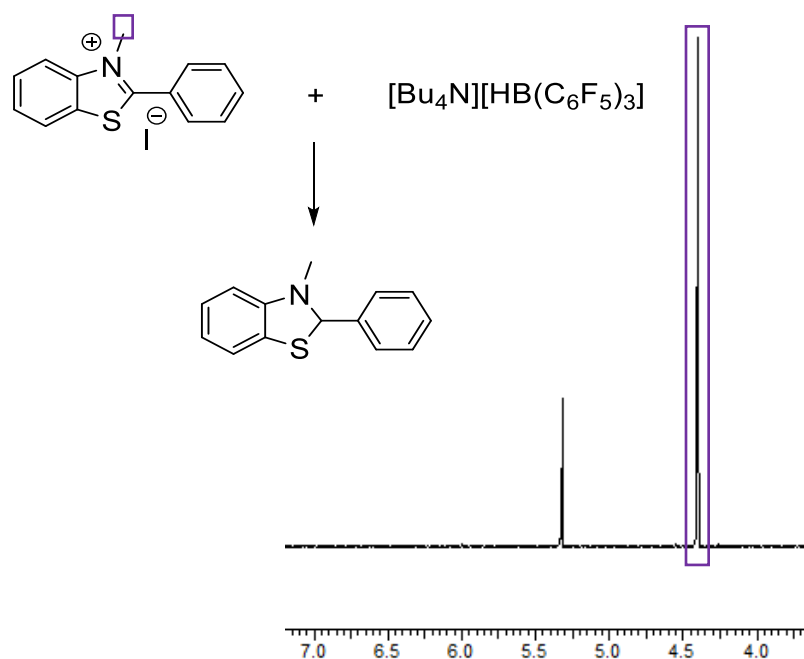


Figure 5.2.2 – Initial ^1H NMR spectrum for the reaction of [*N*-methyl-2-phenylbenzothiazolium][iodide] and $[\text{Bu}_4\text{N}][\text{HB}(\text{C}_6\text{F}_5)_3]$

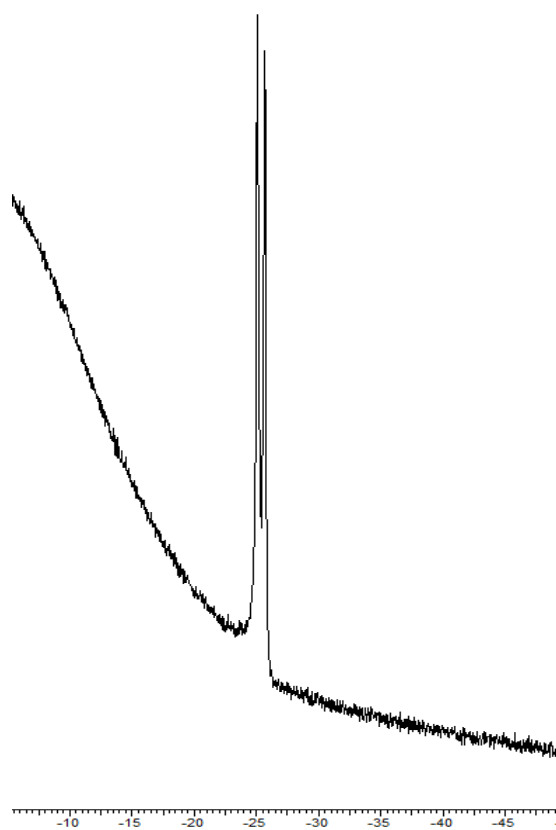


Figure 5.2.3 – Initial ^{11}B NMR spectrum for the reaction of [*N*-methyl-2-phenylbenzothiazolium][iodide] and $[\text{Bu}_4\text{N}][\text{HB}(\text{C}_6\text{F}_5)_3]$

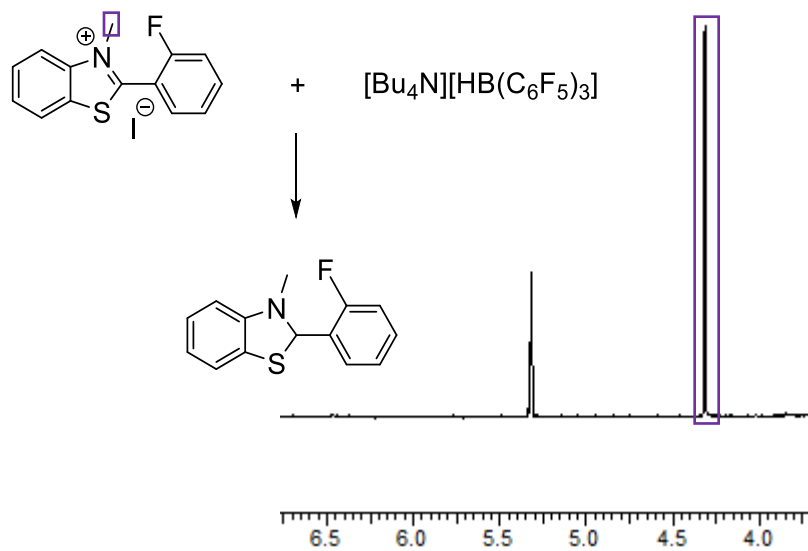


Figure 5.2.4 – Initial ^1H NMR spectrum for the reaction of [*N*-methyl-2-(2-fluorophenyl)benzothiazolium][iodide] and $[\text{Bu}_4\text{N}][\text{HB}(\text{C}_6\text{F}_5)_3]$

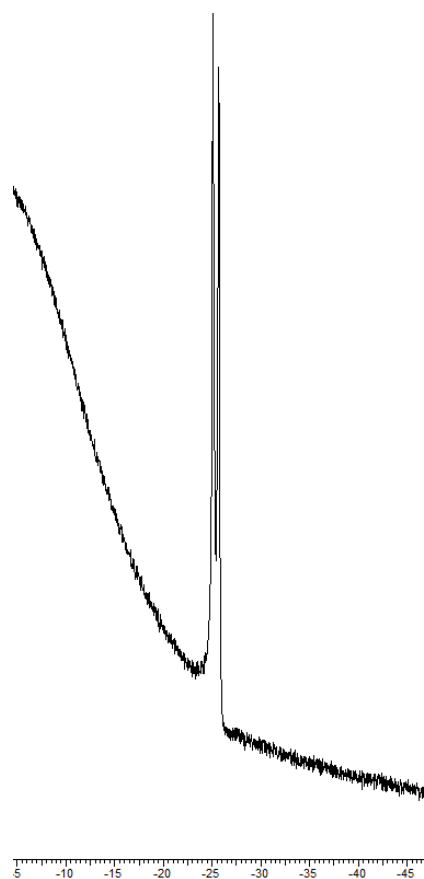


Figure 5.2.5 – Initial ^{11}B NMR spectrum for reaction of [*N*-methyl-2-(2-fluorophenyl)benzothiazolium][iodide] and $[\text{Bu}_4\text{N}][\text{HB}(\text{C}_6\text{F}_5)_3]$

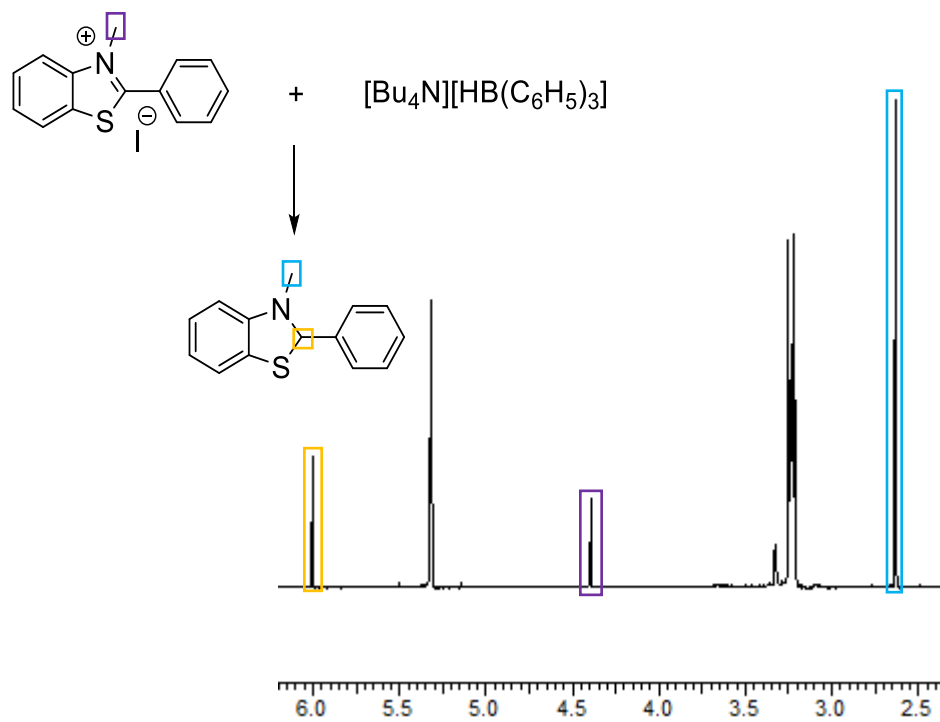


Figure 5.2.6 – Initial ^1H NMR spectrum for the reaction of [*N*-methyl-2-phenylbenzothiazolium][iodide] and $[\text{Bu}_4\text{N}][\text{HB}(\text{C}_6\text{H}_5)_3]$

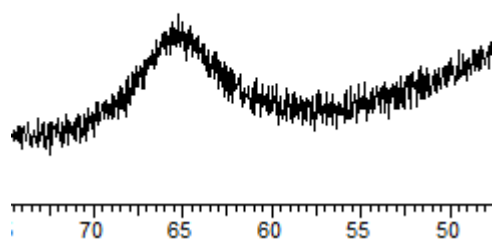


Figure 5.2.7 – Initial ^{11}B NMR spectrum for the reaction of [*N*-methyl-2-phenylbenzothiazolium][iodide] and $[\text{Bu}_4\text{N}][\text{HB}(\text{C}_6\text{H}_5)_3]$

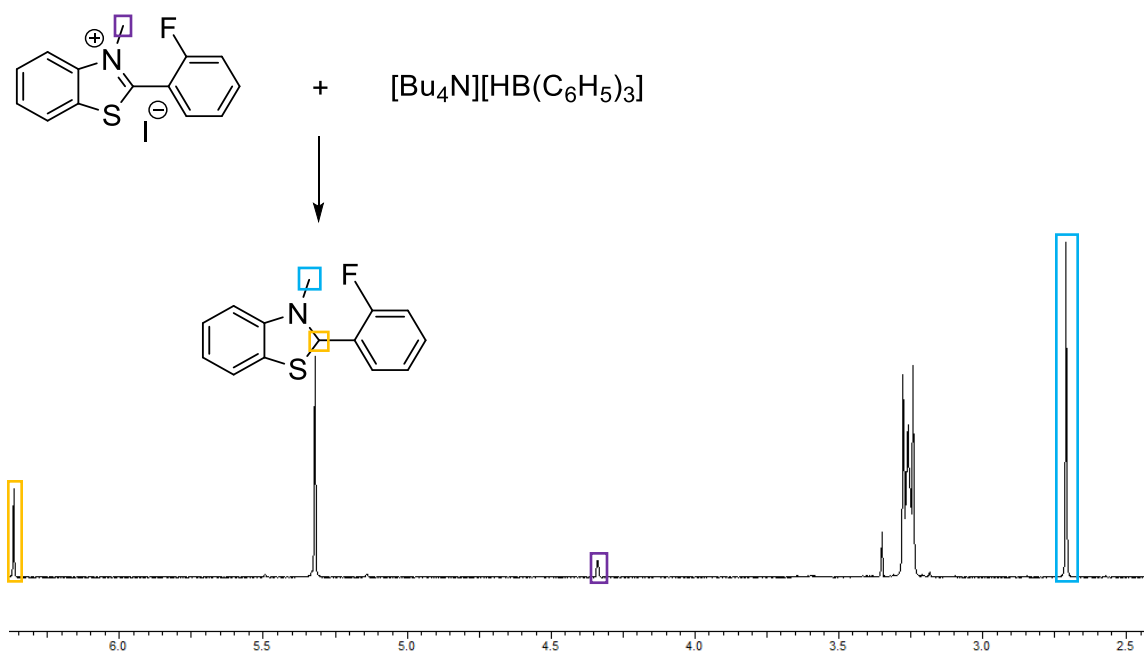


Figure 5.2.8 – Initial ^1H NMR spectrum for the reaction of [*N*-methyl-2-(2-fluorophenyl)benzothiazolium][iodide] and $[\text{Bu}_4\text{N}][\text{HB}(\text{C}_6\text{H}_5)_3]$

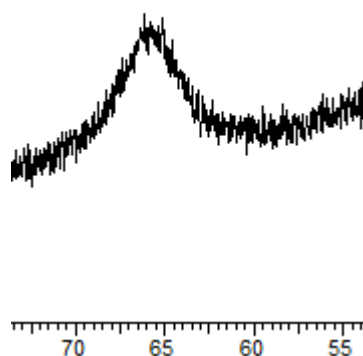


Figure 5.2.9 – Initial ^{11}B NMR spectrum for the reaction of [*N*-methyl-2-(2-fluorophenyl)benzothiazolium][iodide] and $[\text{Bu}_4\text{N}][\text{HB}(\text{C}_6\text{H}_5)_3]$

The reaction between the benzothiazolium salts and tris(pentafluorophenyl)borohydride to transfer the hydride and form the benzothiazoline was slow. The reaction was carried out at room temperature and the initial ^1H and ^{11}B NMR showed no conversion (Figures 5.2.2, 5.2.3, 5.2.4 and 5.2.5). The ^1H and ^{11}B NMR were repeated after 3 days and showed only partial conversion to the benzothiazoline (Figures 5.2.10, 5.2.11, 5.2.12, and 5.2.13).

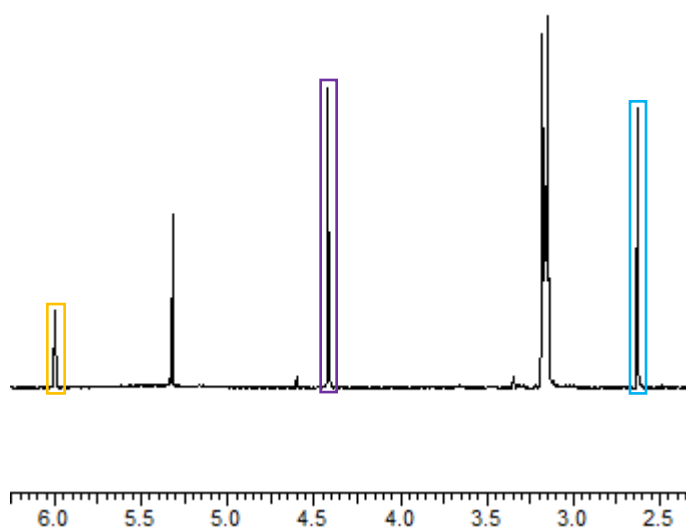


Figure 5.2.10 – ^1H NMR spectrum for the reaction of [*N*-methyl-2-phenylbenzothiazolium][iodide] and $[\text{Bu}_4\text{N}][\text{HB}(\text{C}_6\text{F}_5)_3]$ after 96 h

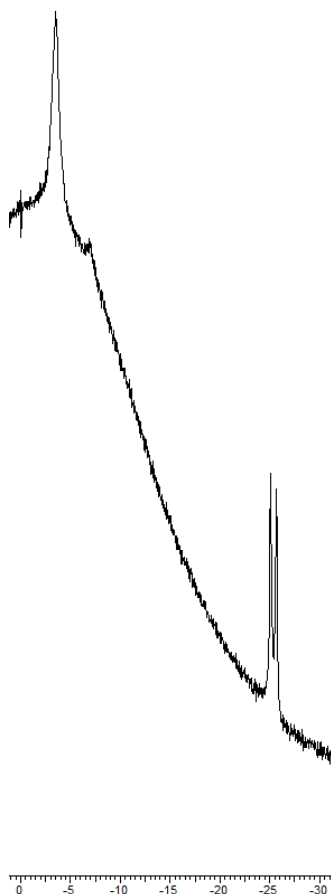


Figure 5.2.11 – ^{11}B NMR spectrum for the reaction of [*N*-methyl-2-phenylbenzothiazolium][iodide] and $[\text{Bu}_4\text{N}][\text{HB}(\text{C}_6\text{F}_5)_3]$ after 96 h

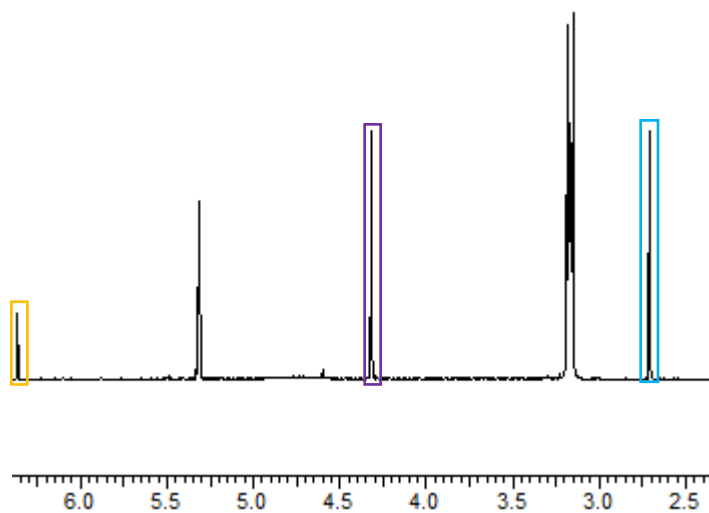


Figure 5.2.12 - ^1H NMR spectrum for the reaction of [*N*-methyl-2-(2-fluorophenyl)benzothiazolium][iodide] and $[\text{Bu}_4\text{N}][\text{HB}(\text{C}_6\text{F}_5)_3]$ after 96 h

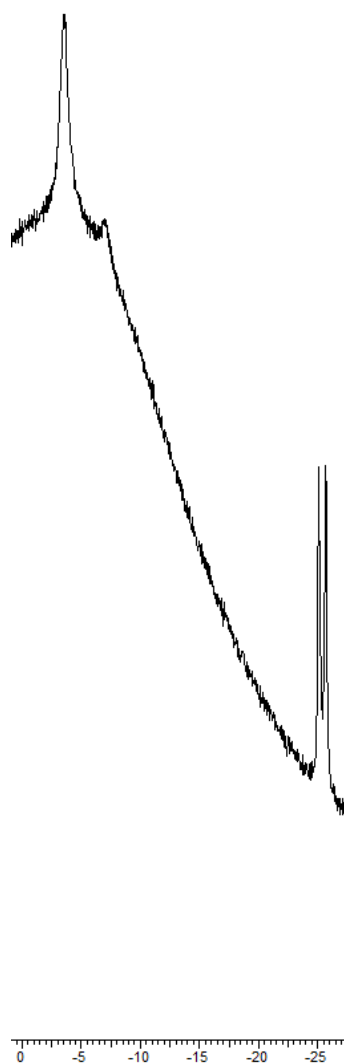


Figure 5.2.13 – ^{11}B NMR spectrum for the reaction of [*N*-methyl-2-(2-fluorophenyl)benzothiazolium][iodide] and $[\text{Bu}_4\text{N}][\text{HB}(\text{C}_6\text{F}_5)_3]$ after 96 h

The ^1H NMR showed singlet peaks at 6.00 ppm and 6.37 ppm for the benzothiazolines, which corresponded to the C2–*H* (Figure 5.2.10 and 5.2.12 respectively – orange). Also present in the ^1H NMR were the singlet peaks at 2.63 ppm and 2.71 ppm which corresponded to the N– CH_3 of the benzothiazoline (blue). However, the singlet peak at 4.42 ppm (**I** – Figure 5.2.10) and 4.32 ppm (**II** – Figure 5.2.12) corresponding to the positively charged nitrogen of N– CH_3 in the benzothiazolium, remained present in the ^1H NMR (purple). This was supported by the ^{11}B NMR, which showed that the doublet was still visible, even after 3 days (**I** - Figure 5.2.11 and **II** – Figure 5.2.13). However, in both spectra (after 96 h) there was a peak at -3.60 ppm, which needed investigation. The reaction between the benzothiazolium and tris(phenyl)borohydride was much quicker for both **I** and **II**. In this instance, the hydride transfer was above 80% complete within 1 h (Figures 5.2.6 and 5.2.8 respectively). The ^1H NMR for the reaction of **I** showed two singlet peaks at 6.00 ppm and 2.63 ppm which again

corresponded to the C2-H (orange) and N-CH₃ (blue), respectively (Figure 5.2.6). The ¹¹B NMR showed a broad peak at 65 ppm, which indicated a free-three coordinate boron, triphenylborane (Figure 5.2.7). There is no doublet visible. This suggested that complete conversion had occurred. The ¹H NMR for the reaction of **II** showed two singlets at 6.37 ppm and 2.71 ppm which corresponded to the C2-H (orange) and N-CH₃ (blue) of the benzothiazoline, respectively (Figure 5.2.8). The ¹¹B NMR again showed a broad peak at 65 ppm and lacked a doublet peak, which suggested the complete conversion to the benzothiazoline using the transfer of the hydride from the borohydride (Figure 5.2.9).

After the successful synthesis of the [N-methyl-2-(4-nitrophenyl)benzothiazolium][BArF₂₀] salt, initial NMR studies were undertaken with borohydride salts readily available in the laboratory. These experiments were assembled under an inert atmosphere (glovebox) in CD₂Cl₂, containing 1:1 mixture of [N-methyl-2-(4-nitrophenyl)benzothiazolium][BArF₂₀] and [Bu₄N][HBPh₃] and [Bu₄N][HBArF₁₅], respectively.

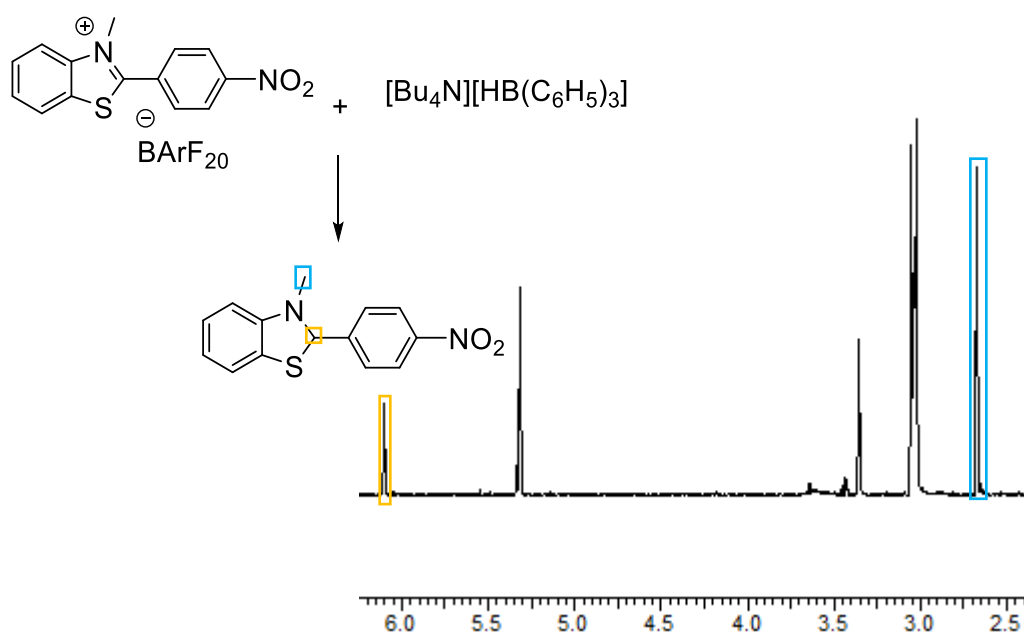


Figure 5.2.14 – Initial ¹H NMR spectrum for the reaction of [N-methyl-2-(4-nitrophenyl)benzothiazolium][BArF₂₀] and [Bu₄N][HBPh₃]

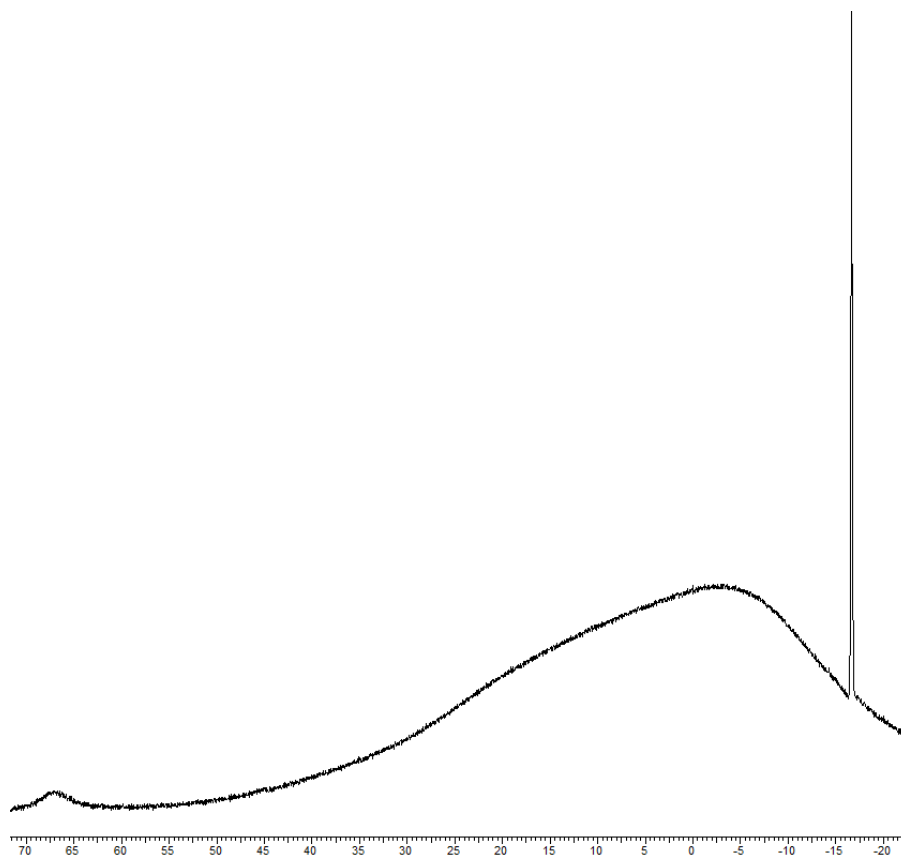


Figure 5.2.15 – Initial ^{11}B NMR spectrum for the reaction of [*N*-methyl-2-(4-nitrophenyl)benzothiazolium][BARF_{20}] and $[\text{Bu}_4\text{N}][\text{HBPh}_3]$

The reaction with triphenylborohydride was a success. The ^1H NMR showed the appearance of a singlet C2–*H* peak (orange) at 6.10 ppm, and the shift of the methyl peak from 4.32 ppm to 2.67 ppm (Figure 5.2.14 - blue). The ^{11}B NMR supported the evidence of the ^1H NMR. No doublet, indicative of a borohydride, was observed (Figure 5.2.15). Instead, a broad signal at ca. 67 ppm was observed, which suggested the three-coordinate boron of triphenylborane. This reaction took place within 1 h. However, triphenylborane is not a sufficiently strong Lewis acid to be used in heterolytic hydrogen cleavage. This can be attributed to the phenyl aromatic π -system donating electron density into the empty $2p_z$ of the boron centre. This decreased the Lewis acidity of the borane.¹⁶⁴

The reaction of [*N*-methyl-2-(4-nitrophenyl)benzothiazolium][BARF_{20}] and tris(pentafluorophenyl)borohydride was slower than the reaction with triphenylborohydride; the conversion of the benzothiazolium to benzothiazoline was 33% complete within 1 h (Figure 5.2.16). This was because BARF_{15} was much more Lewis acidic than BPh_3 and so was more likely to retain the hydride. This was due to the electron-withdrawing fluorines on the aryl rings, which pulled electron density from the aryl system,

which in turn drew electron density from the boron centre, resulting in electron density being withdrawn from the B–H bond. This made the hydride transfer harder and was, therefore, a slower process.

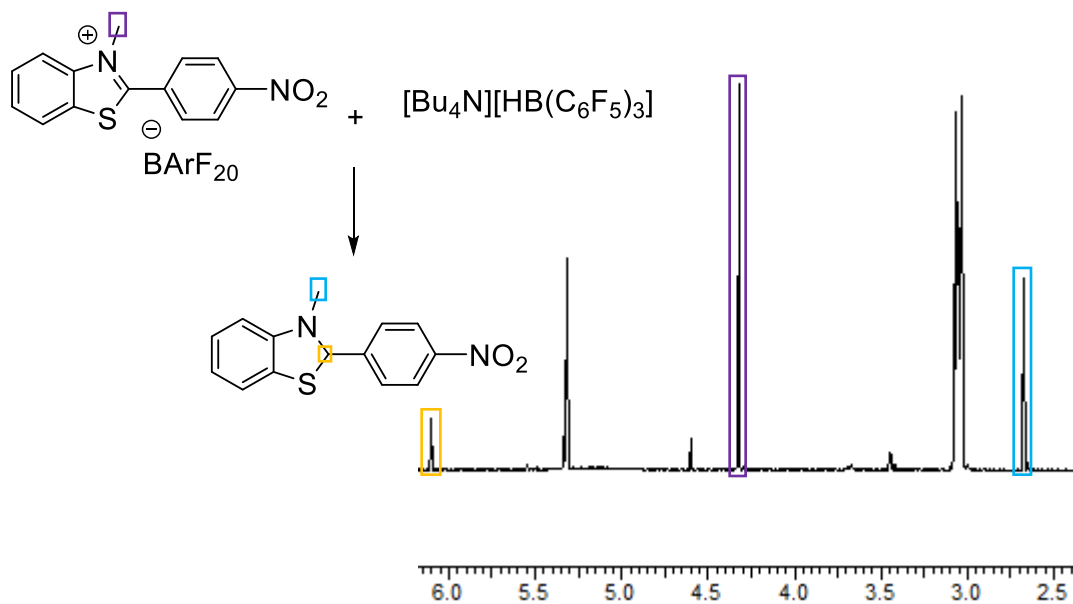


Figure 5.2.16 – Initial ¹H NMR spectrum for the reaction of [N-methyl]-2-(4-nitrophenyl)benzothiazolium[BARF₂₀] and [Bu₄N][HBArF₁₅]

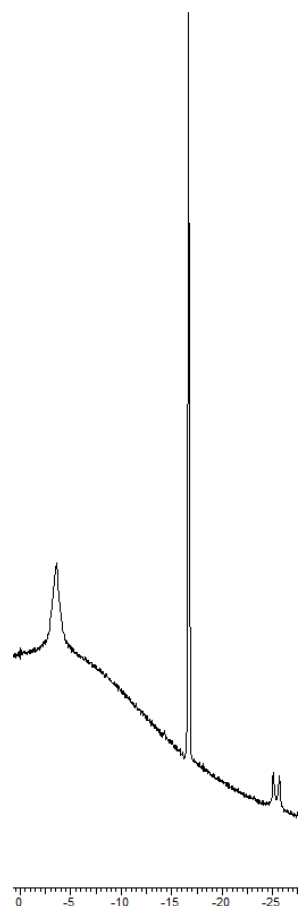


Figure 5.2.17 – Initial ^{11}B NMR spectrum for the reaction of [*N*-methyl-2-(4-nitrophenyl)benzothiazolium][BARF₂₀] and [Bu₄N][HBArF₁₅]

The ^1H NMR showed two singlet peaks at 4.32 ppm and 2.67 ppm, which indicated the methyl groups of the benzothiazolium (purple) and benzothiazoline (blue), respectively (Figure 5.2.16). The ^{11}B NMR also still showed the doublet, indicative of the continued presence of the borohydride. Also, a peak at -3.60 ppm and a sharp singlet peak at -16.66 ppm (Figure 5.2.17) were visible in the ^{11}B NMR; with the latter attributed to the BARF₂₀ counterion. However, the peak at -3.60 ppm (which had also been seen for the reactions of **1** (Figure 5.2.11) and **2** (Figure 5.2.13)) suggested that a boron-sulfur adduct had formed after the transfer of the hydride to form the benzothiazoline; this occurrence was then investigated.

5.3 Adduct formation

NMR experiments were undertaken with BArF₁₅, 2,6-lutidine and [*N*-methyl-2-(4-nitrophenyl)benzothiazolium][BArF₂₀] to determine whether adduct formation was noted. The ¹¹B NMR showed two peaks; one at -3.9 ppm and one at -16.7 ppm (Figure 5.3.1). The latter is the BArF₂₀ peak. A further NMR experiment was carried out measuring BArF₁₅ and 2,6-lutidine in CD₂Cl₂ which showed a peak at -3.92 ppm in ¹¹B NMR (Figure 5.3.2).

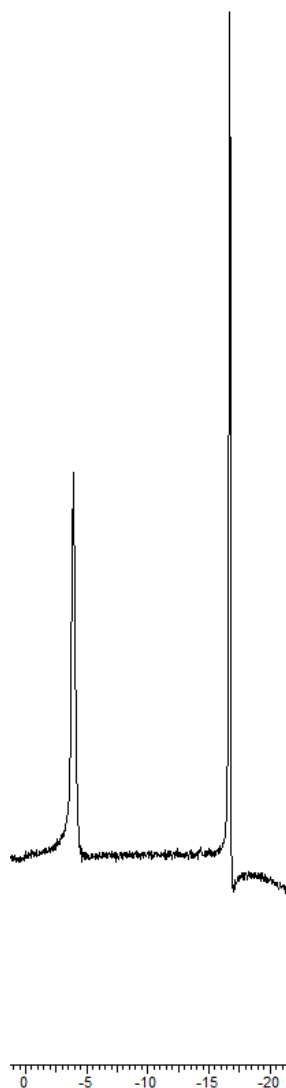


Figure 5.3.1 – ¹¹B NMR spectrum for the reaction between BArF₁₅, 2,6-lutidine and [*N*-methyl-2-(4-nitrophenyl)benzothiazolium][BArF₂₀]

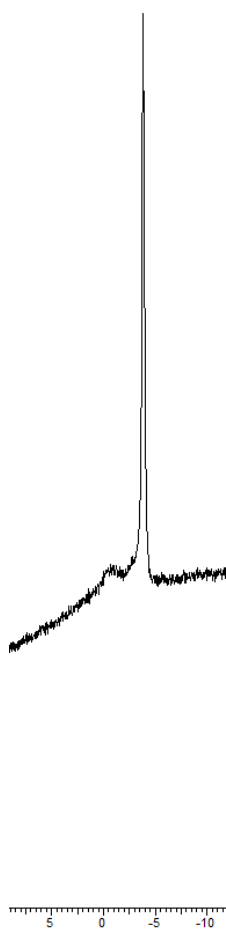


Figure 5.3.2 – ^{11}B NMR spectrum of the reaction between BArF_{15} and 2,6-lutidine

Both these shifts are consistent with that reported by Geier *et al.*, when they carried out a similar experiment.³² This result would suggest that the initial NMR experiment showed a boron-sulfur adduct (Figure 5.2.17), as it is not consistent with a boron-nitrogen adduct of BArF_{15} and 2,6-lutidine. It could be argued that the peak at -3.6 ppm could be another boron-nitrogen adduct, with the nitrogen in the benzothiazoline ring. However, in the case of the benzothiazolium there is no Lewis basicity as there is no lone pair of electrons on the nitrogen because of the double bond to the C2 carbon. In the case of the benzothiazoline, the lone pair on the nitrogen is inaccessible as the orbital faces inwards, and is conjugated with the attached benzene ring. This would imply that there is no Lewis basicity for that nitrogen in the benzothiazolium or benzothiazoline, and suggests the impossibility of an additional boron-nitrogen adduct. However, sulfur has two lone pairs of electrons, facing outwards in the cases of benzothiazolium and benzothiazoline. This would suggest that the formation of a boron-sulfur adduct is possible, and more likely, even though the affinity for adduct formation is higher between boron and nitrogen,¹⁶⁵ than boron and sulfur. Additionally, the

formation of a boron-nitrogen adduct would suggest that BArF_{15} and 2, 6-lutidine are not compatible as an FLP system and that there needs to be more steric bulk to prevent the formation of these adducts. One possible option would be to use a more sterically bulky Lewis base i.e. 2, 2, 6, 6-tetramethylpiperidine (TMP). The ^{11}B NMR for the reaction of BArF_{15} and TMP showed a broad peak ca. 60 ppm which corresponds to a free, three-coordinate borane (Figure 5.3.3). This suggests no adduct formation. This system was subjected to a hydrogen atmosphere and another NMR run. The ^{11}B NMR shows a doublet at -24.16 ppm, indicative a borohydride (Figure 5.3.4). This would suggest that BArF_{15} and TMP are a viable FLP system for hydrogen activation. However, the use of BArF_{15} does not seem viable for the benzothiazolium/benzothiazoline system and therefore another option would be to increase the steric bulk of the Lewis acidic borane (discussed further in section 5.4).

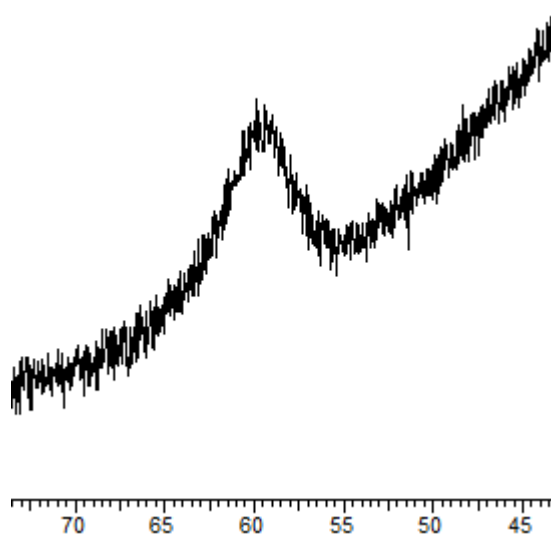


Figure 5.3.3 – ^{11}B NMR spectrum for the reaction of BArF_{15} and TMP

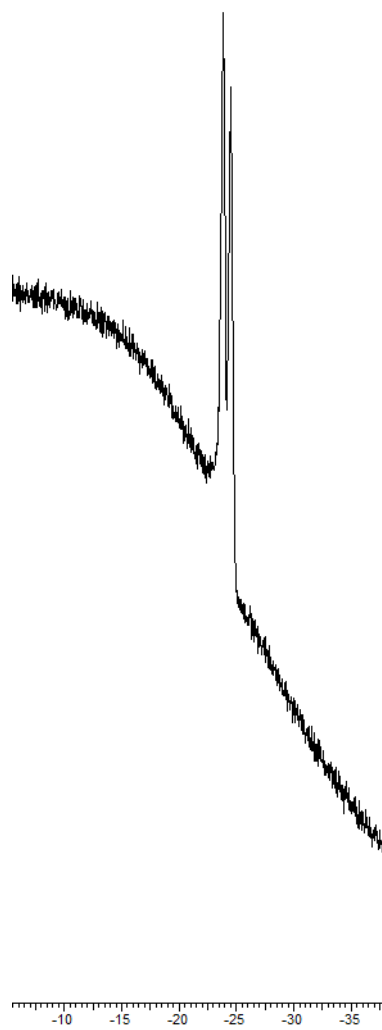


Figure 5.3.4 – ^{11}B NMR spectrum for the reaction of BARF_{15} and TMP after the addition of hydrogen

5.4 Boranes

Sterically-bulky boranes were investigated as a means to avoid boron-nitrogen adducts while maintaining Lewis acidity in order to heterolytically cleave hydrogen. A variety of boranes were readily available in the laboratory so they weren't synthesised for this portion of the project. The boranes that were explored are shown in Figure 5.4.1.

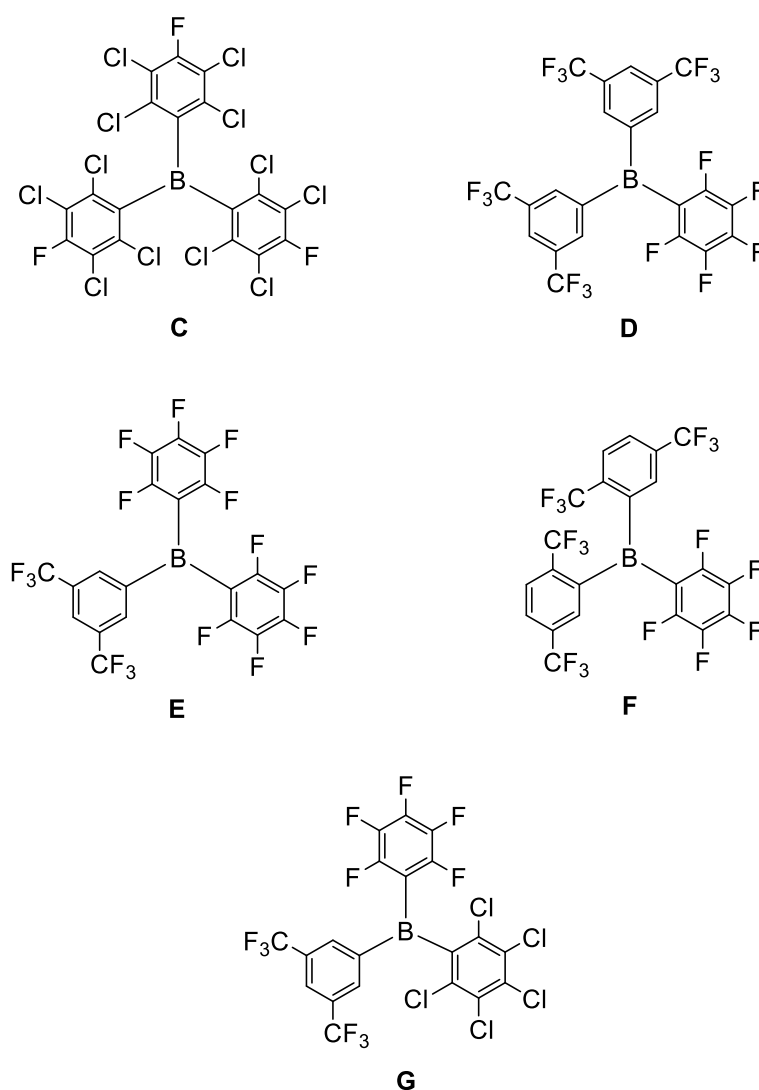


Figure 5.4.1 - Chemical structures of the various different boranes; B(Cl₄F)₃ (C), BArF₁₇ (D), BArF₁₆ (E), BArF₁₇ (F), BArF₁₁Cl₅ (G)

Structures C, F and G have significantly increased steric bulk around the boron centre, in comparison to BArF₁₅ (Figure 5.4.2). The bulk was increased using chlorine in the *ortho* positions or an *ortho* trifluoromethyl substituent, instead of the *ortho* fluorines observed in

BArF₁₅. Structures **D** and **E** do not possess increased steric bulk around the boron centre but were used for comparison.

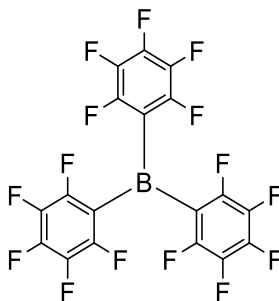


Figure 5.4.2 - Chemical structure of Tris(pentafluorophenyl)borane (BArF₁₅).

The various boranes were assessed in CD₂Cl₂ with the *N*-methyl-2-(4-nitrophenyl)benzothiazoline to see if adduct formation was observed in the ¹¹B NMR. This was done because the adduct formation discussed previously appeared to occur after the hydride transfer to form the benzothiazoline. This is very likely as after the transfer, the boron centre regains its Lewis acidic properties (empty p orbital regained once the hydride transfer has occurred).

The ¹¹B NMR for the reaction between **C** and *N*-methyl-2-(4-nitrophenyl)benzothiazoline showed a broad peak at ca. 67 ppm which is indicative of the free three-coordinate borane. This indicated that no boron-sulfur adduct had formed. The NMR of the reactions of **D**, **E**, **F** and **G** with *N*-methyl-2-(4-nitrophenyl)benzothiazoline also showed similar broad peaks at ca. 66 ppm, on average (65 ppm, 62 ppm, 72 ppm and 65 ppm, respectively). Again, these peaks suggested no boron-sulfur adduct formation with any of the in-house available boranes.

The ¹¹B NMR for the reactions of all 5 boranes (**C–G**) with *N*-methyl-2-(4-nitrophenyl)benzothiazoline can be seen in Figure 5.4.3. No evidence of the formation of a boron-sulfur adduct was observed with any of the listed boranes and the benzothiazoline used.

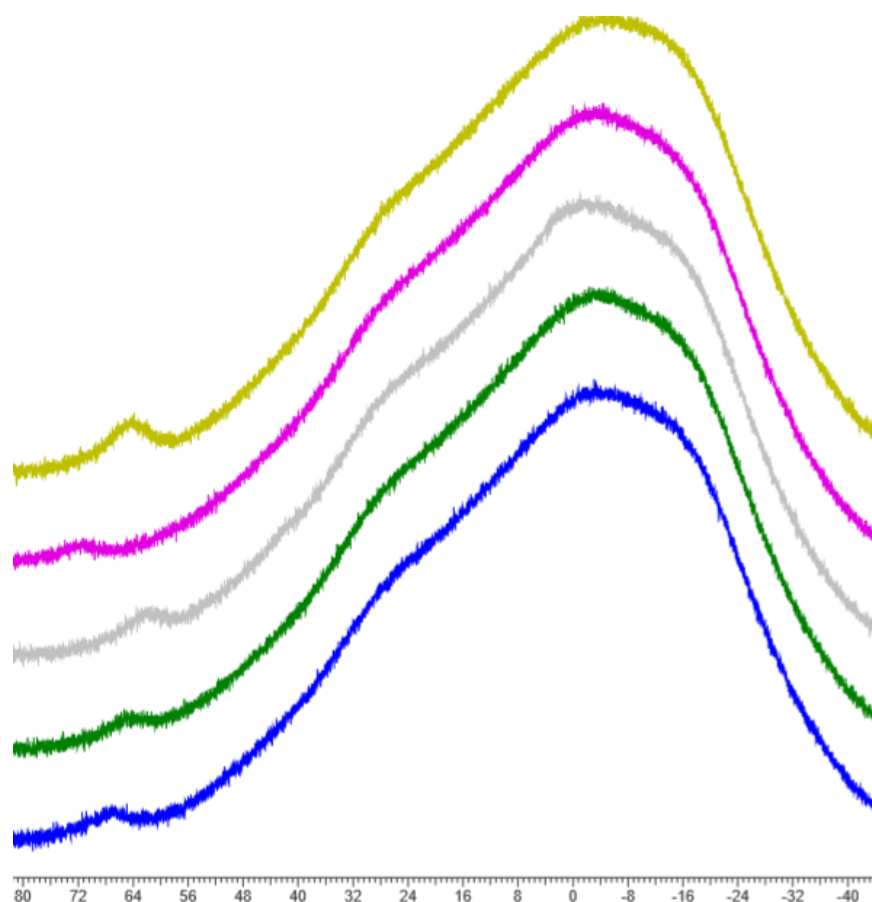


Figure 5.4.3 - The ^{11}B NMR for the reactions of *N*-methyl-2-(4-nitrophenyl)benzothiazoline with various boranes; $\text{B}(\text{CCl}_4\text{F})_3$ (blue), BARF_{17} (mm) (green), BARF_{16} (grey), BARF_{17} (om) (pink), $\text{BARF}_{11}\text{Cl}_5$ (yellow)

$\text{B}(\text{Cl}_4\text{F})_3$ (**C**) has increased steric bulk around the boron centre; the six *ortho*-chloro substituents on both *ortho* positions of each aryl ring, and the increased size of chlorine compared to fluorine contribute to this bulk. Introducing chlorine groups has been shown to increase the twist of the aryl ring, with respect to the boron centre i.e. the molecule is no longer completely planar. The twist in the B–C bond allowed for the alignment of the *ortho*-chloro substituent and the formally vacant $2p_z$ orbital of the boron which facilitated through-space donation of the chlorine lone pair in to the empty orbital.¹⁶⁴ This in turn decreases the Lewis acidity of the borane and prevented the formation of boron-sulfur adduct.

BARF_{17} (**D**) does not have increased steric bulk around the boron centre, as the two aryl rings contain trifluoromethyl substituents in the 3- and 5- positions. However, no boron-sulfur adduct formation occurred. It has been shown that having small *ortho*-substituents (H in this case) increases the symmetry of the molecule and decreases twist in B–C bond. This, in turn, increases the overlap of the boron $2p_z$ orbital and the π -orbitals of the aromatic ring,¹⁶⁴ decreasing the Lewis acidity of the borane.

Similarly to **D**, BArF_{16} (**E**) does not have increased steric bulkiness around the boron centre, but possessed a single aryl ring containing trifluoromethyl substituents in the 3- and 5-positions. This again exhibited similar behaviour to that discussed for **D**, and displayed decreased Lewis acidity. The decreased Lewis acidity in **B** and **C** accounts for the lack of boron-sulfur adduct formation.

BArF_{17} (**F**) does display increased steric bulk around the boron centre, with a single *ortho*-trifluoromethyl substituent present on two of the three aryl rings. Similar to **C**, this decreased Lewis acidity because of the through-space donation of electrons from the fluorines into the vacant $2p_z$ orbital of the boron.

$\text{BArF}_{11}\text{Cl}_5$ (**G**) also displayed an increase in steric bulk around the boron centre, with a single aryl ring possessing *ortho*-chloro substituents in the 2- and 6-positions. This borane also contains an aryl ring with trifluoromethyl groups on the 3- and 5-positions. The incorporation of these substituted aryl rings is likely to decrease Lewis acidity in the same way as discussed for **C** and **D** respectively. This decrease in Lewis acidity made the formation of boron-sulfur adducts less likely. Each of the in-house available boranes was identified as a viable option for moving forward without adduct formation.

Boron centre electrophilicity and borane Lewis acidity are closely correlated. The incorporation of an *ortho*-trifluoromethyl substituent significantly decreases the electrophilicity of the boron due to the through-space donation (Figure 5.4.4) mentioned previously.

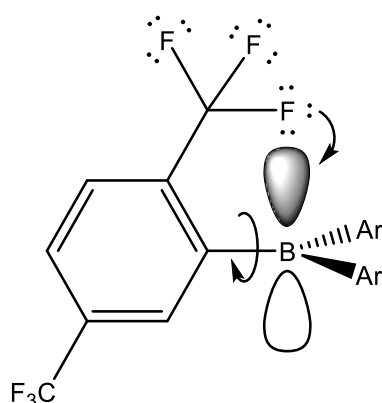


Figure 5.4.4 - The through-space donation of the lone pair of electrons from a fluorine of the *ortho*-substituted trifluoromethyl group into the formally vacant $2p_z$ orbital of the boron centre

A pentachlorophenyl substituent has similar effects on Lewis acidity as a pentafluorophenyl substituent.¹⁶⁶ The lone pair of both *ortho*-chloro substituents are donated into the vacant $2p_z$ orbital of the boron (Figure 5.4.5). With the pentafluorophenyl substituent, you see donation of the fluorine $2p$ orbital into the π^* orbital of the aromatic ring.¹⁶⁴

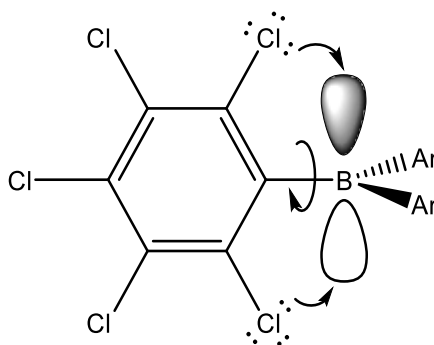


Figure 5.4.5 - The through-space donation of the lone pair of electrons from the *ortho*-chloro substituents on the aryl ring, into the formally vacant $2p_z$ orbital of the boron centre

Both pentachlorophenyl and pentafluorophenyl substituents increase the electrophilicity of the boron centre, compared to *ortho*-trifluoromethyl.⁸⁸ Means to enable quantification of Lewis acidity have previously been reported.^{167–168} One study used an array of different Lewis acids (boranes) with a single Lewis base (Triethylphosphine oxide) to form a boron-phosphorus adduct.^{167–168} The ^{31}P NMR was recorded with the intent to measure increased Lewis acidity through increased deshielding of the phosphorus atom bound to the boron resulting in a downfield shift. However, using this approach alone does not tackle the issue of electronics, nor sterics, with respect to *ortho*-substituents and Lewis acidity in the free three-coordinate borane. Furthermore, it does not address the change in electronics due to the formation of the adduct (boron formally becoming tetrahedral in geometry from trigonal planar). A study published in 2014 using the Gutmann-Beckett method for quantification reported multiple electronic effects that could influence the Lewis acidity of boron compounds.¹⁶⁹ This study aimed to increase the Lewis acidity of the boron centre. While BARF_{15} has been identified as an ideal boron based Lewis acid,¹⁷⁰ there has been a lot of research into increasing Lewis acidity. Perfluorinated 9-boraphenylfluorene has displayed greater Lewis acidity than that of BARF_{15} .^{171–172} However, for the purpose of this project a decrease in Lewis acidity through increased steric bulk around the boron centre was required in order to hinder the formation of boron-sulfur adducts.

Studies comparing the Lewis acidity of boranes with the rate of hydrogen cleavage, using tri-*tert*-butylphosphine as the Lewis base with a variety of different triarylboranes have been reported.¹⁶⁴ The cleavage reaction of the Lewis acid/base of tris(pentafluorophenyl)borane and P^tBu₃ with the addition of hydrogen and formation of a tri-*tert*-butylphosphonium cation and the tris(pentafluorophenyl)borohydride was complete within 5 h. The reaction was carried out with several additional boranes but resulted in an increased reaction time; the slowest reaction involved BArCl₁₀F₆ and showed only 23% completion in 96 h¹⁶⁴ (Figure 5.4.6).

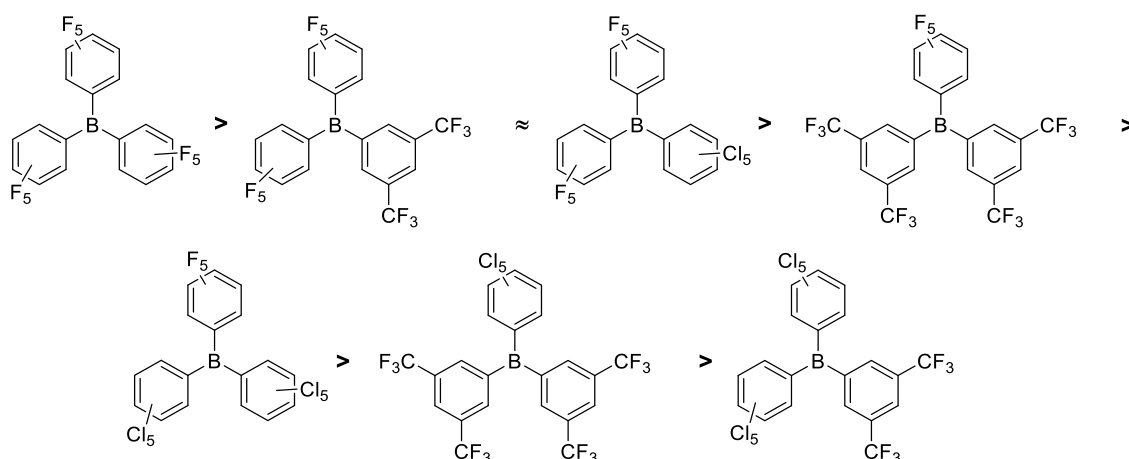


Figure 5.4.6 - The chemical structures of the different boranes, in order of rate of hydrogen cleavage, with the Lewis base tri-*tert*-butylphosphine¹⁶⁴

Using the information from Figure 5.4.6 it can be suggested that the boranes that were tested here for adduct formation (Figure 5.4.1) would react and cleave hydrogen very slowly, if at all, in the case of B(CCl₄F)₃. This is due to the substantial increase in *ortho* shielding of the boron centre and donation into the empty boron orbital. The decreased Lewis acidity of the boranes in Figure 5.4.1 can also explain why the boron-sulfur adduct is not observed in the ¹¹B NMR with these compounds.

6. Conclusion and future work

Following the literature for the synthesis of the *N*-methyl-2-(aryl)benzothiazolines, several compounds were successfully synthesised. However, several alterations had to be made in order to synthesise compounds containing electron-withdrawing substituents.

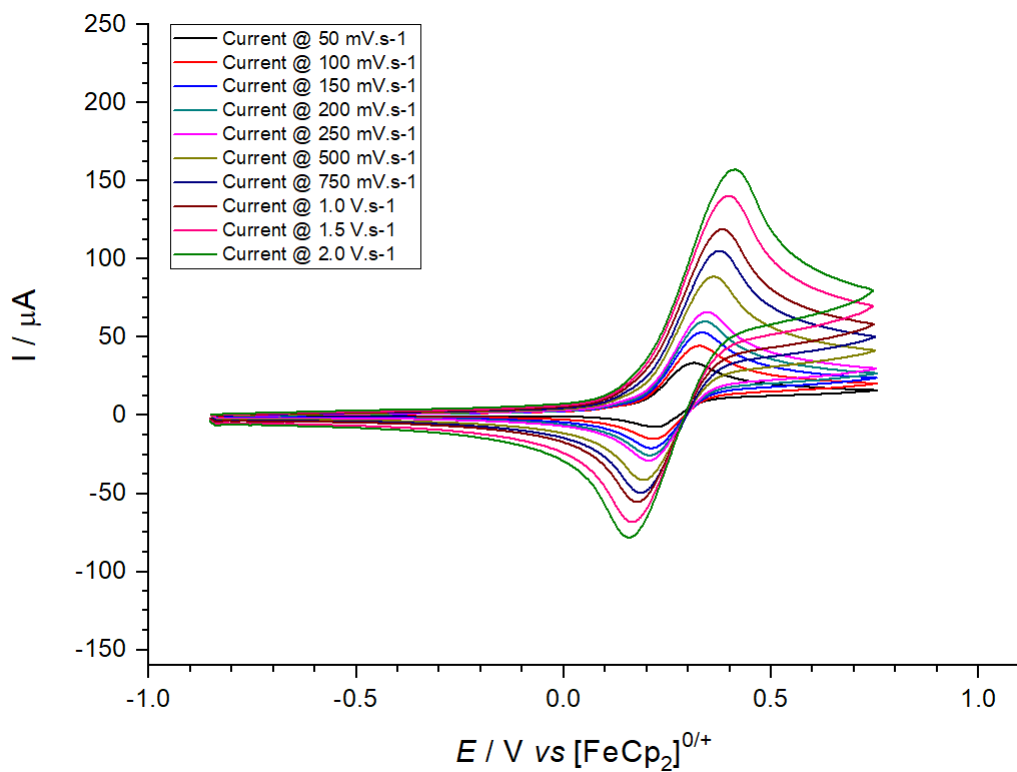
The electrochemical analysis of the *N*-methyl-2-(aryl)benzothiazolines was performed and showed that the C2 substituent can influence the ease and position of oxidation/reduction. It was also shown that a more complicated process occurred for the phenyl substituent.

The hydride transfer experiments showed that it is possible for hydride transfer from a borohydride to the benzothiazolium can take place but there were complications with the formation of a boron-sulfur adduct. Further investigation into sterics and Lewis acidity needs to be undertaken in order to find a borane that is Lewis acidic enough to heterolytically cleave hydrogen in an FLP system. However, the borane also needs to avoid forming a Lewis acid-base adduct with the sulfur of the benzothiazoline, suggesting a narrow target margin for Lewis acidity. Using a different FLP system is also a possibility, or a reagent lacking boron altogether to remove the possibility of boron-sulfur adduct formation. However, further research into this area is required.

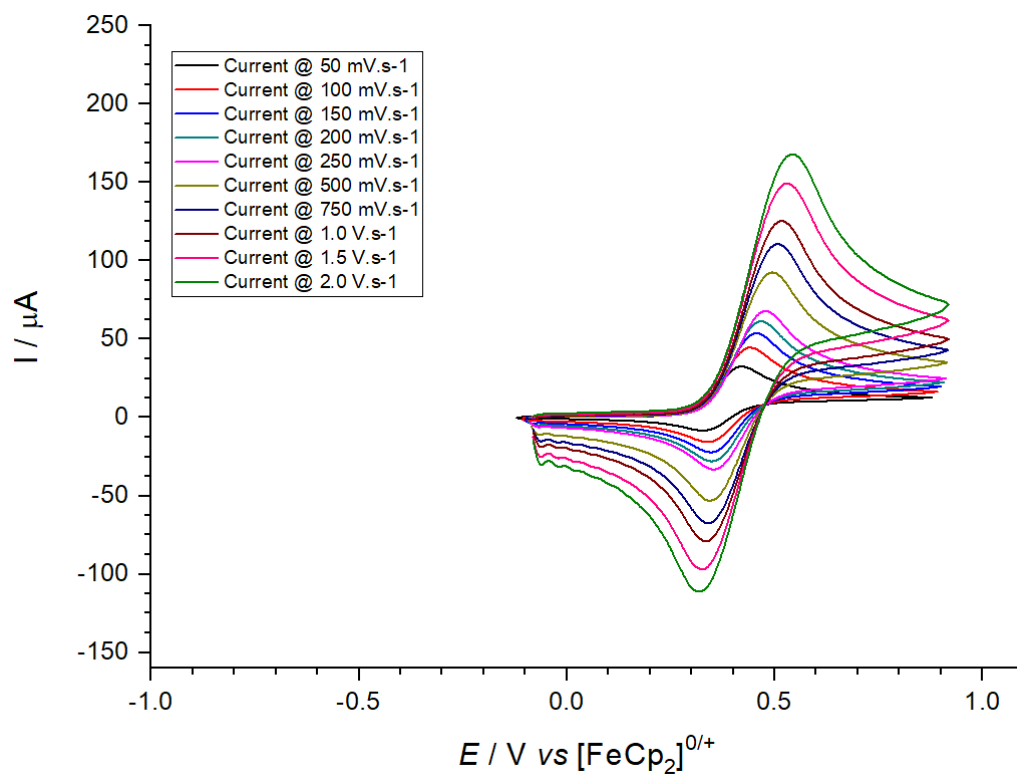
There is a possibility of testing the disulfide linked imines, as variations have previously been tested for their antibacterial activities against both gram-positive and gram-negative bacteria.¹⁷³⁻¹⁷⁴

The use of *N*-methyl-2-(aryl)benzimidazolines could be a possibility of another class of carbon-based Lewis acids which would prevent the formation of a boron-sulfur adduct; and a viable continuation of this work.

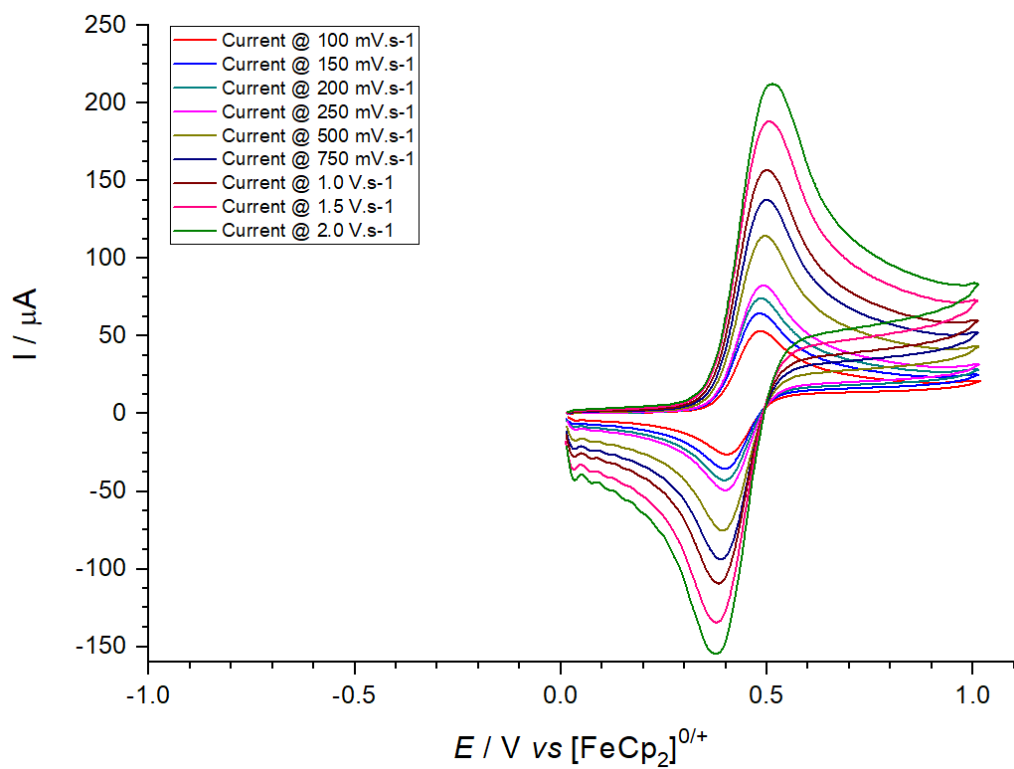
7. Appendix



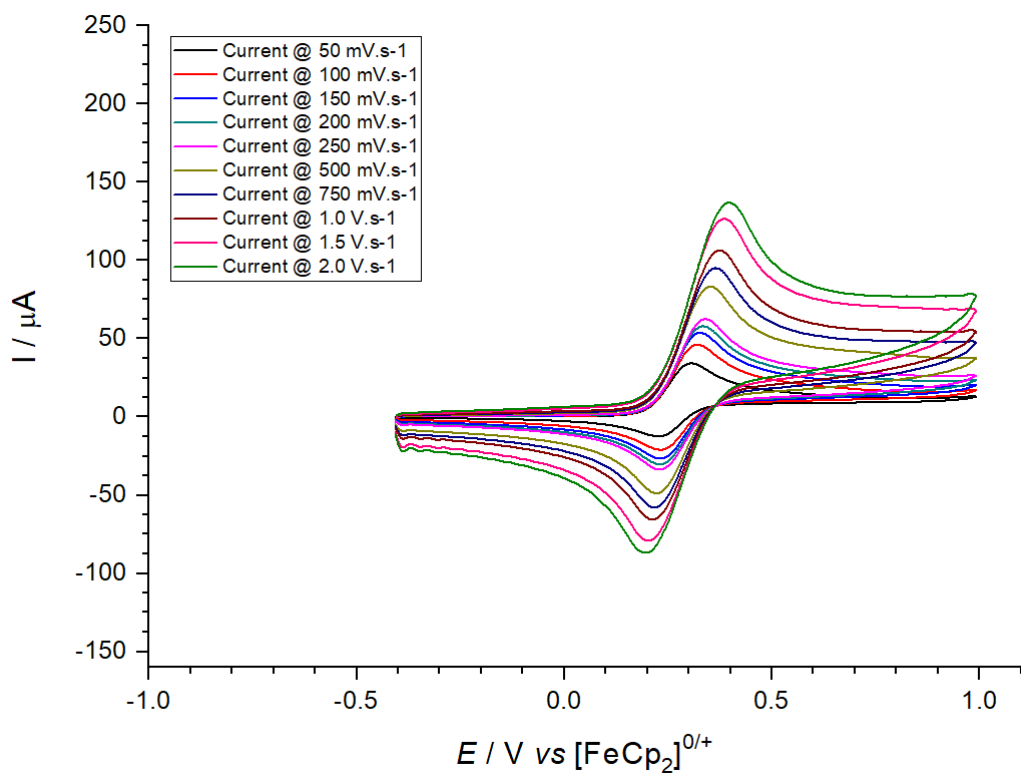
A1 - VSR cyclic voltammetry for *N*-methyl-2-(2-fluorophenyl)benzothiazoline, **BNZ2**



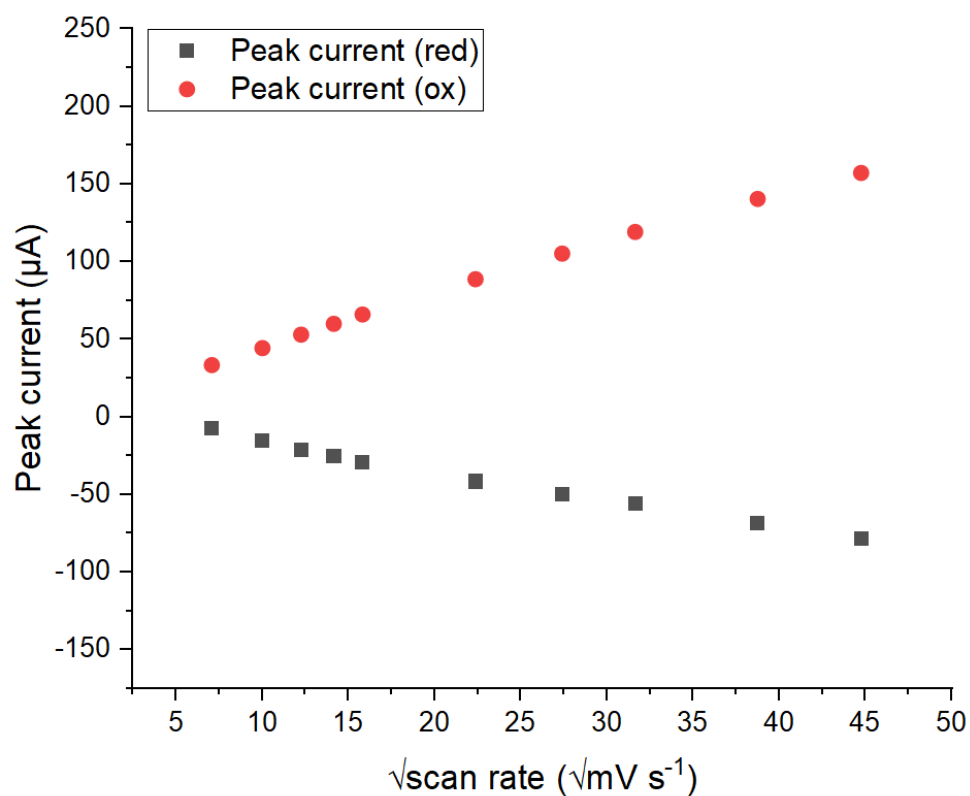
A2 - VSR cyclic voltammetry of *N*-methyl-2-(3,5-di-*tert*-butyl-2-hydroxyphenyl)benzothiazoline, **BNZ4**



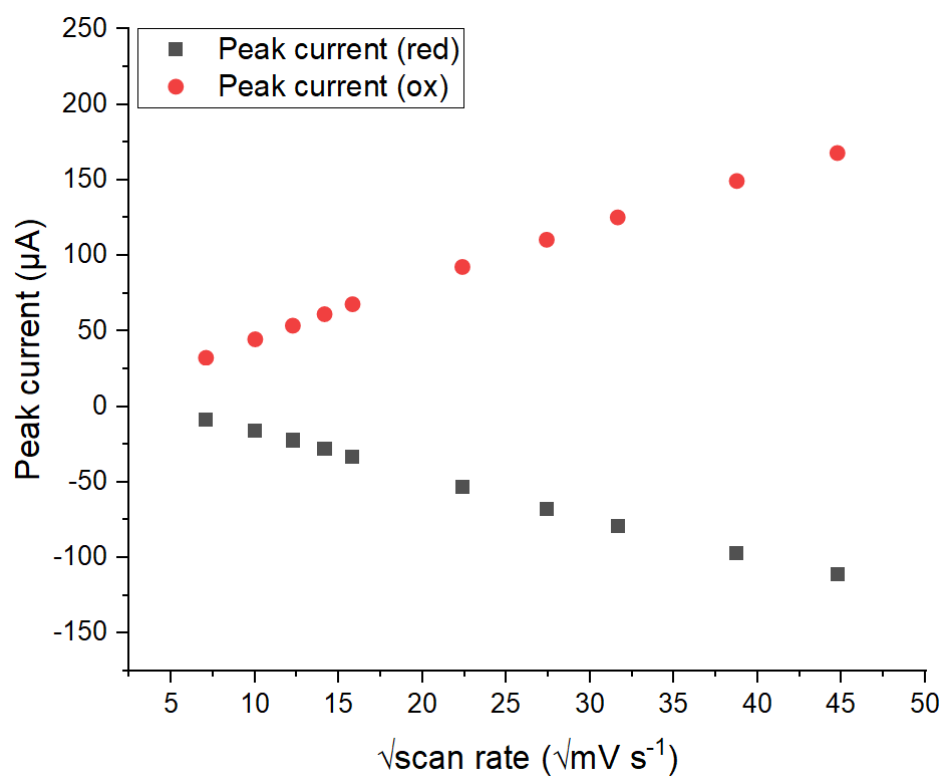
A3 - VSR cyclic voltammetry of *N*-methyl-2-(3-nitrophenyl)benzothiazoline, **BNZ7**



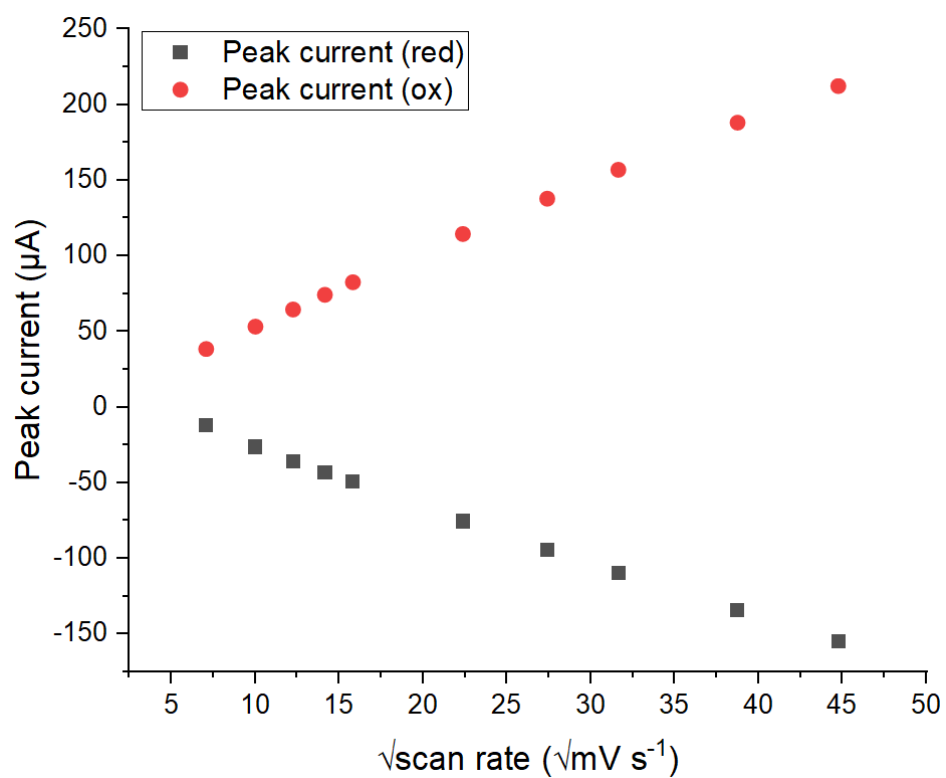
A4 - VSR cyclic voltammetry of *N*-methyl-2-(3,5-di-*tert*-butyl-2-methoxyphenyl)benzothiazoline, **BNZ8**



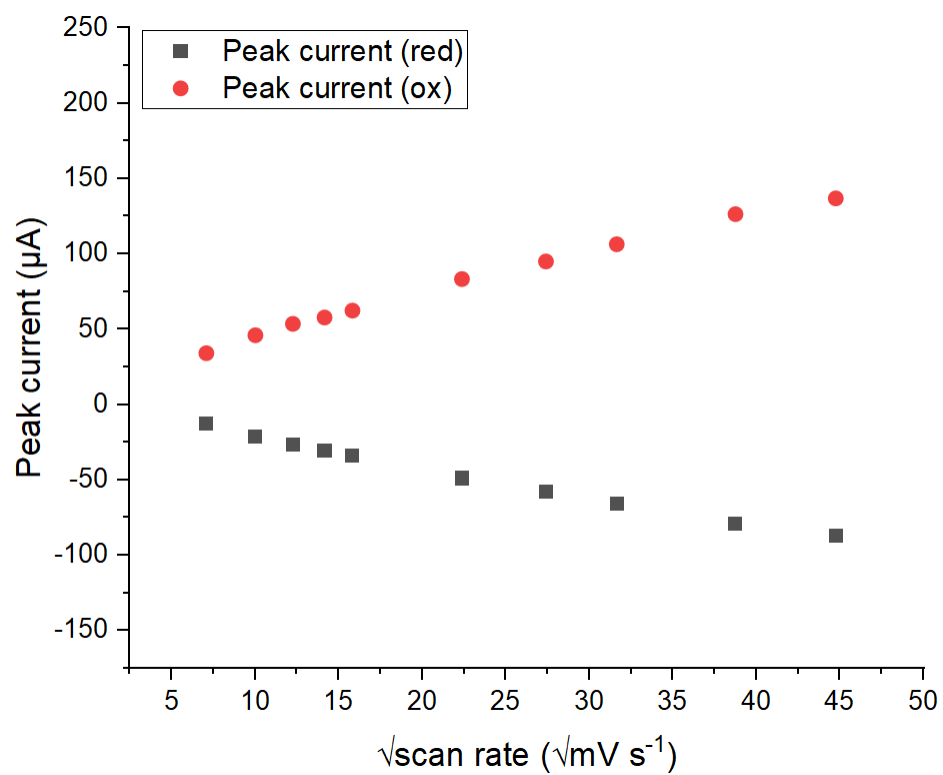
A5 - Randles-Sevcik plot for *N*-methyl-2-(2-fluorophenyl)benzothiazoline, **BNZ2**



A6 - Randles-Sevcik plot for *N*-methyl-2-(3,5-di-*tert*-butyl-2-hydroxyphenyl)benzothiazoline, **BNZ4**



A7 - Randles-Sevcik plot for *N*-methyl-2-(3-nitrophenyl)benzothiazoline, **BNZ7**



A8 - Randles-Sevcik plot for *N*-methyl-2-(3,5-di-*tert*-butyl-2-methoxyphenyl)benzothiazoline, **BNZ8**

8. References

1. Schlapbach L. and Züttel A., *Nature*, **2002**, 414, 353–358
2. Lui K., Song C. and Subramani V., *Hydrogen and Syngas Production and Purification Technologies*, Wiley & Sons, Hoboken, NJ, **2010**
3. Ogden J. M., *Physics Today*, **2002**, 55, 69–75
4. IPCC, *Fourth Assessment Report (AR4) - Climate Change 2007: Synthesis Report*, Intergovernmental Panel on Climate Change, Geneva, Switzerland, **2007**
5. Sorrell S., Speirs J., Bentley R., Brandt A. and Miller R., *Energy Policy*, **2010**, 38, 5290–5295
6. Bentley R. and Boyle G., *Environ. Plann. B.*, **2008**, 35, 609–626
7. Barbir F., *PEM Fuel Cells: Theory and Practice*, **2013**, Academic Press, Waltham, MA
8. Rohland B., Nitsch J. and Wendt H., *J. Power Sources*, **1992**, 37, 271–277
9. Zou X. and Zhang Y., *Chem. Soc. Rev.*, **2015**, 44, 5148–5180
10. Das D. and Veziroglu T. N., *Int. J. Hyd. Energ.*, **2001**, 26, 13–28
11. Ni M., Leung D. Y. C., Leung M. K. H. and Sumathy K., *Fuel Process. Technol.*, **2006**, 87, 461–472
12. Holladay J. D., Hu J., King D. L. and Wang Y., *Catal. Today*, **2009**, 139, 244–260
13. Sanchez N., Ruiz R. Y., Cifuentes B. and Cobo M., *Int. J. Hyd. Energ.*, **2016**, 41, 5640–5651
14. Bridgwater A. V., *Fuel*, **1995**, 74, 631–653
15. Xu J. and Froment G. F., *AIChE J.*, **1989**, 35, 88–96
16. Pritchard J., Filonenko G. A., van Putten R., Hensen E. J. M. and Pidko E. A., *Chem. Soc. Rev.*, **2015**, 44, 3808–3833
17. Ullrich J. and Breit B., *ACS Catal.*, **2018**, 8, 785–789
18. Mondy S., Lenglet A., Cosson V., Pelletier S., Pateyron S., Gillard F., Scholte M., Brocard L., Couzigou J.-M., Tcherkez G., Pean M. and Ratet P., *Plant, Cell & Env.*, **2014**, 37, 54–69
19. Sigfridsson K., Liedel N., Sanganas O., Chernev P., Lenz O., Yoon K.-S., Nishihara H, Parkin A, Armstrong F., Dementin S., Rousset M De Lacey A. and Haumann M., *Biochim. Biophys. Acta, Bioenerg.*, **2015**, 1847, 162–170
20. Lui T., Li B., Popescu C. V., Bilko A., Pérez L. M., Hall M. B. and Darensbourg M. Y., *Chem. Eur. J.*, **2010**, 16, 3083–3089

21. Siebel J. F., Adamska-Venkatesh A., Weber K., Rumpel S., Reijerse E. and Lubitz W., *Biochemistry*, **2015**, 54, 1474–1483
22. Albertini M., Vallese F., Di Valenti M., Berto P., Giacometti G. M., Constantini P. and Carbonera D., *Int. J. Hyd. Energ.*, **2014**, 39, 18574–18582
23. Vignais P. M. and Billoud B., *Chem. Rev.*, **2007**, 107, 4206–4272
24. Hallenbeck P. C. and Benemann J. R., *Int. J. Hyd. Energ.*, **2002**, 27, 1185–1193
25. Lai C.-H., Reibenspies J. H. and Darensbourg M. Y., *Angew. Chem. Int. Ed. Engl.*, **1996**, 35, 2390–2393
26. Osterloh F., Saak W., Haase D. and Pohl S., *Chem. Commun.*, **1997**, 979–980
27. Sellman D., Geipel F. and Heinemann F. W., *Chem. Eur. J.*, **2002**, 8, 958–966
28. Verhagen J. A. W., Ellis D. D., Luts M., Spek A. L. and Bouwman E., *J. Chem. Soc., Dalton Trans.*, **2002**, 1275–1280
29. Wilson A. D., Newell R. H., McNevin M. J., Muckerman J. T., Rakowski Dubois M. and Dubois D. L., *J. Am. Chem. Soc.*, **2006**, 128, 358–366
30. Ozawa H., Haga M. and Sakai K., *J. Am. Chem. Soc.*, **2006**, 128, 4926–4927
31. Karunadasa H. I., Montalvo E., Sun Y., Majda M., Long J. R. and Chang C. J., *Science*, **2012**, 335, 698–702
32. Li L., Duan L., Fen W., Li C., Wang M., Hagfeldt A. and Sun L., *Chem. Commun.*, **2012**, 48, 988–990
33. Pullen S., Fei H., Orthaber A., Cohen S. M. and Ott S., *J. Am. Chem. Soc.*, **2013**, 135, 16997–17003
34. Rakowski Dubois M. and Dubois D. L., *Chem. Soc. Rev.*, **2009**, 38, 62–72
35. Low J. J. and Goddard W. A., *Organometallics*, **1986**, 5, 609–622
36. Jourdan A., Gonzalez-Zamora E. and Zhu J., *J. Org. Chem.*, **2002**, 67, 3163–3164
37. Frey G. D., Lavallo V., Donnadiu B., Schoeller W. W. and Bertrand G., *Science*, **2007**, 316, 439–441
38. Bardi U. and Caporali S., *Minerals*, **2014**, 4, 388–398
39. Haddad A. Z., Garabato B. D., Kozlowski P. M., Buchanan R. M. and Grapperhaus C. A., *J. Am. Chem. Soc.*, **2016**, 138, 7844–7847
40. Zheng Y., Jiao Y., Zhu Y., Li L. H., Han Y., Chen Y., Du A., Jaroniec M. and Qiao S. Z., *Nat. Commun.*, **2014**, 5, 1–8
41. Cui W., Liu Q., Cheng N., Asiri A. M. and Sun X., *Chem. Commun.*, **2014**, 50, 9340–9342
42. Qu L., Liu Y., Baek J.-B. and Dai L., *ACS Nano.*, **2010**, 4, 1321–1326

43. Wang S., Zhang L., Xia Z., Roy A., Chang D. W., Baek J.-B. and Dai L., *Angew. Chem. Int. Ed.*, **2012**, 51, 4209–4212
44. Tao L., Wang Q., Dou S., Ma Z., Huo J., Wang S. and Dai L., *Chem. Commun.*, **2016**, 52, 2764–2767
45. Ma Z., Dou S., Shen A., Tao L., Dai L. and Wang S., *Angew. Chem. Int. Ed.*, **2015**, 54, 1888–1892
46. Li D., Jia Y., Chang G., Chen J., Liu H., Wang J., Hu Y., Xia Y., Yang D. and Yao X., *Chem.*, **2018**, 4, 2345–2356
47. Balogun M.-S., Qiu W., Yang H., Fan W., Huang Y., Fang P., Li G., Ji H. and Tong Y., *Energy Environ. Sci.*, **2016**, 9, 3411–3416
48. Qiu W., Xie X.-Y., Qiu J., Fang W.-H., Liang R., Ren X., Ji X., Cui G., Asiri A. M., Cui G., Tang B. and Sun X., *Nat. Commun.*, **2018**, 9, 1–8
49. Lv C., Yan C., Chen G., Ding Y., Sun J., Zhou Y. and Yu G., *Angew. Chem.*, **2018**, 130, 6181–6184
50. Wu J., Ma S., Sun J., Gold J. I., Tiwary C., Kim B., Zhu L., Chopra N., Odeh I. N., Vajtai R., Yu A. Z., Luo R., Lou J., Ding G., Kenis P. J. A. and Ajayan P. M., *Nat. Commun.*, **2016**, 7, 1–6
51. Ghausi M. A., Xie J., Li Q., Wang X., Yang R., Wu M., Wang Y. and Dai L., *Angew. Chem.*, **2018**, 130, 13319–13323
52. Berry G. D., Pasternak A. D., Rambach G. D., Smith J. R. and Schock R. N., *Energy*, **1996**, 21, 289–303
53. Wait A. F., Parkin A., Morley G. M., dos Santos L. and Armstrong F. A., *J. Phys. Chem.*, **2010**, 114, 12003–12009
54. Grove W. R., *Phil. Mag. (III)*, **1842**, 417–420
55. Appleby A. J., *Int. J. Hydrog. Energy*, **1994**, 19, 175–180
56. Brumfiel G., *Nature*, **2003**, 104
57. Deng J., Ren P., Deng D., Yu L., Yang F. and Bao X., *Energy Environ. Sci.*, **2014**, 9, 1919–1923
58. Kreuer K. D., *J. Membr. Sci.*, **2001**, 185, 29–39
59. Karayakin A. A., Morozov S. V., Karayakina E. E., Varfolomeyev S. D., Zorin N. A. and Cosnier S., *Electrochem. Commun.*, **2002**, 4, 417–420
60. Contestabile, M., Offer G. J., Slade R., Jaeger F. and Thoenes M., *Energy Environ. Sci.*, **2011**, 4, 3754–3772
61. Potera C., *Environ. Health Perspect.*, **2007**, 115, A38–A41

62. Manoharan Y., Hosseini S. E., Butler B., Alzahrani H., Fou Snr. B. T., Ashuri T. and Krohn J., *Appl. Sci.*, **2019**, 9, 2296
63. Midilli A., Ay M., Dincer I. and Rosen M. A., *Renew. Sust. Energ. Rev.*, **2005**, 9, 255–271
64. Staffell I., Scamman D., Abad A. V., Balcombe P., Dodds P. E., Ekins P., Shah N. and Ward K. R., *Energy Environ. Sci.*, **2019**, 12, 463–491
65. Runyon J. W., Steinhof O., Rasika Dias H. V., Calabrese J. C., Marshall W. J. and Arduengo III A. J., *Aust. J. Chem.*, **2011**, 64, 1165–1172
66. Wallace J. S. and Ward C. A., *Int. J. Hydrog. Energy*, **1983**, 8, 255–268
67. Chalk S. G. and Miller J. F., *J. Power Sources*, **2006**, 159, 73–80
68. Brown H. C., Schlesinger H. I. and Cardon S. Z., *J. Am. Chem. Soc.*, **1942**, 64, 325–329
69. McCahill J. S. J., Welch G. C. and Stephan D. W., *Angew. Chem. Int. Ed.*, **2007**, 46, 4968–4971
70. Wang H., Fröhlich R., Kehr G. and Erker G., *Chem. Commun.*, **2008**, 5966–5968
71. Parks D. J. and Piers W. E., *J. Am. Chem. Soc.*, **1996**, 118, 9440–9441
72. Fontaine F.-G. and Stephan D. W., *Phil. Trans. R. Soc.*, **2017**, 375: 20170004
73. Welch G. C., San Juan R. R., Masuda J. D. and Stephan D. W., *Science*, **2006**, 314, 1124–1126
74. Sumerin V., Schulz F., Atsumi M., Wang C., Nieger M., Leskelä M., Repo T., Pyykkö P. and Rieger B., *J. Am. Chem. Soc.*, **2008**, 130, 14117–14119
75. Stephan D. W. and Erker G., *Angew. Chem. Int. Ed.*, **2010**, 49, 46–76
76. Ramos A., Lough A. J. and Stephan D. W., *Chem. Commun.*, **2009**, 1118–1120
77. Sumerin V., Schulz F., Nieger M., Leskelä M., Repo T. and Rieger B., *Angew. Chem. Int. Ed.*, **2008**, 47, 6001–6003
78. Chase P. A. and Stephan D. W., *Angew. Chem.*, **2008**, 120, 7543–7547
79. Geier S. J., Chase P. A. and Stephan D. W., *Chem. Commun.*, **2010**, 46, 4884–4886
80. Holschumacher D., Bannenberg T., Hrib C. G., Jones P. G. and Tamm M., *Angew. Chem. Int. Ed.*, **2008**, 47, 7428–7432
81. Geier S. J., Gille A. L., Gilbert T. M. and Stephan D. W., *Inorg. Chem.*, **2009**, 48, 10466–10474
82. Geier S. J. and Stephan D. W., *J. Am. Chem. Soc.*, **2009**, 131, 3476–3477
83. Chase P. A., Welch G. C. Jurca T. and Stephan D. W., *Angew. Chem. Int. Ed.*, **2007**, 46, 8050–8053

84. Hamza A., Stirling A., Rokob T. A. and Pápai I., *Int. J. Quant. Chem.*, **2009**, 109, 2416–2425
85. Lu Z., Wang Y., Liu J., Lin Y.-J., Li Z. H. and Wang H., *Organometallics*, **2013**, 32, 6753–6758
86. Binding S. C., Zaher H., Chadwick F. M. and O’Hare D., *Dalton Trans.*, **2012**, 41, 9061–9066
87. Scott D. J., Fuchter M. J. and Ashley A. E., *Angew. Chem. Int. Ed.*, **2014**, 53, 10218–10222
88. Herrington T. J., Thom A. J. W., White A. J. P. and Ashley A. E., *Dalton Trans.*, **2012**, 41, 9019–9022
89. Farrell J. M., Hatnean J. A. and Stephan D. W., *J. Am. Chem. Soc.*, **2012**, 134, 15728–15731
90. Lawrence E. J., Herrington T. J., Ashley A. E. and Wildgoose G. G., *Angew. Chem. Int. Ed.*, **2014**, 53, 9922–9925
91. Ménard G. and Stephan D. W., *Angew. Chem.*, **2012**, 124, 8397–8400
92. Weicker S. A. and Stephan D. W., *Bull. Chem. Soc. Jpn.*, **2015**, 88, 1003–1016
93. Misumi Y., Seino H. and Mizobe Y., *J. Am. Chem. Soc.*, **2009**, 131, 14636–14637
94. Owen G. R., *Chem. Commun.*, **2016**, 52, 10712–10726
95. Owen G. R., *Chem. Soc. Rev.*, **2012**, 41, 3535–3546
96. Tsoureas N., Kuo Y.-Y., Haddow M. F. and Owen G. R., *Chem. Commun.*, **2011**, 47, 484–486
97. Geri J. B. and Szymczak N. K., *J. Am. Chem. Soc.*, **2015**, 137, 12808–12814
98. Ohki Y., Matsuura N., Marumoto T., Kawaguchi H. and Tatsumi K., *J. Am. Chem. Soc.*, **2003**, 125, 7978–7988
99. Matsumoto T., Nakaya Y. and Tatsumi K., *Angew. Chem. Int. Ed.*, **2008**, 47, 1913–1915
100. Ohki Y., Sakamoto M. and Tasumi K., *J. Am. Chem. Soc.*, **2008**, 130, 11610–11611
101. Sweeney Z. K., Polse J. L., Bergman R. G. and Andersen R. A., *Organometallics*, **1999**, 18, 5502–5510
102. Sweeney Z. K., Polse J. L., Andersen R. A., Bergman R. G. and Kubinec M. G., *J. Am. Chem. Soc.*, **1997**, 119, 4543–4544
103. Budlezaar P. H. M., Hughes D. L., Bochmann M., Macchioni A. and Rocchigiani L., *Chem. Commun.*, **2020**, 56, 2542–2545
104. Campos J., *J. Am. Chem. Soc.*, **2017**, 139, 2944–2947

105. Harman W. H. and Peters J. C., *J. Am. Chem. Soc.*, **2012**, 134, 5080–5082
106. Fong H., Moret M.-E., Lee Y. and Peters J. C., *Organometallics*, **2013**, 32, 3053–3062
107. Devillard M., Declercq R., Nicolas E., Ehlers A. W., Backs J., Saffon-Merceron N., Bouhadir G., Slootweg J. C., Uhl W. and Bourissou D., *J. Am. Chem. Soc.*, **2016**, 138, 4917–4926
108. Inés B., Holle S., Goddard R. and Alcarazo M., *Angew. Chem. Int. Ed.*, **2010**, 49, 8389–8391
109. Lawrence E. J., Clark E. R., Curless L. D., Courtney J. M., Blagg R. J., Ingleson M. J. and Wildgoose G. G., *Chem. Sci.*, **2016**, 7, 2537–2543
110. Fasano V., Radcliffe J. E., Curless L. D. and Ingleson M. J., *Chem. Eur. J.*, **2017**, 23, 187–193
111. Williams, D. B. G. and Lawton, M., *J. Org. Chem.*, **2010**, 75, 8351–8354
112. Togashi, M., Urano, Y., Kojima, H., Terai, T., Hanaoka, K., Igarashi, K., Hirata, Y. and Nagano, T., *Org. Lett.*, **2010**, 12, 1704–1707
113. LeSuer, R. J., Buttolph, C. and Geiger, W. E., *Anal. Chem.*, **2004**, 76, 6395–6401
114. Hünig S., Scheutzow D., Schlaf H. and Quast H., *Liebigs Ann. Chem.*, **1972**, 765, 110–125
115. CrysAlisPro 1.171.40.68a, **2019**, Rigaku Oxford Diffraction
116. Sheldrick G. M., **2015**, *Acta Cryst.*, A71, 3–8
117. Sheldrick G. M., **2015**, *Acta Cryst.*, C71, 3–8
118. Chikashita H., Ishimoto N., Komazawa S. and Itoh K., *Heterocycles*, **1985**, 23, 2509–2514
119. Chikashita H., Komazawa S., Ishimoto N., Inoue K. and Itoh K., *Bull. Chem. Soc. Jpn.*, **1989**, 62, 1215–1225
120. Kil H. J. and Lee I.-S. H., *J. Phys. Chem. A.*, **2009**, 113, 10704–10709
121. Ravetz B. D., Pun A. B., Churchill E. M., Congreve D. N., Rovis T. and Campos L. M., *Nature*, **2019**, 565, 343–346
122. Sirgamalla R., Kommakula A., Konduru S., Ponakanti R., Devaram J. and Boda S., *Chem. Data Collect.*, **2020**, 27, 100362
123. Sharma K., Singh R. V. and Fahmi N., *Spectrochimica Acta Part A*, **2011**, 78, 80–87
124. Miyamatsu H., Ueno S., Shimizu M., Hosono J., Tomari M., Seida K., Suzuki T. and Wada J., *J. Med. Chem.*, **1974**, 17, 491
125. Bradshaw T. D., Wrigley S., Shi D.-F., Schultz R. J., Paull K. D. and Stevens M. F. G., *Br. J. Cancer*, **1998**, 77, 745

126. Wells G., Bradshaw T. D., Diana P., Seaton A., Shi D.-F., Westwell A. D. and Stevens M. F. G., *Bioorg. Med. Chem. Lett.*, **2000**, 10, 513
127. Hamby J. M. and Showalter H. D. H., *Pharmacol. Ther.*, **1999**, 82, 169
128. Wördehoff M. M. and Hoyer W., *Bio Protoc.*, **2018**, 8 (14)
129. Garmaise D. L., Paris G. Y., Komlossy J., Chambers C. H. and McCrae R. C., *J. Med. Chem.*, **1969**, 12, 30–36
130. Green A. G., *Ber. Dtsch. Chem. Ges.*, **1889**, 22, 968–973
131. Tang J., Zhang B.-N., Ge M., Zhu L., Wang Y., Chen Y. and Xia P., *Chin. J. Chem.*, **2008**, 26, 1447–1453
132. Sakamoto T., Mori K. and Akiyama T., *Org. Lett.*, **2012**, 14, 3312–3315
133. Banerjee S., Payra S., Saha A. and Sereda G., *Tetrahedron Lett.*, **2014**, 55, 5515–5520
134. Shelkar R., Sarode S. and Nagarkar J., *Tetrahedron Lett.*, **2013**, 54, 6986–6990
135. Riadi Y., Mamouni R., Azzalou R., El Haddad M., Routier S., Guillaumet G. and Lazar S., *Tetrahedron Lett.*, **2011**, 52, 3492–3495
136. Hu R., Li X., Tong Y., Miao D., Pan Q., Jiang Z., Gan H. and Han S., *Synlett.*, **2016**, 27, A–D
137. Soroko I., Bhole Y. and Livingston A. G., *Green Chem.*, **2011**, 13, 162–168
138. Trofimov B. A., *J. Sulfur Chem.*, **1992**, 11, 207–227
139. Zhou C. and Larock R. C., *J. Org. Chem.*, **2006**, 71, 3184–3191
140. Azeredo J. B., Godoi M., Martins G. M., Silveira C. C. and Braga A. L., *J. Org. Chem.*, **2014**, 79, 4125–4130
141. Vieira A. A., Azeredo J. B., Godoi M., Santi C., da Silva Júnior E. N. and Braga A. L., *J. Org. Chem.*, **2015**, 80, 2120–2127
142. Reddy M. R., Rao N. N., Ramakrishna K. and Meshram H. M., *Tetrahedron Lett.*, **2014**, 55, 4758–4762
143. Sun M.-A., Wang Y., Zhang Q., Xia Y., Ge W. and Guo D., *BMC Genomics*, **2017**, 18, 279
144. Clayden J., Greeves N. and Warren S., *Organic Chemistry Second Edition*, **2012**, Oxford University Press
145. Sankar M., Nowicka E., Carter E., Murphy D. M., Knight D. W., Bethell D. and Hutchings G. J., *Nat. Commun.*, **2014**, 5, 3332
146. Hori M., Kataoka T., Shimizu H., Imai Y. and Fujimura H., *Yakugaku Zasshi.*, **1978**, 98, 1019–27

147. Elgrishi N., Rountree K. J., McCarthy B. D., Rountree E. S., Eisenhart T. T. and Dempsey J. L., *J. Chem. Educ.*, **2018**, 95, 197–206
148. Gritzner G. and Kůta J., *Electrochim. Acta*, **1984**, 29, 869–873
149. Bard A. J. and Faulkner L., *Electrochemical Methods: Fundamentals and Applications*, **2001**, John Wiley & Sons
150. Compton R. G. and Banks C. E., *Understanding Voltammetry*, **2011**, Imperial College Press, London
151. Einstein A., *Ann. Phys.*, **1905**, 322, 549–560
152. von Smoluchowski M., *Ann. Phys.*, **1906**, 326, 756–780
153. Atkins P. and de Paula J., *Atkins' Physical Chemistry*, **2006**, OUP Oxford
154. LeSuer R. J., Buttolph C. and Geiger W. E., *Anal. Chem.*, **2004**, 76, 6395–6401
155. Rosenthal M. R., *J. Chem. Educ.*, **1973**, 50, 331
156. Marks T. J. and Seyam A. M., *Inorg. Chem.*, **1974**, 13, 1624–1627
157. Chen E. Y.-X. and Lancaster S. J., *Comprehensive Inorganic Chemistry II: From Elements to Applications*, **2013**, Elsevier, Oxford
158. Martin E., Hughes D. L. and Lancaster S. J., *Inorg. Chim. Acta*, **2010**, 363, 275–278
159. Nishida H., Takada N., Yoshimura M., Sonoda T. and Kobayashi H., *Bull. Chem. Soc. Jpn.*, **1984**, 57, 2600–2604
160. O'Toole T. R., Younathan J. N., Sullivan B. P. and Meyer T. J., *Inorg. Chem.*, **1989**, 28, 3923–3926
161. Domingo L. R., Perez P. and Contreras R., *J. Org. Chem.*, **2003**, 68, 6060–6062
162. Zhu X.-Q., Zhang M.-T., Yu A., Wang C.-H. and Cheng J.-P., *J. Am. Chem. Soc.*, **2008**, 130, 2501–2516
163. Richter D., Tan Y., Antipova A., Zhu X.-Q. and Mayr H., *Chem. Asian J.*, **2009**, 4, 1824–1829
164. Blagg R. J., Simmons T. R., Hatton G. R., Courtney J. M., Bennett E. L., Lawrence E. J. and Wildgoose G. G., *Dalton Trans.*, **2016**, 45, 6032–6043
165. Laurence C. and Gal J.-F., *Lewis Basicity and Affinity Scales: Data and Measurement*, **2010**, John Wiley & Sons Ltd
166. Zhao H., Reibenspies J. H. and Gabbai F. P., *Dalton Trans.*, **2013**, 42, 608–610
167. Mayer U., Gutmann V. and Gerger W., *Monatshefte für Chemie*, **1975**, 106, 1235–1257
168. Beckett M. A., Strickland G. C., Holland J. R. and Varma K. S., *Polymer*, **1996**, 37, 4629–4631

169. Sivaev I. B. and Bregadze V. I., *Coord. Chem. Rev*, **2014**, 270-271, 75–88
170. Skara G., Vleeschouwer F. D., Geerlings P., De Proft F. and Pinter B., *Sci. Rep.*, **2017**, 7, 16024
171. Chase P. A., Piers W. E. and Patrick B. O., *J. Am. Chem. Soc.*, **2000**, 122, 12911–12912
172. Chase P. A., Romero P. E., Piers W. E., Parvez M. and Patrick B. O., *Can. J. Chem.*, **2005**, 83, 2098–2105
173. Bhowon M. G., Jhaumeer-Laulloo S., Dowlut M., Curpen S. and Jumnoodoo V., *Transit. Met. Chem.*, **2005**, 30, 35–39
174. Bhowon M. G., Jhaumeer-Laulloo S., Soukhee N., Allibacus A. and Shiboo V., *J. Coord. Chem.*, **2007**, 60, 1335–1343